Environmental Chemistry Letters (2021) 19:1295–1334
https://doi.org/10.1007/s10311-020-01119-1

REVIEW

Transition metal-based metal–organic frameworks for environmental applications: a review

Yeisy C. López[1,2] · Herlys Viltres[1] · Nishesh Kumar Gupta[3,4] · Próspero Acevedo-Peña[1] · Carolina Leyva[1] · Yasaman Ghaffari[3,4] · Anjali Gupta[5] · Suho Kim[3,4] · Jiyeol Bae[4] · Kwang Soo Kim[3,4]

Received: 7 July 2020 / Accepted: 10 October 2020 / Published online: 27 January 2021

Abstract

Rapid industrialization is deteriorating air and water quality by exposing life to a wide range of pollutants, thus calling for efficient and affordable remediation strategies. Metal–organic frameworks (MOFs) are emerging materials for environmental remediation applications due to their high surface area, ordered porous structure, and application-specific tailoring of properties. In particular, transition metal-based frameworks are advanced adsorbents and catalysts for the remediation of organic and gaseous pollutants. Physicochemical properties are mainly dependent on the choice of the metal center, the oxidation state, and organic linkers. Bimetallic-, polyoxometalate-, and metal oxide-incorporated frameworks find applications as photocatalysts for decontamination of dyes, phenolic compounds, pesticides and pharmaceutical drugs under ultraviolet (UV)/visible radiations. Large surface area coupled with high activity of transition metal frameworks allows the capture and removal of inorganic and volatile organic pollutants. Transition metal frameworks convert gaseous pollutants into value-added chemicals. Frameworks containing synthetic and natural fibers are currently studied to remove chemical warfare agents.

Keywords Adsorption · Gaseous pollutants · Metal–organic frameworks · Photocatalysis · Transition metals · Wastewater remediation

Abbreviations

$AgIO_3$/MIL-53 (Fe)	Fe-based MOF composited with $AgIO_3$
BiOBr/UiO-66	Zr-based MOF combined with BiOBr
CdBDC	Cadmium 1,4-benzenedicarboxylate
Co_2Cl_2(BBTA)	Co_2Cl_2(1H,5H-benzo(1,2-d),(4,5-d′)bistriazole)
$Co_2Cl_2(btdd)(H_2O)_2$	Co_2Cl_2(bis(1H-1,2,3-triazolo[4,5-b],[4′,5′-i])dibenzo[1,4]dioxin)$(H_2O)_2$
Co–DMOF–TM	Co_2(1,4-benzenedicarboxylate)$_2$(1,4-diazabicyclo[2.2.2]octane)
CPL-1	Cu_2(2,3-pyrazinedicarboxylate)$_2$(pyrazine)
CTAB-modified UiO-66	Cetyltrimethylammonium bromide-modified UiO-66
Cu_2Cl_2(BBTA)	Cu_2Cl_2(1H,5H-benzo(1,2-d),(4,5-d′)bistriazole)
$Cu_2O@SiO_2$	Silica-coated copper oxide(I) nanocages
Cu_2O@ZIF-8	Cu_2O loaded within ZIF-8
Cu-BDC(ted)$_{0.5}$	Cu(1,4-benzenedicarboxylate)(triethylenediamine)$_{0.5}$
CuBDC	Copper 1,4-benzenedicarboxylate
CuBTC	Copper benzene-1,3,5-tricarboxylate

✉ Kwang Soo Kim
kskim@kict.re.kr

[1] Instituto Politécnico Nacional, Centro de Investigación en Ciencia Aplicada Y Tecnología Avanzada, CDMX, Mexico

[2] Laboratorio de Bioninorgánica, Facultad de Química, Universidad de La Habana, La Habana, Cuba

[3] University of Science and Technology (UST), Daejeon, Republic of Korea

[4] Department of Land, Water, and Environment Research, Korea Institute of Civil Engineering and Building Technology (KICT), Goyang, Republic of Korea

[5] Department of Chemistry, Dayalbagh Educational Institute, Agra, India

CuBTC-P	Non-thermal plasma-treated CuBTC
D-M-Fe	Fe-based MOF (MIL-53 (Fe)) modified with D-sorbitol
Fe_3O_4@MOF-2	Zn-based MOF-supported Fe_3O_4 nanoparticles
Fe_3O_4@SiO_2	Magnetite nanoparticles coated with silica
Fe_3O_4@SiO_2 @Zn–TDPAT	Zn-based MOF with TDPAT loaded with Fe_3O_4@SiO_2
Fe_3O_4-COOH @ZIF-8/Ag/Ag_3PO_4	Fe_3O_4 with carboxylate and Ag/Ag_3PO_4 nanoparticles
Fe-BTC	Iron benzene-1,3,5-tricarboxylate
Fe-M MOFs	Bimetallic Fe-based MOF, M: transition metal
Fe-Zn BDC BMOF	Iron zinc bimetallic MOF with BDC
HKUST-1	Cu-based MOF using trimesic acid
HPU-5	{[Co(5-(3,5-Di-pyridin-4-yl-[1,2,4]triazol-1-ylmethyl)-isophthalic acid)]$(CH_3CN)_{0.5}(H_2O)_5\}_n$
HPU-6	{[Mn_2((5-(3,5-Di-pyridin-4-yl-[1,2,4]triazol-1-ylmethyl)-isophthalic acid))$_2$ $(H_2O)_2$]$(CH_3OH)_2(H_2O)_3$ $(DMA)_2$}
IRMOF-3	Zn_4O(2-aminoterephthalate)$_3$
KAUST-7	$Ni(NbOF_5)(pyrazine)_2{\cdot}2H_2O$
KAUST-8	$[Ni(AlF_5(OH_2))(pyrazine)_2{\cdot}2H_2O$
LED	Light-emitting diode
M.MIL-100(Fe) @ZnO NS	Fe (III)-based MOF modified with ZnO nanospheres
MFM-520	Zn_2(4,4-bipyridyl-3,3′,5,5′-tetracarboxylate)
MFM-601	$Zr_6(\mu_3\text{-}O)_4(\mu_3\text{-}OH)_4(OH)_4(H_2O)_4$(4,4′,4″,4‴-(1,4-Phenylenebis(pyridine-4,2,6-triyl))tetrabenzoate)$_2$
MIL(Fe)/Fe-SPC	Fe-doped nanospongy porous biocarbon (SPC) composited with Fe-based MOF
MIL-100(Fe)	$Fe_3(H_2O)_3O$[1,3,5-benzenetricarboxylate]$_2{\cdot}nH_2O$
MIL-101(Cr)	$Cr_3F(H_2O)_2O$[benzene dicarboxylate]$_3{\cdot}nH_2O$
MIL-101(Fe)	$Fe_3O(H_2O)_2Cl$(1,4-benzenedicarboxylate)$_3$
MIL-101-NH_2(Cr)	$Cr_3F(H_2O)_2O$[2-aminoterephthalate]$_3{\cdot}nH_2O$
MIL-125(Ti)@TiO_2	Ti based MOF with encapsulated TiO_2
MIL-125(Ti)	$Ti_8O_8(OH)_4$(1,4-benzenedicarboxylate)$_6$
MIL-47(V)	V^{IV}(O)(1,4-benzenedicarboxylate)
MIL-53(Fe)	[Fe(OH).(benzene dicarboxylate).H_2O]
$Mn_2Cl_2(btdd)(H_2O)_2$	Mn_2Cl_2(bis(1H-1,2,3-triazolo[4,5-b],[4′,5′-i])dibenzo[1,4]dioxin)$(H_2O)_2$
MOF 1	3D-[$Zn_4(\mu_4\text{-}O)$(6-oxo-6,7-dihydro-5H-dibenzo[d,f][1,3]-diazepine-3,9-dicarboxylate)$_3$]
MOF 3	[Zn_2(6-oxo-6,7-dihydro-5H-dibenzo[d,f][1,3]-diazepine-3,9-dicarboxylate)$_2$(4,4′-bipyridine)]
MOF 4	[Zn_2(6-oxo-6,7-dihydro-5H-dibenzo[d,f][1,3]-diazepine-3,9-dicarboxylate)$_2$(1,2-bis(4-pyridyl)ethane)]
MOF	Metal-organic framework
MOF-177	Zn_4O(4,4′,4″-benzene-1,3,5-triyltribenzoate)$_2$
MOF-5	Zn_4O(1,4-benzenedicarboxylate)$_3$
MOF-74(Zn)	Zn_2(2,5-dihydroxyterephthalate)
MOF-808	$Zr_6O_4(OH)_4$(benzene-1,3,5-tricarboxylate)$_2$
NH_2-MIL-125(Ti)	$Ti_8O_8(OH)_4$(2-aminoterephthalate)$_6$
Ni(bdc)(ted)$_{0.5}$	Ni(1,4-benzenedicarboxylate)(triethylenediamine)$_{0.5}$
Ni_2Cl_2(BBTA)	Ni_2Cl_2(1H,5H-benzo(1,2-d),(4,5-d′)bistriazole)
$Ni_2Cl_2(btdd)(H_2O)_2$	Ni_2Cl_2(bis(1H-1,2,3-triazolo[4,5-b],[4′,5′-i])dibenzo [1,4]dioxin)$(H_2O)_2$
Ni–DMOF–TM	Ni_2(1,4-benzenedicarboxylate)$_2$(1,4-diazabicyclo[2.2.2]octane)
NU-1000	$Zr_6(\mu_3\text{-}OH)_8(OH)_8$(1,3,6,8-tetrakis(p-benzoic acid)pyrene)$_2$
NU-1401	$Zr_6(\mu_3\text{-}O)_4(\mu_3\text{-}OH)_4(HCOO)_4(OH)_4$ $(H_2O)_4(C_{30}H_{10}N_2O_{12})$
PCN-222(Zr)	$Zr_6(\mu_3\text{-}O)_8(OH)_8$(tetrakis(4-carboxyphenyl)porphyrin)$_2$
PMo_{12}@UiO-66 @H_2SMIPs	$H_3PMo_{12}O_{40}$@UiO-66@ H_2S molecular imprinted polymers
PW@HKUST-1H_3	Keggin-type polyoxometalate encapsulated in CuBTC MOF
$PW_{12}O_{40}{\cdot}nH_2O$	
TDPAT	2,4,6-tris(3,5-dicarboxy phenylamino)-1,3,5-triazine
TiO_2@NH_2-MIL-88B(Fe)	Iron-based MOF with TiO_2 grafted on the surface

TiO_2@NH_2-UiO-66	Zr-based MOF with encapsulated TiO_2
UiO-66/g-C_3N_4/Ag(15)	Zr-based MOF modified with graphite carbonitride and silver nanoparticles
UiO-66	$Zr_6O_4(OH)_4$(1,4-benzenedicarboxylate)$_6$
UiO-66-NH_2	$Zr_6O_4(OH)_4$(2-aminobenzenedicarboxylate)$_6$
UiO-67	$Zr_6O_4(OH)_4$(biphenyl-4,4'-dicarboxylate)$_6$
UiO-68-TBTD	Triazolobenzothiadiazole-$Zr_6O_4(OH)_4$(p,p'-terphenyldicarboxylate)$_6$
UMCM-313	$Zr_6(\mu_3\text{-}O)_4(\mu_3\text{-}OH)_4(OH)_4(H_2O)_4$(2,5,8,11-tetrakis(4-carboxyphenyl)perylene)$_2$
WO_3/MIL-53(Fe)	Fe-based MOF combined with WO_3
XY-M-Fe	Fe-based MOF (MIL-53 (Fe)) modified with xylitol
ZIF-67	Co(2-methylimidazole)$_2$
ZIF-8	Zn(2-methylimidazole)$_2$
Zn(bdc)(ted)$_{0.5}$	Zn(1,4-benzenedicarboxylate)(triethylenediamine)$_{0.5}$
ZnBDC	Zinc 1,4-benzenedicarboxylate
Zn–DMOF–TM	Zn_2(1,4-benzenedicarboxylate)$_2$(1,4-diazabicyclo[2.2.2]octane)
Zn–TDPAT	Zn-based MOF with TDPAT
α-Fe_2O_3@MIL-101(Cr)@TiO_2	Cr-based MOF modified with α-Fe_2O_3 and TiO_2-modified ZIF-8
α-Fe_2O_3@UiO-66	UiO-66 MOF loaded with hematite nanoclusters
30UiO-66/$CdIn_2S_4$	Zr-based MOF combined with mixed metal sulfide ($CdIn_2S_4$)
1-NO_3-OH·20H_2O	$Cu_9(OH)_6Cl_2$(1-imidazol-1-yl-3-(1,2,4-triazol-4-yl)propane)$_6$(bdc)$_3$](NO_3)$_2$(OH)$_2$

Introduction

According to the 2020 edition of the World Water Development Report, 1.6 billion people lack access to clean water (UNESCO 2019). Moreover, the quality of water sources is rapidly decreasing due to the incorporation of highly toxic chemicals. Anthropogenic activities, such as agricultural and industrial, are responsible for releasing hazardous compounds, including dyes, pesticides, phenolic, and chlorinated compounds. Furthermore, daily activities have been adding emerging contaminants such as pharmaceuticals, personal care products, and endocrine-disrupting compounds at trace concentrations. These toxic and carcinogenic micropollutants could be a severe threat to the environment (De Andrade et al. 2018; Rojas and Horcajada 2020). Another high-priority environmental concern is associated with the increasing demand for fossil fuels such as coal, petroleum, and natural gas. The uncontrolled burning of fossil fuels leads to the emission of obnoxious and toxic gases, generally termed as CO_x, NO_x, and SO_x, along with volatile organic compounds and volatile sulfur-organic compounds. These gases severely deteriorate air quality and are directly or indirectly linked to global warming and acid rains (Kim 2018; Han et al. 2019).

Numerous physicochemical and biological methods for water and air decontamination have been developed. Many of these strategies have limited applicability, difficulty in scaling up, and high operational cost. Such is the case of ultrafiltration, reverse osmosis, or biological treatment of water due to large energy consumption, high cost, or slow operational kinetics. In the case of air decontamination processes, the accepted method of chemical adsorption involves high energy consumption and experiences solvent loss. In that sense, the development of economical, robust, and scalable technologies remained a challenging task for environmental engineers and researchers.

The discovery of metal–organic frameworks (MOFs) opened the door for the development of porous materials for gas storage at ambient conditions. Among the attractive physicochemical properties of these inorganic–organic hybrids are a large surface area ($\sim$ 1000–10,000 $m^2\ g^{-1}$), pore volume, excellent water and thermal stability, and an enormous structural variability (more than 60,000 MOFs have been reported in the Cambridge crystallographic database by changing metal centers and/or organic linkers). Such features allow the design of MOFs for a wide variety of applications in CO_2 capture, gas storage, gas separation, sensing, catalysis of organic reactions, adsorption, activation of small molecules, and biomedical imaging. The increasing publications per year index related to the use of MOFs for environmental applications corroborate the increasing interest in the field (Fig. 1a). Furthermore, the application of MOFs is not restricted to one specific type of pollutant. MOF-based materials have been used for the removal of heavy metals, recovery of precious metals (Geisse et al. 2019; Lou et al. 2019; Jiang et al. 2019), the capture of NO_x, CO_2, and other toxic gases (Kim 2018; McGrath et al. 2019) and photocatalytic degradation of

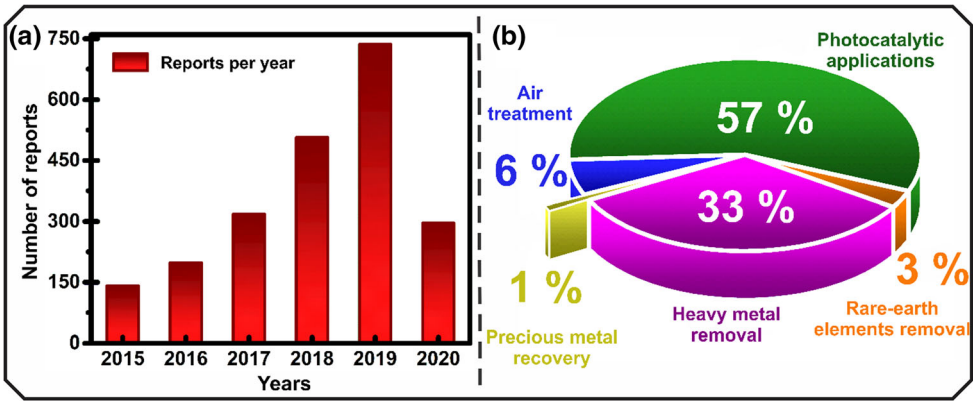

Fig. 1 **b** Number of publications per year related to metal–organic frameworks (MOFs) for environmental applications (2015–2020), **b** publications percent of MOFs for heavy metal removal, recovery of precious metal and rare-earth elements, air treatment, and photocatalytic degradation of organic compounds (Statics extracted from *Web of Science database:*(Clarivate Accelerating innovation 2019) Keywords used: MOFs, environmental applications, water remediation, air decontamination)

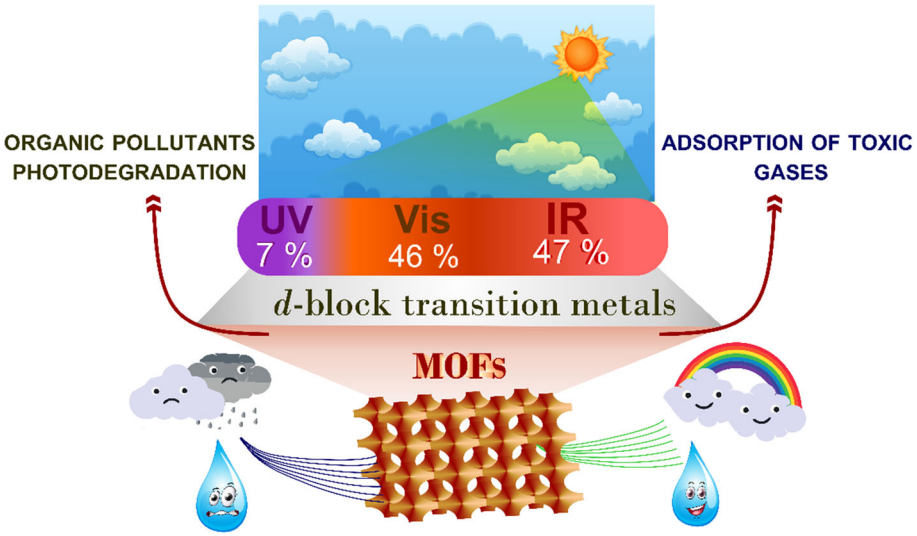

Fig. 2 Transition metal-based metal–organic framework (MOF) for environmental applications. The broad ultraviolet/visible absorption range of MOF-based materials makes them excellent candidates for photodegradation of organic compounds, while the large surface area and porosity boost their use as materials for toxic gas decontamination

different organic and inorganic pollutants (Fig. 1b) (Bedia et al. 2019).

Heterogeneous photocatalysis is an efficient strategy for eliminating organic pollutants, where semiconductors such as TiO_2, ZnO, and ZnS remain the most popular choices. However, the use of these photocatalysts presents some significant drawbacks such as poor material recovery, fast electron–hole pair recombination, and low solar activity due to a wide bandgap energy ($E_g \sim$ 3.2–3.7 eV). The oxides and sulfides of some 3*d*-block transition metals are known to have a narrow bandgap energy (1.11 eV for $CoFe_2O_4$), making them suitable for exploiting the entire UV–visible region of the solar spectrum (Gupta et al. 2020c). MOFs with Zn(II), Cu(I)/Cu(II), Co(II)/Co(III), and Fe(II)/Fe(III) as metal centers are capable of acting as photocatalysts, allowing the degradation of organic pollutants under UV/visible light. The organic linkers in the MOF structure can act as light "receptionists," activating the transition metal centers via ligand-to-metal cluster charge transfer. The excited MOF is capable of producing electron–hole pairs that can be transferred to the surface and participate in photo-redox reactions. The weak coordination of *d*-block transition metals with ligands within the MOF favors the creation of coordination vacancies where the coordinatively unsaturated metal centers behave as Lewis acid catalytic sites (Kökçam-Demir et al. 2020). Moreover, the light-harvesting properties of these coordination polymers could be tuned by using conjugated organic linkers. The MOFs could exploit the entire solar spectrum and are considered as next-generation photocatalysts. Since one of the first applications of MOFs was gas capture and storage, it is possible to use MOFs as adsorbents/catalysts for the removal of toxic gases, which may come out as an economical and direct approach to alleviate the growing level of air pollution (Fig. 2).

This review provides an updated overview of transition metal-based MOFs materials for environmental applications, particularly organic pollutants degradation and air decontamination strategies. The first section is dedicated to the more recent synthetic approaches for upgrading the catalytic centers of MOFs with a focus on the strategies related to the metallic nodes. The relevant physical and chemical properties of the MOF, such as surface area, thermal stability, resistance to acidic or basic media, as well as the optical properties, are discussed in the subsequent section. Major sections of this review highlight the applicability of MOFs in the catalytic degradation of organic dyes, pharmaceutical drugs, pesticides, and phenolic compounds. The adsorptive and catalytic removal of inorganic and organic gaseous pollutants using MOFs has been discussed in great lengths in the interest of readers. MOF's potential to remediate harmful toxicants like chemical warfare agents have been addressed to broaden the domain of the coordination polymers in environmental applications. Finally, we have addressed the challenges and prospects of MOFs in air and water decontamination.

Synthesis of metal–organic frameworks

The photocatalytic activity of metal–organic frameworks (MOFs) is due to its high porosity and excellent light absorption capability. Opposite to zeolites and aluminophosphates, which present a restricted number of building units, SiO_4/AlO_4 and AlO_4/PO_4, respectively, tuning of linkers or metal nodes provides a more extensive range of surface area, porosity, and chemical environment in MOFs. The coordination polymers are versatile materials that allow a rational design of the active catalytic site and its environment with a remarkable degree of exactitude (Gascon et al. 2014). In particular, MOFs containing transition metals as nodes have gained interest due to significant structural and morphological variability. In that sense, MOFs containing Zn, Cu, Cd, Co, and Fe centers have been reported as photocatalysts for the degradation of organic pollutants under UV/visible source (Vu et al. 2019; Cheng et al. 2020). The metal nodes usually have one or more weakly coordinated ligands (water molecules or solvents) that can be eliminated without altering the crystal structure. Once the coordination vacancy is formed, the metal center behaves as Lewis acid, accepting electrons

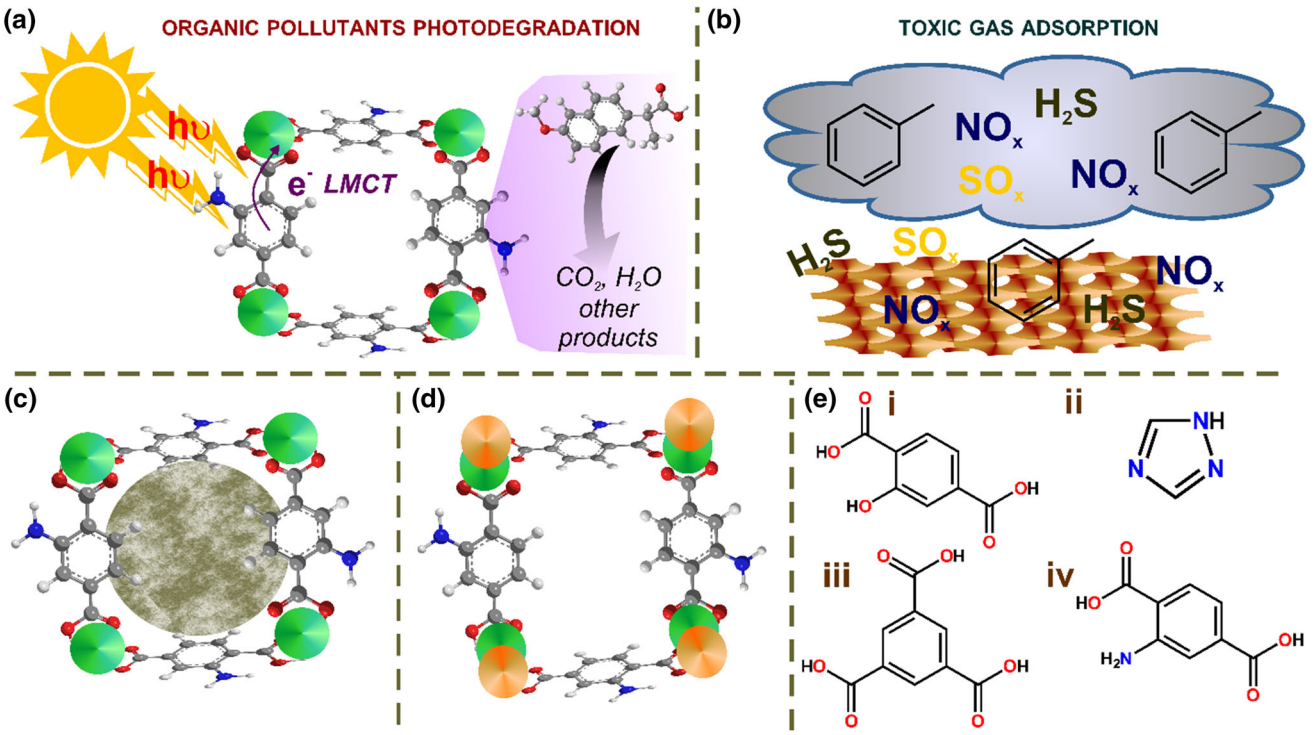

Fig. 3 **a** Organic pollutants photodegradation using metal–organic frameworks (MOFs) showing the excitation of the organic linker after irradiation and the transference of the excited electron to the metal node through ligand-to-metal charge transfer, **b** toxic gases physical adsorption on MOFs surface, **c** encapsulation of photoactive species inside MOF pores, **d** modification of metal nodes (bimetallic MOFs, metal oxides or polyoxometalates), **e** commonly used organic ligands for enhancing the light-harvesting ability of MOF: i. 2-hydroxyterephthalic acid, ii. 1,2,4-triazole, iii. trimesic acid, iv. 2-aminoterephthalic acid

from a photosensitive molecule present in the media (Fig. 3a). However, not only the metallic node plays a major role in the MOF photocatalytic performance, the organic linker and the pore space could participate as well in the photo-redox reaction. The encapsulation of a photocatalytic active species inside the MOF pores represents another strategy to ensure high photocatalytic performance (Fig. 3c) (Chandra et al. 2019; Malik and Nath 2019). Besides, the porous structure of the inorganic polymers favors the charge transfer by lowering the recombination rate for electron–hole pairs due to the narrow distance that charge carriers must travel to be transported to the pore surface (Li et al. 2018b).

Finally, the organic linkers are responsible for absorbing photons and inducing a charge-separate state by single electron transfer from the ligand to the metal nodes (Dhakshinamoorthy et al. 2016). The extent of conjugation in the ligand (and the metal coordination) determines the energetic requirements for a favorable transition. In that sense, the preferred ligands are aromatic polycarboxylates, 2-aminoterephthalic acid, and porphyrins (Fig. 3e) (Dhakshinamoorthy et al. 2016). As mentioned earlier, MOF applications can be extended to the physicochemical adsorption (Fig. 3b) and catalytic degradation of toxic gases. The variation of metal nodes, i.e., the introduction of another metal ion (Fig. 3d), leads to variation in the porosity of the material and active sites for adsorption, influencing the gas capture capacity (He et al. 2020). In the following subsections, an overview of synthetic approaches for MOFs with engineered photocatalytic centers has been provided with a focus on the modification of metallic nodes of the MOFs and/or encapsulation of active species. More detailed information on the synthesis of MOFs can be collected from the previously published reviews (Stock and Biswas 2012; Lee et al. 2013).

Monometallic ion-based metal–organic frameworks

Materials scientists develop strategies that allow the designing of specific materials with desired characteristics (Howarth et al. 2017; Liu et al. 2017b; Diercks et al. 2018). Different aspects have to be considered for photocatalytic applications, such as absorption of photons in the entire solar spectrum, efficient charge separation, presence of catalytic centers, and fast charge transfer kinetics (Zeng et al. 2016; Gong et al. 2020; Pratim Bag and Sahoo 2020). Metal–organic frameworks (MOFs) represent one of the most diverse family of materials with characteristics that are required for photocatalytic applications: the organic linker may behave as a photon absorber and the isolated metallic ions as catalytic centers to promote the charge transfer or the formation of oxidant species (Cheng et al. 2018; Kang et al. 2019). Till now, thousands of MOFs have been reported with a well-controlled structure in one-, two-, or three-dimensions obtained by changing the metal centers and/or the organic linkers (Gangu et al. 2016; Safaei et al. 2019).

The literature has plenty of specialized synthetic routes for the fabrication of MOFs (Bayliss et al. 2014; Yap et al. 2017; Guo et al. 2019; Zhu and Liu 2019). This large variety offers the possibility of obtaining MOFs with diverse properties such as vacancies, crystallinity, and morphology that could contribute to their performance. Figure 4 summarizes some of the most common strategies adopted for the synthesis of MOFs. These techniques have been extensively reviewed and are commonly employed to obtain MOFs for different applications (Flügel et al. 2012; Lee et al. 2013; Rubio-Martinez et al. 2017; Zhang et al. 2017). Although solvothermal is the most popular strategy for synthesizing MOFs, other strategies have been reported to obtain the solids at mild conditions (Klimakow et al. 2010; Khan and Jhung 2015; Mehta et al. 2018; Vaitsis et al. 2019). Moreover, several green strategies have been developed to avoid high energy consumption or the generation of many residues (Sánchez-Sánchez et al. 2015; Reinsch 2016). Lee et al. (2015) compare seven different synthetic routes on the properties of ZIF-8 (Lee et al. 2015). Sonochemical and dry-gel routes offer lower-sized particles. Solvothermal and mechanochemical are attractive for incorporating magnetite nanoparticles into MOFs. The route followed for the synthesis of the material has an impact on the MOF yield.

Template-directed synthesis of MOFs is a strategy to form composite@MOF photocatalysts (Yang et al. 2019b). It could enhance the charge separation and transfer process, improving the photocatalytic behavior. Synthetic routes like Langmuir–Blodgett (Benito et al. 2016) and electrodeposition (Li et al. 2016) could be used for the development of MOF films. Another strategy to improve photocatalytic properties could be the exfoliation of the MOF to obtain 2D structures. In this way, the metallic centers would be more accessible for catalytic reactions (Zhu and Liu 2019). The synthesis method should be selected based on the linker and metal salt required to prepare the MOF with controlled composition and morphology. The employment of additives to achieve the directional growth of porous solids is a recurrent strategy to control the shape and size and obtain exotic morphologies (Ranft et al. 2013; Liu et al. 2018a).

Bimetallic ions-based metal–organic frameworks

The presence of second metal in a bimetallic catalyst has a synergistic effect on its catalytic activity, which has been reviewed extensively in the literature (Notar Francesco et al. 2014). The introduction of a second metal ion as the

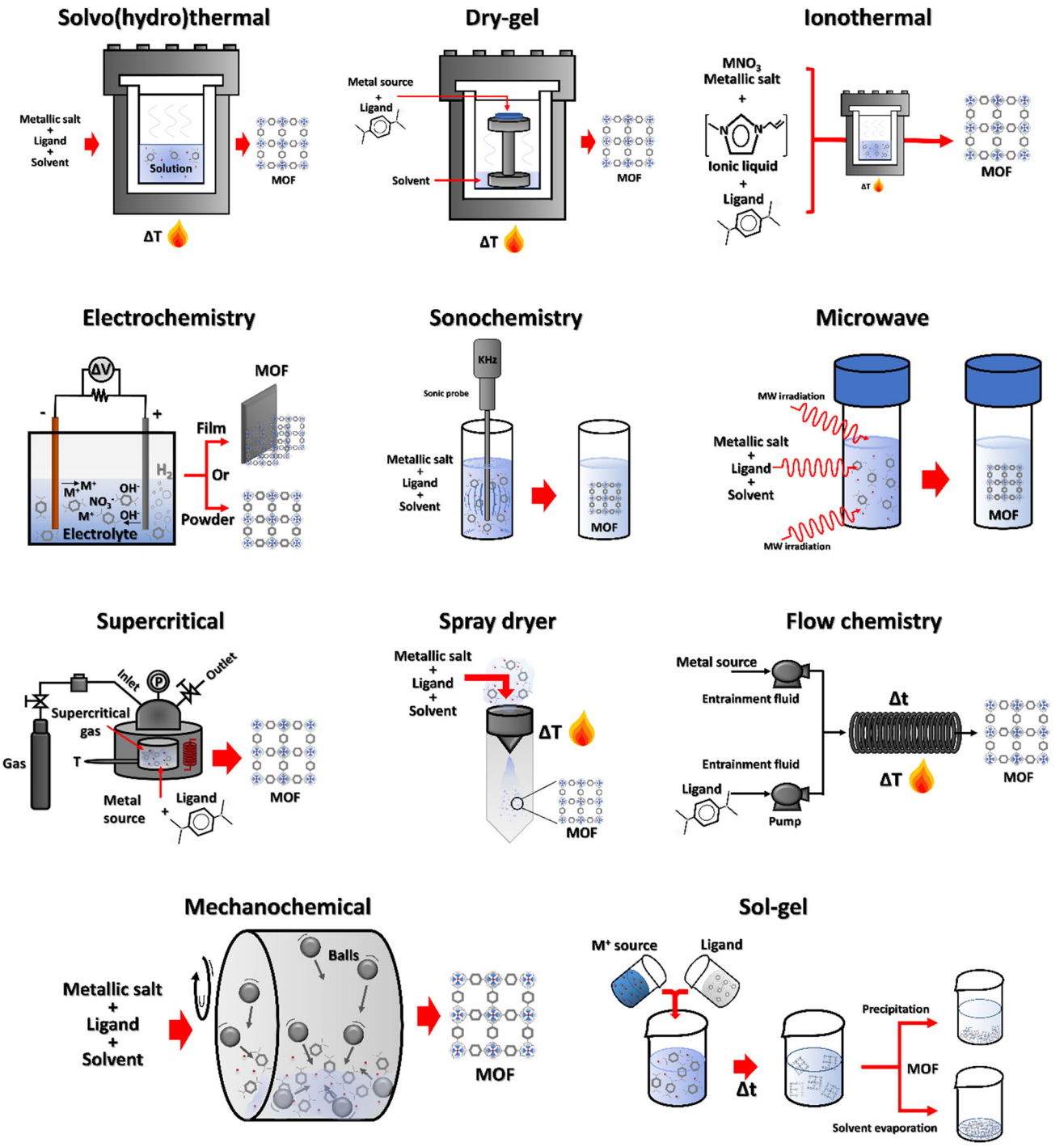

Fig. 4 Synthetic approaches for preparing metal–organic frameworks: solvo/hydrothermal, ionothermal, electrochemistry, spry dryer, microwave, sol–gel, mechanochemical, dry-gel, sonochemistry, supercritical, flow chemistry

node for preparing metal–organic frameworks (MOFs) enhances the photocatalytic performance of the material, compared to their single metal analogs. The improved catalytic response is most likely related to synergistic effects among the components of the MOF-based photo-responsive material. The possibility of multiple oxidation states in many of the transition metals enables easy electron transfer, making their redox chemistry attractive. Iron-based bimetallic MOFs generated hydroxyl (˙OH) radicals from heterogeneous Fenton reaction with hydrogen peroxide (H_2O_2) (Zhao et al. 2017; Tang and Wang 2020). Sun et al. (2017) fabricated a family of bimetallic Fe-M MOFs using manganese, cobalt, and nickel as the second metal (M). The bimetallic MOFs were synthesized via the

solvothermal reaction of terephthalic acid with variable Fe/M ratios. The Fe–M MOFs were tested for heterogeneous Fenton-like degradation of phenolic compounds. The better catalytic performance of Fe–Mn MOF, compared to the other two bimetallic MOFs, has to do with the redox chemistry of Co and Ni and their role in the Fenton reaction. A priori, either the Co(III)/Co(II) or Mn(III)/Mn(II) could decompose H_2O_2 and generate $^{\cdot}OH$ radicals. However, the lower incorporation of Co ions into the Fe–MOF skeleton hinders the $^{\cdot}OH$ radical formation and, subsequently, Fe–Co–MOF photocatalytic efficiency. Unlike Mn(II), Ni(II) does not participate in the Fenton reaction, which leads to poor degradation performance of Fe–Ni-MOF (Sun et al. 2017). Thus, it is highly recommendable to choose suitable second metal ions as these occupy catalytic centers and lower the catalytic activity, if not chosen properly.

Li et al. (2019a) reported a FeCo bimetallic MOF synthesized via a solvothermal method. The metallic precursors, $FeCl_2.4H_2O$ and $Co(NO_3)_2.6H_2O$ were dissolved in ŃN-dimethylformamide/HF mixture with 2-hydroxyterephthalic acid as the organic linker. After mixing, the suspension was transferred into a Teflon sealed reactor and subjected to different time–temperature conditions. Fe(II) is considered as the most effective transition metal to activate H_2O_2 and peroxydisulfate, while Co(II) quickly generates sulfate radical ($SO_4^{\cdot-}$) and $^{\cdot}OH$ radicals from peroxymonosulfate. Both processes are possible due to the oxidation of the metal ions in the presence of oxidants. The formation of highly reactive species, $SO_4^{\cdot-}$ and $^{\cdot}OH$ radicals, allowed the prepared material to degrade methylene blue without any light source. Thus, the combination of Fe(II) and Co(II) in the MOF skeleton enhanced the catalytic activity compared to single Fe- or Co-based MOF (Li et al. 2019a). Fe-Zn bimetallic MOF was reported for photocatalytic degradation of methylene blue under visible light. The incorporation of a second metal node to the MOF structure lowered the bandgap to the visible light range, making the photodegradation process more efficient. The bimetallic MOF was prepared through a one-pot solvothermal method. The transition metal salts were dispersed in ŃN-dimethylformamide/ethanol mixture with terephthalic acid as the linker. The mixture was thoroughly stirred and then heated at 150 °C for 20 h in a Teflon-lined stainless-steel Parr autoclave, yielding pale-yellow crystals. The prepared Fe-Zn bimetallic MOF exhibited good magnetic behavior, which further improved the catalyst recovery. Moreover, the aromatic linker is an accepted ligand to improve light response and transfer of the excited electrons, in this case, most likely to Fe(III) ions, considering that Zn(II) reduction to Zn is highly unlikely within the MOF structure. The Fe(III) ion behaves as a Lewis acid, which can easily reduce to Fe(II) by accepting an electron (Tiwari et al. 2019).

Gómez-Aviles et al. (2019) proposed a one-pot partial substitution of Ti ions with Zr in the NH_2-MIL-125(Ti). For the in situ substitution of Ti ions, different proportions of Zr(IV) butoxide solution and titanium isopropoxide were added in a 2-aminoterephthalic acid/N′N-dimethylformamide mixture under stirring. The reaction mixture was stirred, transferred to a Teflon-lined autoclave, and heated at 150 °C for 16 h, leading to the formation of yellow-colored crystals. The presence of amino groups (offering one pair of free electrons in the aromatic ligand structure) enables efficient metal–ligand charge transfer and extends the lifetime of the photo-excited states, which lowers the electron–hole recombination rate. In the mixed Ti-Zr metallic centers, there were new energy levels (due to the incorporation of Zr ions) below the conduction band or above the valence band, acting as new states for electron excitation, thus suppressing the charge recombination process. MOFs with low Zr(IV) content exhibited elevated porosity, high crystallinity, and low bandgap, which favored the acetaminophen degradation (Gómez-Avilés et al. 2019). He et al. (2020) reported the partial substitution of Cu with Fe and Co in HKUST-1 for CO_2 capture. The spray method is based on atomizing the precursor solutions (Cu, Co, and Fe salts; trimesic acid) into microdroplets. The microdroplets are carried through the tube furnace by airflow (5 L min^{-1}) at 200 °C. In the tube, the solvent evaporates with the initiation of the nucleation and crystallization processes. The incorporation of the second metal ion led to the expansion of the unit cell, resulting in a slightly higher surface area and pore volume (He et al. 2020).

Metal oxide-based metal–organic frameworks

The electron–hole recombination rates in monometallic and bimetallic metal–organic frameworks (MOFs) are still higher, which limits their photocatalytic activity. Aiming to reduce the charge recombination rate, loading MOFs with metal oxides is considered a suitable solution. Metal oxide semiconductors such as Fe_3O_4, α-Fe_2O_3, Cu_2O, TiO_2, and ZnO are popular choices due to their excellent photocatalytic activity. In that sense, a novel proposal is the modification (in situ/post-synthesis) of MOFs with other photocatalytic metal oxide semiconductors. Ahmad et al. (2019) synthesized M.MIL-100(Fe)@ZnO nanostructure for effective photo-Fenton-induced degradation of toxic organic compounds. Metal–organic assemblies were used as a template for preparing the stable mesoporous M.MIL-100(Fe) by the in situ self-assembly method. The metal–organic assemble precursor was prepared by dissolving metal precursors and organic linkers in dimethylformamide

and transferring the mixture into a Teflon liner autoclave. The suspension was sonicated, sealed, and heated for 12 h at 150 °C. The powder collected by centrifugation was dispersed in 0.1 M HCl under stirring to destroy the template, leading to the formation of M.MIL-100(Fe). The ZnO nanospheres were loaded onto the M.MIL-100(Fe). The lower electron–hole recombination rate of ZnO and the MOF-ZnO heterojunction enhanced the degradation performance (Ahmad et al. 2019).

TiO_2 has been considered as one of the most employed semiconductor oxides in the preparation of photocatalysts, including the modification of MOFs for the degradation of volatile organic compounds and dyes. Various approaches have been adopted to introduce TiO_2 in the MOF structure, either within the pores or onto the surface. Yao et al. (2018) proposed the encapsulation of TiO_2 inside the pores of NH_2-UiO-66 for visible-light-responsive-photodegradation of volatile organic compounds. The TiO_2 nanoparticles were prepared separately by a microwave-assisted method. The TiO_2@MOF was obtained by self-assembly of the MOF around Zr(IV) ions pre-coordinated to the TiO_2. $ZrCl_4$ and TiO_2 nanoparticles were dispersed in ŃN-dimethylformamide and 2-aminoterephthalic/acetic acid mixture was added. The reaction mixture was heated for 24 h at 120 °C under stirring, forming a yellow solid as the final product. The highly porous structure of the TiO_2@-MOF led to enhanced volatile organic compounds capture, where 2-aminoterephthalic acid acted as a light-harvesting center and photocatalytic active site in the same space (Yao et al. 2018). Li et al. (2018d) reported a different synthetic strategy for preparing TiO_2@NH_2-MIL-88B(Fe). Ferric chloride and tetrabutyl titanate were used as metallic precursors with 2-aminoterephthalic acid as the organic ligand in the solvothermal synthesis. Unlike the material reported by Yao, TiO_2 nanoparticles were equally distributed on the materiaĺs surface (Li et al. 2018d). Zhu and Yan (2018) presented another encapsulation strategy, where TiO_2 particles and the MOF were synthesized separately by the solvothermal method. TiO_2 was magnetically dispersed in ŃN-dimethylformamide for 3 h, followed by the addition of MIL-125(Ti) to achieve co-precipitation of TiO_2 and MOF without stirring. MIL-125(Ti)@TiO_2 was separated and heated at 150 °C for 6 h to get the final product. The Ti-based MOF behaved as a light sensitizer, transferring photons to TiO_2. The synergistic effect of encapsulated TiO_2 and Ti in the MOF enhanced the degradation of rhodamine B than the non-encapsulated TiO_2 particles (Zhu and Yan 2018).

Li et al. (2018a) developed the first report on the incorporation of unstable Cu_2O nanocages inside ZIF-8 through a template protection-sacrifice method. The reported strategy is based on the preparation of the Cu_2O nanocages separately and capping with a silica shell to cover the surface. The Cu_2O@SiO_2 was loaded into the ZIF-8, followed by etching of the silica layer with the NaOH solution to yield hybrid Cu_2O@ZIF-8. The porous framework of the ZIF-8, along with the hollow morphology, achieved after etching SiO_2, expedite the diffusion of pollutants and offer a suitable space and surrounding for catalytic reactions. This approach protected Cu_2O inside the hybrid Cu_2O@ZIF-8 from oxidation after the catalytic hydrogenation of *p*-nitrophenol (Li et al. 2018a). Zhang et al. (2019b) reported the encapsulation of α-Fe_2O_3 nanoclusters in the pores of UiO-66 for visible-light-responsive photocatalysis. UiO-66 was synthesized via a solvothermal route using $ZrCl_4$ and terephthalic acid in ŃN-dimethylformamide/acetic acid. The thermally activated MOF was suspended in an iron acetylacetonate solution and was stirred for 6 h. The prepared material was calcined for 6 h at 300 °C, which led to the formation of α-Fe_2O_3 nanoclusters within the pores of UiO-66 (Zhang et al. 2019b).

Polyoxometalate-based metal–organic frameworks

Polyoxometalates are poly-structures of cations linked through polyanion clusters with MO_x (x = 5,6) as the building units. Most often, transition metals such as W, Mo, V, and Nb in their highest oxidation state make polyoxometalates (Wang and Yang 2015; Jiang et al. 2018). The use of polyoxometalate units leads to open network metal–organic frameworks (MOFs). Polyoxometalate can either be a part of the MOF skeleton or encapsulated within the pores. Since revising all different types of polyoxometalate-based MOFs is beyond this review's scope, limited information on the synthesis of polyoxometalate-based MOFs has been presented. A typical feature of polyoxometalate is the abundance of oxygen in its structure, acting as electron donors (Lewis base). At the same time, the transition metal ions provide empty orbitals to accept electrons, behaving as Lewis acids. Consequently, these structural assemblies can participate in redox reactions (Wang and Yang 2015). polyoxometalates have been used for a wide variety of applications due to their attractive redox behavior, tunable acid–base properties, and resistance to oxidative decomposition, sensitivity toward light and electricity, and high thermal stability. However, their high water solubility hinders their use as heterogeneous photocatalysts. The development of polyoxometalate-MOF is an attractive proposal to enhance its water stability (Chen and Zhang 2019). Zhao et al. (2018) reported two stable 3D Keggin-type polyoxometalate-based $[Cu(I)_{12}(trz)_8]$ MOFs for photocatalysis. Two different polyoxometalates, $[\alpha\text{-}SiW_{12}O_{40}]^{4-}$ and $[\alpha\text{-}PW_{12}O_{40}]^{3-}$ used in the fabrication of MOFs resulted in different physical properties of the MOF. The

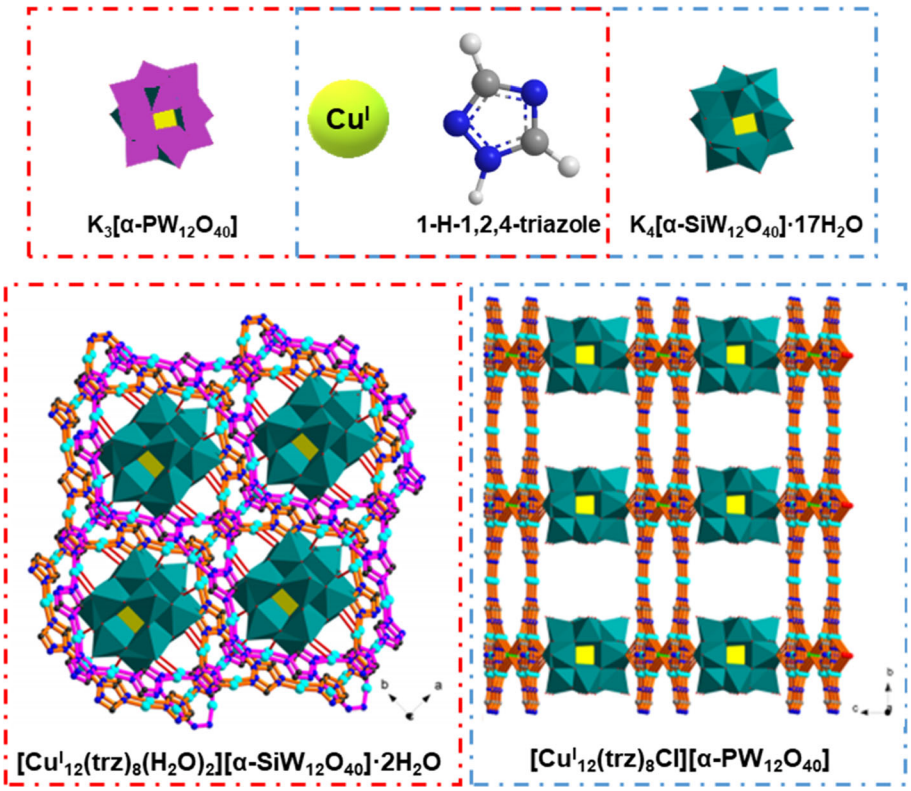

Fig. 5 Formation processes of 3D Keggin-type polyoxometalate-based metal–organic frameworks using copper(I), 1-H-1,2,4-triazole with different polyoxometalate structures $[\alpha\text{-}SiW_{12}O_{40}]^{4-}$ and $[\alpha\text{-}PW_{12}O_{40}]^{3-}$ (Zhao et al. 2018)

$[Cu(I)_{12}(trz)_8(H_2O)_2][\alpha\text{-}SiW_{12}O_{40}]\cdot 2H_2O$ was prepared by a hydrothermal approach using $Cu(NO_3)_2\cdot 3H_2O$, 1-H-1,2,4-triazole (trz), $K_4[\alpha\text{-}SiW_{12}O_{40}]\cdot 17H_2O$, and isonicotinic acid as a mixture in distilled water. The mixture was transferred into a Teflon-lined stainless-steel autoclave and heated for 72 h at 170 °C, yielding a yellow solid as the final product. The other polyoxometalate-MOF, $[Cu(I)_{12}(trz)_8Cl][\alpha\text{-}PW_{12}O_{40}]$ was developed following the same experimental procedure by replacing the Si-W–O Keggin polyoxometalate with $K_3[\alpha\text{-}PW_{12}O_{40}]$, resulting in dark brown crystals (Fig. 5). Despite structural differences between the MOFs, both presented relative narrow band-gap, resulting in efficient photocatalytic degradation of rhodamine B under visible light. Cu(I)-trz units connected with polyoxometalates promoted electron transfer between polyoxometalates by reducing the deactivation of excited states. Thus, introducing polyoxometalates into MOFs promotes visible-light response and separation of photo-generated electron–hole pairs.

Polyoxometalate may be used for improving the water stability of some MOFs, besides boosting photocatalytic activity. Chen et al. (2018) develop a cage-like Cu-MOF with $H_4SiW_{12}O_{40}$ as the polyoxometalate accommodated in cages of the Cu-MOF. The polyoxometalate-MOF $([(Cu_4Cl)(4\text{-}(4\text{-carboxyphenyl})\text{-}1,2,4\text{-triazole}))_4].(HSiW_{12}O_{40}).31H_2O$ was prepared by a solvothermal reaction. The 4-(4-carboxyphenyl)-1,2,4-triazole), $CuCl_2.3H_2O$, and $H_4SiW_{12}O_{40}$ were dispersed in a water/CH_3CN mixture and heated at 120 °C for 48 h in a Teflon reactor, yielding green strip crystals as the final product. The Keggin-type polyoxometalate was introduced in the octahedral cages, resulting in a 3D arrangement of the SiW_{12} in the cages sharing $[Cu_4Cl]^{7+}$ vertices. The polyoxometalate-modified MOF was water-stable with an excellent photocatalytic response (Chen et al. 2018a). Zhong et al. (2018) proposed a similar approach to obtain robust and improved catalytic material by one-pot encapsulation of the $H_3PW_{12}O_{40}\cdot nH_2O$ Keggin-type polyoxometalate in the HKUST-1, $[Cu_2(BTC)_{4/3}(H_2O)_2]_6[HPW_{12}O_{40}]$, named as PW@HKUST-1 by employing a novel liquid-assisted grinding method. The synthetic procedure consisted of dissolving the $Cu(NO_3)_2\text{-}3H_2O$ and $H_3PW_{12}O_{40}$ at pH 4. The solvent was evaporated, and the powder was mixed with 1,3,5-benzene tricarboxylic acid and ethanol for 5 min in an agate mortar, resulting in a blue solid. The catalytic activity of the PW@HKUST-1 was found to be considerably higher than of the polyoxometalate and HKUST-1 (Zhong et al. 2018).

Physicochemical properties of metal–organic frameworks

Metal–organic frameworks (MOFs) are characterized by ultra-high surface area, tunable pore size and shape, and chemical functionality. Physicochemical properties can be tuned by changing the metallic nodes and the organic

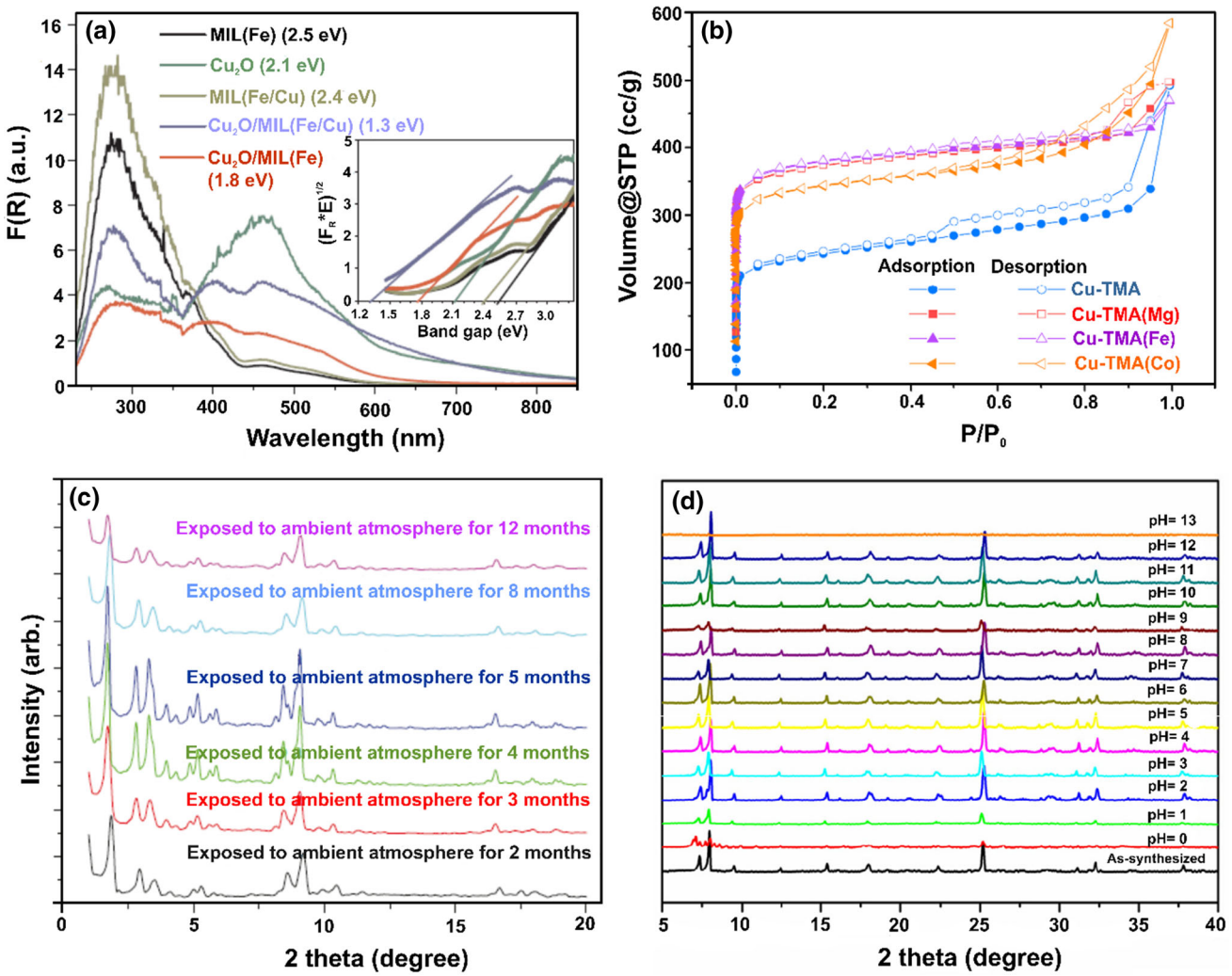

Fig. 6 **a** Ultraviolet–visible diffuse reflectance spectroscopy and optical band gap energy estimation in the inset (Zhong et al. 2020), **b** nitrogen sorption isotherms at 77 K (He et al. 2020), **c** X-ray diffraction (XRD) patterns of MIL-101 exposed to the ambient atmosphere for several months (Du et al. 2019), **d** X-ray diffraction patterns for $[(Cu_4Cl)(CPT)_4]\cdot(HSiW_{12}O_{40})\cdot 31H_2O$ soaked in water with pH 0–13 for one day (Chen et al. 2018a) (Reprinted with permission from Elsevier)

linkers constituting the MOF. The great variety of possible nodes-organic linkers combinations make these coordination polymers very suitable platforms for multiple applications such as drug delivery/release, gas storage, separation, and heterogeneous catalysis (Wang et al. 2015; Chen et al. 2020a). The MOF surface area, pore size, water stability, and bandgap are vital parameters for improving the material's photocatalytic response. On the same note, for the removal of gaseous pollutants, the MOF should have a large surface area, suitable pore size, thermal and catalytic stability, and ability to withstand exposure to the harsh environment.

Photodegradation is a surface phenomenon where the reactive species generated by photocatalytic reactions attack the pollutants adsorbed on the surface. Hence, the greater the surface area, the higher the adsorption capacity, favoring the photodegradation of the pollutant. Pore size and volume are also of keen importance for adsorption and photocatalytic degradation. A wider pore size expedites the entrance of the targeted pollutant near to the photoactive sites, increasing the material performance. Various reports suggest that using mixed metal ions as the inorganic building units of MOFs provides a way to tune their acid–base and redox properties. Specifically, the secondary metal sites' presence may improve the surface area of the resulting bimetallic MOFs due to the expansion of unit cells (Fig. 6b). Moreover, the bimetallic MOF's pore volume increases with the atomic radii of the secondary metal ion (He et al. 2020).

Light-harvesting ability in the solar spectrum is another fundamental property of a photocatalyst. From a practical point of view, organic linkers should absorb light in the

visible region. MOF-based materials aim to facilitate easy electron transportation and increase the lifetime of photogenerated electron–hole pairs (Abazari and Mahjoub 2018). The light absorption in the visible region is marked by a low bandgap value ($E_g \sim$ 1.6–3.2 eV) of the photocatalyst (Fig. 6a). Bimetallic and semiconductor metal oxides-based MOF, as well as their composites, can be used in the photodegradation of organic pollutants under the solar spectrum (Chen et al. 2020b). Another commonly used strategy for improving visible-light response is the use of conjugated organic or amine-functionalized linkers, which improve the electronic transference and the formation of charge carriers (Gómez-Avilés et al. 2019).

The structural stability of MOFs under strong acidic/alkaline conditions is of paramount importance to achieve the commercialization of MOFs for different environmental applications. The best approach to determine the structural stability is to expose the material to harsh conditions such as solutions of varying pH and then analyze either the solution phase for possible leaching of organic linkers/metal nodes or MOF structure by X-ray diffraction. An insignificant variation in the X-ray diffraction pattern of the MOF before and after being exposed to basic or acid media ensures high structural stability of the material (Fig. 6d) (Chen et al. 2018a). The removal of gaseous pollutants also requires MOF to be highly stable in the atmospheric conditions as structural instability leads to pore blockage and decrease in surface area, severely affecting the diffusion of gaseous pollutants inside the pores. Prolonged exposure of MOFs to ambient atmosphere could lower the stability by oxidizing the metal nodes (Fig. 6c) (Du et al. 2019).

Metal–organic frameworks for wastewater remediation

Without any pretreatment, industrial and municipal wastewaters are being dumped into clean water sources, adding all sorts of toxic organic chemicals. Metal–organic frameworks (MOFs) are in the limelight as an effective alternative to reduce the impact of these pollutants on human health by capturing and degrading them into non-toxic products. These coordination polymers have been employed in the design and development of novel adsorbents and photocatalysts to remove organic pollutants. In the following subsections, a general overview of the most updated reports on MOFs for wastewater remediation has been presented, which are primarily focused on the elimination of organic pollutants. Table 1 highlights the degradation performance of MOF-based photocatalysts for organic dyes, pharmaceutical drugs, pesticides, and phenolic compounds.

Degradation of organic dyes

The majority of industrial wastewater is composed of dyes, toxic organic compounds, and colored substances. It is estimated that around 15% of the global dye production (nearly 800,000 tons per year) is directly discharged into water sources, without any pretreatment (Sarkar et al. 2017; Tarkwa et al. 2019). Consumer goods industries like textile, leather, paper and pulp, plastic, electroplating, food, medicine, and cosmetics are majorly responsible for dye pollution (Gupta et al. 2005). There are several dye classifications, including azo dyes, anthraquinone, indigoide, triphenylmethyl, and sulfur and phthalocyanine derivatives (Martínez-Huitle and Brillas 2009). As much as 70% of the synthetic dyes used in the industrial activities are azo dyes (those with azo-functional group "–N=N–") (Gupta et al. 2020c). Organic dyes present complex and diverse chemical structures that put them in the category of persistent pollutants (the hydrolysis half-life of reactive blue 19 is 46 years) under ambient environmental conditions (Hao et al. 2000). Also, it has been reported that the textile wastewaters exhibit low dissolved oxygen, indicating that the organic dyes are non-biodegradable compounds (Hao et al. 2000).

Organic dyes in water can have toxic effects on human health, such as allergic reactions, dermatitis, nausea, and mental disorders. Many of the azo dyes have genotoxic, mutagenic, and carcinogenic effects on living beings. Moreover, they can react with disinfectants present in the water yielding hazardous by-products (Chung 2016; Gupta et al. 2020c). The presence of colored substances in water bodies leads to lower penetration of sunlight through the water. Consequently, a decreased photosynthesis rate and low dissolved oxygen levels are typical of dye polluted waters, interfering with the life cycle of aquatic life forms (Hassan and Carr 2018). A representative number of the commonly used dyes are highly soluble in water, hindering the removal of these pollutants by conventional methods. Consequently, the removal of dyes from water has become a significant challenge for stakeholders. The most employed strategies for dealing with colored waters are adsorption and degradation. Various porous materials have been investigated to remove dyes from aqueous media such as metal oxides (Gupta et al. 2020b), clays (Gil et al. 2011), mesoporous silica (Jadhav et al. 2019), activated carbon (Demirbas 2009), and graphene oxides (Gupta et al. 2020a). The popularity of metal–organic frameworks (MOFs) for the removal of organic dyes is based on their large surface area, high porosity, ability to interact with organic dyes via electrostatic interactions, and metal sites for the catalytic degradation of adsorbed dye molecules.

Table 1 Transition metal-based metal–organic frameworks as catalysts for the degradation of organic pollutants

Photocatalyst	Pollutant	Experimental conditions				Oxidizing system	Efficiency (TOC) (%)	References
		pH	Time (min)	Dostt age (g L^{-1})	C (mg L^{-1})			
MIL-53 (Fe)	Rhodamine B	–	180	0.40	10	H_2O_2/Xe lamp	90 (–)	Liu et al. (2019)
AgI/MIL-53(Fe)	Rhodamine B	–	200	0.30	5	Xe lamp	100 (–)	Han et al. (2018)
CdS@NH_2- MIL-125(Ti)	Rhodamine B	–	120	0.15	180	Xe lamp	97 (–)	Wang et al. (2019b)
BiOBr/NH_2-MIL-125(Ti)	Rhodamine B	–	100	0.20	20	Xe lamp	80 (–)	Zhu et al. (2016)
BiOI@MIL-88A(Fe)@g-C_3N_4	Rhodamine B	–	180	0.10	10	Xe lamp	75 (–)	Khasevani and Gholami (2018)
	Acid blue 92						88 (–)	
CuS/UiO-66	Rhodamine B	–	60	0.15	10	H_2O_2/Xe lamp	90 (–)	Chen et al. (2019a)
	Methyl orange						40 (–)	
1-NO_3-OH·20H_2O	Rhodamine B	–	120	0.40	10	H_2O_2/Xe lamp	92 (–)	Zheng et al. (2018)
Prussian blue	Rhodamine B	–	120	–	7.5	H_2O_2	80 (%)	Liu et al. (2011)
HPU-5	Rhodamine B	–	150	0.07	10	H_2O_2/Hg lamp	99 (–)	Li et al. (2017)
HPU-6	Methyl orange						83 (–)	
	Rhodamine B						78 (–)	
	Methyl orange						31 (–)	
α-Fe_2O_3@UiO-66	methylene blue	–	60	1.00	12.8	Xe lamp	100 (–)	Zhang et al. (2019b)
Fe_3O_4/Cu_3(BTC)$_2$	Methylene blue	4	120	0.6	100	H_2O_2	85 (–)	Sun et al. (2019b)
TiO_2@NH_2-MIL-88B(Fe)	methylene blue	7.0	150	0.20	100	H_2O_2/LED lamp	100 (–)	Li et al. (2018d)
[Mn(3,4-dimethylthieno[2,3-b]thiophene-2,5-dicarboxylic acid)(DMF)]	Methylene blue	–	70	1.00	10	Hg lamp	91 (–)	(Fang et al. (2018)
BiOI/$ZnFe_2O_4$/MIL-88B(Fe)	Methylene blue	–	120	0.10	10	LED	65 (–)	(Khasevani and Gholami (2019b)
	Acid blue 92						73 (–)	
[CoNi(μ_3-bdc)$_2$(μ_2-pyrazine)$_2$]@$CuWO_4$	Methylene blue	–	135	0.10	10	LED	98 (–)	(Ramezanalizadeh and Manteghi (2018)
CuTz-1	Methylene blue	6.5	8	0.60	12	H_2O_2/Xe lamp	100 (–)	(Liu et al. (2018b)
	Methyl orange	6.8	15	0.60	12		98 (–)	
	Rhodamine B	6.6	22	0.60	12		100 (–)	
MIL-100 (Fe)	Basic blue 41	5.0	180	0.04	20	UV-C	100 (–)	(Mahmoodi et al. (2018)
MIL-100(Fe)@MIL-53(Fe)	Methyl orange	7.0	80	0.50	10	H_2O_2/Xe lamp	100 (–)	(Abdpour et al. (2018)
$Cd_{0.5}Zn_{0.5}S$@UIO-66@g-C_3N_4	Methyl orange	–	120	0.20	20	Xe lamp	82 (–)	(Liang et al. (2018b)
Ag_3PO_4/$BiPO_4$@MIL-88B(Fe)@g-C_3N_4	Acid blue 92	–	60	0.10	10	Xe lamp	85 (–)	(Khasevani et al. (2017)
MIL-88A/BiOI	Acid blue 92 methylene blue	–	80	0.10	–	Xe lamp	80 (–)	(Khasevani and Gholami (2019a)
							45 (–)	
MIL-101(Cr)	Remazol black B	7.0	45	0.50	50	UV	100 (–)	Du et al. (2019)
MIL-125-NH_2@Zr	Acetaminophen	7.0	90	0.25	5	Xe lamp	100 (65)	Gómez-Avilés et al. (2019)
MIL-53(Al)-NH_2–Sm_2O_3–ZnO	Amoxicillin	5.0	90	0.30	–	H_2O_2/UV-C	100 (88)	Abazari and Mahjoub Abazari and Mahjoub (2018)

Table 1 (continued)

Photocatalyst	Pollutant	Experimental conditions				Oxidizing system	Efficiency (TOC) (%)	References
		pH	Time (min)	Dostt age (g L^{-1})	C (mg L^{-1})			
MIL-53(Fe)	clofibric acid	3.0	270	0.10	40	H_2O_2/Xe lamp	98 (–)	Gao et al. (2017)
	Carbamazepine						90 (–)	
Fe_2O_3/TiO_2@MIL-101	Diclofenac ciprofloxacin	7.0	350	0.30	17	LED	97 (–)	Tilgner et al. (2018)
	levofloxacin	7.0	350	0.30	18		70 (–)	
		7.0	350	0.30	15		70 (–)	
Siloxane-based Cu-MOF	Doxorrubicin	7.0	20	1.50	30	H_2O_2/Sunlight	100 (–)	Racles et al. (2019)
MIL-100(Fe) @Pd	Doxorubicin theophylline	4.0	150	0.12	20	H_2O_2/Xe lamp	100 (69)	Liang et al. (2015)
							100 (45)	
Ag/AgCl@MIL-88A(Fe)	Ibuprofen	–	210	0.40	10	Xe lamp	100 (91)	Huang et al. (2018)
CdS@MIL-125(Ti)-NH_2	Oxytetracycline	–	120	0.15	180	Xe lamp	98 (–)	Wang et al. (2019b)
Bio-MOF-11-Co	Sulfachloropyradazine	5.5	30	0.05	45	H_2O_2/ peroxydisulfate/ peroxymonosulfate	100 (85)	Azhar et al. (2018)
CUS-MIL-100(Fe)	Sulfamethazine	4.0	180	0.50	–	H_2O_2	98 (52)	Tang and Wang (2018)
MIL-53(Fe)	sulfamethazine	5.8	60	0.20	5	Fe(III)/percarbonate/ LED	90 (55)	Li et al. (2018c)
MIL-88B-Fe@CNT	Sulfamethoxazole	4.0	30	0.10	25	H_2O_2	100 (–)	Zhang et al. (2019a)
Magnetic MIL-100(Fe)	Sulfadiazine	4.0	300	1.00	5	H_2O_2/Xe lamp	90 (–)	Tian et al. (2018)
MIL-53(Fe)-NH_2@g-C_3N_4/PDI	tetracycline	6.0	150	0.40	50	H_2O_2/LED	90 (78)	Li et al. (2019c)
	carbamazepine						78 (–)	
MIL-101(Fe)/TiO_2	Tetracycline	7.0	10	0.80	20	Solar light	93 (–)	He et al. (2019)
MIL-125(Ti)@In_2S_3	tetracycline	5.9	60	0.30	46	Xe lamp	63 (17)	Wang et al. (2016)
UiO-66@Co	Tetracycline	5.4	60	0.20	20	Xe lamp	94 (14)	Cao et al. (2018)
M.MIL-100 (Fe) @ZnO NS	atrazine	2.0	120	0.20	5	H_2O_2/Xe arc lamp	92 (49)	Ahmad et al. (2019)
BiOBr/UiO-66	Atrazine	5.7	–	0.50	5	Xe lamp	88 (–)	Xue et al. (2018)
Fe_3O_4@MOF-2	diazinon	3.0	120	0.70	30	Persulfate/ultrasonic	98 (83)	Sajjadi et al. (2019)
Fe_3O_4-COOH@ZIF-8/ Ag/Ag_3PO_4	Diazinon	7.0	55	0.20	20	W lamp	63 (–)	Naimi Joubani et al. (2020)
UiO-66/g-C_3N_4/Ag(15)	2,4-dichlorophenoxyacetic acid	–	180	0.40	20	H_2O_2/Xe lamp	84 (–)	Feng et al. (2019)
WO_3/MIL-53(Fe)	2,4-dichlorophenoxyacetic acid	2.5	240	0.50	45	Solar light	100 (–)	Oladipo (2018)
α-Fe_2O_3@MIL-101(Cr)@TiO_2	Paraquat	7.0	45	0.20	20	UV lamp	87 (–)	Khodkar et al. (2019)
$AgIO_3$/MIL-53(Fe)	Methyl malathion chlorpyrifos	5.0	60	0.05	20	Sunlight	100 (70)	Oladipo et al. (2018)
							100 (70)	
Cu_2O/MIL(Fe/Cu)	thiacloprid	7.4	18	0.50	80	H_2O_2/Xe lamp	100 (82)	Zhong et al. (2020)
MIL(Fe)/Fe-SPC	Thiamethoxam	5	180	1.00	60	H_2O_2/ultrasonic	100 (95)	Wei et al. (2018)
D-M-Fe	Thiamethoxam	5.0	60	0.50	5	$Na_2S_2O_8$/	50 (–)	Mei et al. (2019)
XY-M-Fe						LED lamp	96 (–)	
30UiO-66/$CdIn_2S_4$	Triclosan	7.1	180	0.50	10	Xe lamp	92 (90)	Bariki et al. (2020)

Table 1 (continued)

Photocatalyst	Pollutant	Experimental conditions				Oxidizing system	Efficiency (TOC) (%)	References
		pH	Time (min)	Dostt age (g L^{-1})	C (mg L^{-1})			
MOF-5	2,6-di-tert-butylphenol	–	180	4.00	40	Hg lamp	92 (–)	Llabrés i Xamena et al. (2007)
Pd@MIL-100(Fe)	Bisphenol A	4.0	240	0.12	20	H_2O_2/Xe lamp	65 (21)	Liang et al. (2015)
H, Zn and Cd (Fe–L)Cl	2-chlorophenol	3.0	80	1.00	40	H_2O_2/Hg lamp	73 (–)	Li et al. (2015a)
Fe_3O_4/MIL-53(Fe)	*p*-nitrophenol	–	150	0.40	10	H_2O_2/halogen tungsten lamp	60 (–)	Zhang et al. (2015)
Cd-Zn TMU-5	phenol	–	120	0.50	50	UV-C	87.6 (–) 78 (–)	Masoomi et al. (2016)
[Zn(5-aminoisophthalic acid)(H_2O)]	phenol	–	140	–	30	Hg lamp	67 (–)	Wang et al. (2017)
[CoNi(μ_3-tp)$_2$(μ_2-pyz)$_2$]/$CuWO_4$	*p*-nitrophenol	–	105	0.20	10	LED visible light	81 (–)	Ramezanalizadeh and Manteghi (2018)
[Zn(BDC)(DMF)]	*p*-nitrophenol	6.0	15	0.50	10	H_2O_2/$NaBH_4$/solar light	97 (–)	Samuel et al. (2018)
MIL-100(Fe)/ZnO	Phenol Bisphenol A	2.0	120	0.20	5	H_2O_2/Xe arc lamp	92 (–) 86 (–)	Ahmad et al. (2019)
Fe_3O_4@GO@MIL-100(Fe)	2,4-dichlorophenol	5.5	100	0.20	50	H_2O_2/Xe lamp	100 (60)	Gong et al. (2019a)
NH_2-MIL-125(Ti)/BiOCl	Bisphenol A	–	240	0.50	10	Xe lamp	65 (–)	Hu et al. (2019)
g-C_3N_4/PDI@NH_2-MIL-53(Fe)	Bisphenol A *p*-nitrophenol tetracycline carbamazepine	–	10 30 60 150	0.40	50	H_2O_2/LED white lamp	100 (–) 100 (–) 90 (–) 78 (–)	Li et al. (2019c)
Pt-UiO-66-NH_2	Phenol	–	300	–		H_2O_2/metal halide lamp	(–) (70)	Chen et al. (2020c)

As discussed in previous sections, most MOFs have limitations in harvesting the entire solar spectrum, which could be resolved by coupling MOF with other semiconductors and sensitizers. Wang et al. (2019b) developed CdS@NH_2-MIL-125(Ti) heterostructure by depositing Ti-MOF over CdS nanorods. The CdS@MOF showed faster rhodamine B degradation under visible light as compared to CdS and MOF. The composite had a strong covalent conjunction from the Cd–Se–Ti bonding interactions, which resulted in a lower recombination rate of photogenerated electron–hole pairs and accelerated charge carrier transport (Wang et al. 2019b). Zhua et al. (2016) fabricated BiOBr/NH_2-MIL-125(Ti) composite for the degradation of rhodamine B under visible-light illumination. A low recombination rate of charge carriers and Ti^{3+}–Ti^{4+} intervalence electron transfer led to the formation of $O_2^{\cdot-}$ over reduced Ti^{3+} (formed by the reduction of Ti^{4+} in the Ti–O cluster of MOF) (Zhu et al. 2016). Han et al. (2018) fabricated AgI/MIL-53(Fe) composite for complete visible-light-assisted degradation of rhodamine B within 180 min. The composite showed a higher rate constant (0.030 min^{-1}) as compared to AgI (0.012 min^{-1}) and MIL-53(Fe) (0.010 min^{-1}). The introduction of AgI in MOF significantly inhibited the recombination rate of the photogenerated electron–hole pairs (Han et al. 2018). α-Fe_2O_3 nanoparticles were strategically confined in the pores of UiO-66 to develop α-Fe_2O_3@UiO-66 heterostructure. Under visible light, the photocatalyst was able to degrade ~ 100% of dye within 50 min. The growth of α-Fe_2O_3 was confined to the pores UiO-66 and

formed nanoclusters with a diameter of < 2 nm. The electron–hole transport distances shortened in the nanoclusters, which led to the transportation of electrons from bulk to the surface. A higher photocurrent intensity of α-Fe_2O_3@UiO-66 heterostructure under visible-light irradiation confirmed the phenomenon. The increased surface reaction sites and shortened carrier transport distance improved the photocatalytic activity of the heterostructure (Zhang et al. 2019b). Malik and Nath (2019) reported photocatalytic degradation of methylene blue dye over CdS@ZIF-8 in near-neutral conditions. The by-products generated during the photodegradation of methylene blue dye were analyzed by gas chromatography (GC)-mass spectrometry (MS). The analysis showed a small presence of intermediates after 2 h of irradiation, probably due to faster mineralization. Four major peaks at m/z ∼ 283, 256, 167, and 125 were due to methylene blue dye, 3-amino-7-(dimethylamino)phenothiazin-5-ium, N-(3,4-dihydroxyphenyl)-N-methylformamide, and 4-aminobenzene-1,2-diol, respectively. Thus, it was conclusive that reactive oxygen species ($^{\cdot}OH$, $^{\cdot}O_2^-$) attacked N–CH_3 bonds leading to the oxidation of methyl groups to HCHO or HCOOH. The $^{\cdot}OH$ radicals cleaved the central heterocyclic ring by attacking C–S and C–N bonds for complete mineralization (Malik and Nath 2019).

Abdpour et al. (2018) introduced a hybrid photocatalyst with MIL-100(Fe) and MIL-53(Fe) as *p*-type and *n*-type semiconductor materials, respectively. Decorating MIL-100(Fe) on the surface of MIL-53(Fe) resulted in electrostatic self-assembly of positive charged MIL-53 (Fe) and the negative charged MIL-100(Fe). This electrostatic interaction led to the development of a large heterojunction space, which facilitated an easy electron–hole transfer between MIL-53(Fe) and MIL-100(Fe) and increased the lifetime of the electron–hole pairs. This *p*–*n* heterojunction led to complete degradation of methyl orange within 80 min of visible-light illumination at neutral pH (Abdpour et al. 2018). A BiOI/$ZnFe_2O_4$/MIL-88B(Fe) ternary nanocomposite with *n*-*p*-*n* heterojunction was fabricated by the deposition of BiOI (*p*-type) and $ZnFe_2O_4$ (*n*-type) over MIL-88B(Fe) (*n*-type). The nanocomposite had a better dye degradation efficiency under visible light than the constituent photocatalysts. The electron-capturing through Fe-oxo clusters of MOF by converting Fe^{3+} to Fe^{2+} and transporting properties of MOF coupled with improved visible-light response and charge carrier transfer rate of BiOI/$ZnFe_2O_4$ led to an excellent photo-induced electron–hole pairs separation in the ternary composite (Khasevani and Gholami 2019b). Khasevani et al. (2017) successfully fabricated a novel quaternary Ag_3PO_4/$BiPO_4$@MIL-88B(Fe)@g-C_3N_4 nanocomposite. The nanocomposite showed low charge transfer resistance and superior charge separation efficiency, which was reflected in the acid blue 92 degradation under visible-light irradiation. Moreover, an excellent visible-light-harvesting ability, enhanced transportation, and mobility of photogenerated electrons in the specific π-conjugated networks of MIL-88B(Fe)@g-C_3N_4 had a unique role to play in the generation of reactive oxidation species (Khasevani et al. 2017).

Efforts in developing multi-step approaches have not been reflected in their photocatalytic efficiency. Most of these nanocomposites are far from harvesting the entire solar spectrum. For harnessing the visible part of the solar light, Liu et al. (2018b) developed a novel CuTz-1 for rapid photocatalytic degradation of multiple cationic, anionic, azo, and triarylmethane dyes in the presence of H_2O_2. CuTz-1 needed only 8, 15, and 22 min to completely degrade methyl orange, rhodamine B, and methylene blue dye. The faster degradation kinetics of the MOF could be linked to the predominance of Fenton-like reaction between Cu^+ and H_2O_2, which generated $^{\cdot}OH$ radicals for the degradation process. The effectiveness of the MOF was demonstrated by degrading a mixed solution of all four dyes under Xenon lamp irradiation and natural sunlight, where complete degradation was achieved within 21 and 80 min, respectively (Liu et al. 2018b).

Degradation of pharmaceutical drugs

In recent decades, thousands of tons of pharmaceutical drugs have been consumed, which led to the presence of more than 150 active pharmaceutical ingredients in sewage effluents and surface waters (Jones et al. 2005; Rayaroth et al. 2016). A large amount of these chemicals is excreted un-metabolized or as active metabolites, veto the removal processes in wastewater treatment plants, and enter the environment. Also, pharmaceutical products have a long half-life, leading to their accumulation beyond detectable limits and ultimately reaching life cycles. Some of them can have high environmental persistence longer than a year (Patel et al. 2019). The toxicity level of these compounds is estimated at trace level (ppb) for aquatic flora. These chemicals can also produce acute or chronic effects in humans. More accurately, estrogens hormones can induce endocrine disorders, which may restrict reproductive and sexual development (Prosser and Sibley 2015; Patel et al. 2019). Thus, there is a necessity to find effective methods for their complete removal from water even at trace levels. Catalytic degradation is one of the promising methodologies with improved treatment of persistent pollutants. The search for a suitable catalytic system is a debatable issue as each system is known for its pros and cons on the terms of affordability, ease of operation, and the formation of by-products. The ease of operation and possible mineralization make photocatalysis a viable option.

Gao et al. (2017) reported MIL-53(Fe) for the removal of clofibric acid and carbamazepine from deionized water, municipal wastewater, and river water. These compounds are drugs used to treat high blood lipids and epilepsy, respectively, but inhibit metabolism, reproduction, and embryonic development. The metal–organic framework (MOF)/H_2O_2/visible system degraded 98.2 and 90.1% (deionized water), 94 and 88% (river water), and 71 and 86% (municipal wastewater) of clofibric acid and carbamazepine, respectively, in 270 min. Apart from slow kinetics and requirement of a very low operational pH of 3, the process led to the formation of humic acid-like and fulvic acid-like organic matter as by-products, which require additional treatment process for complete removal from water (Gao et al. 2017). Fe-MOF with Fe(II)/Fe(III) coordinatively unsaturated centers, CUS-MIL-100(Fe), was developed for sulfamethazine degradation. The MOF could degrade 100% of sulfamethazine with 52% mineralization in 180 min using the heterogeneous Fenton reaction (Tang and Wang 2018). Fenton-like process and photocatalysis are better systems for the rapid mineralization of pollutants. MIL-53(Fe) in a modified visible/MIL-53(Fe)/Fe(III)/percarbonate system degraded 90% of sulfamethazine with 55% mineralization within 60 min. It was due to the significant contribution of Fenton reactions where adsorbed Fe(III) on MIL-53(Fe) reduced to Fe(II) by capturing photogenerated electron (Li et al. 2018c).

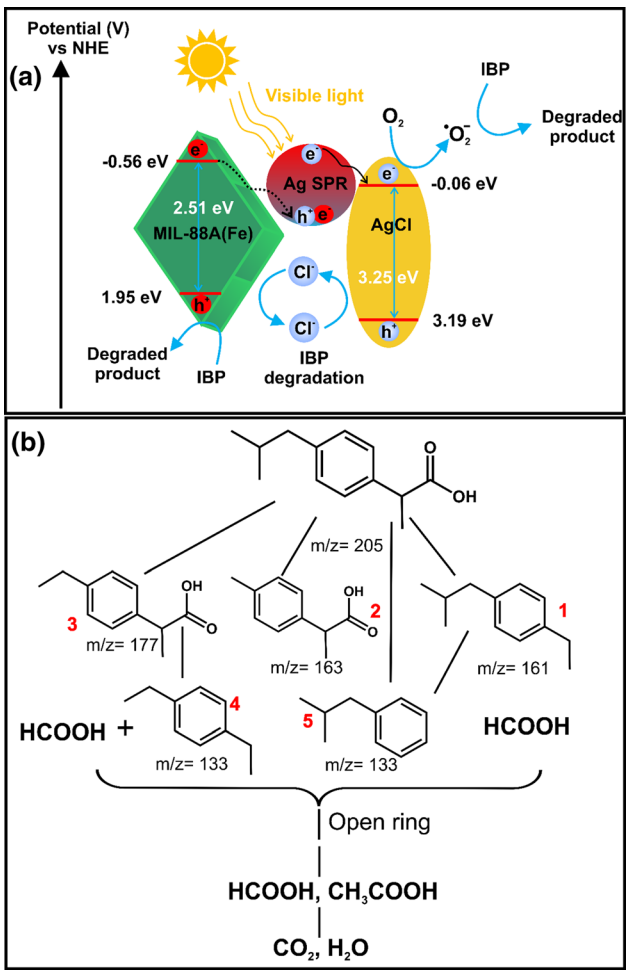

Fig. 7 **a** Photodegradation of ibuprofen over Ag/AgCl@MIL-88A(Fe) nanocomposite under visible-light irradiation, **b** proposed photocatalytic degradation pathway of ibuprofen with the presence of ACMA-2 nanocomposite (Huang et al. 2018)

MIL-125-NH_2@Zr was fabricated for the photocatalytic degradation of acetaminophen under solar irradiation. Acetaminophen is a popular antipyretic and analgesic drug and has been detected in urban wastewaters. The doping of Ti-MOF with Zr provided energy levels below the conduction band or above the valence band, which acted as new states for electron transfer and decreased the possibility of charge recombination. These improved optical properties led to the complete degradation of acetaminophen with 65% mineralization in 180 min. Even after 180 min of irradiation, no aromatic intermediate was detected, and only organic acids, such as maleic, malonic, and oxalic acids were observed, which showed the extraordinary mineralization capability of the bimetallic MOF (Gómez-Avilés et al. 2019). Ag/AgCl is a composite photocatalyst known for a high surface plasmon resonance, enhancing the visible-light-harvesting ability. Huang et al. (2018) integrated Ag/AgCl with MIL-88A(Fe) to form Ag/AgCl@MIL-88A(Fe) nanocomposite for ibuprofen (popular nonsteroidal anti-inflammatory drug) degradation. The nanocomposite was faster than its constituents, illustrating that Ag/AgCl incorporation to MOFs is an excellent approach in harnessing visible light (Fig. 7a). The intermediates and end-products of ibuprofen degradation were probed by ion chromatography (IC) and liquid chromatography (LC)-MS–MS. The ion chromatography analysis confirmed the formation of formic and acetic acid as the end-products where the concentration of both acids increased with the irradiation time. The ibuprofen degradation was initiated by the cleaving of the alkyl side chain (forming 2 and 3 as intermediates), decarboxylation (forming 1 as intermediate), or both at the same time (forming 4 and 5 as intermediates). Since C–C bonds in aliphatic side chains are less stable than C=C bonds in aromatic rings, these bonds are cleaved first by the reactive species, which is followed by ring-opening and complete mineralization of ibuprofen (Fig. 7b) (Huang et al. 2018).

Degradation of pesticides

The use of pesticides represents a widespread strategy to control the growth of unwanted plants and animals to safeguard agricultural production. More than 5.5 million tons of pesticides are released every year into the

environment (Yang et al. 2019a; Oladipo et al. 2020; Pirsaheb and Moradi 2020). Herbicides are considered as the principal pesticide (∼ 45%), followed by insecticides, fungicides, and bactericides (Mahour et al. 2014; Rawtani et al. 2018). Human exposure to pesticides causes carcinogenicity, neurotoxicity, reproductive toxicity, and metabolic toxicity (Oladipo et al. 2018; Khodkar et al. 2019). Also, prolonged exposure to these chemicals can significantly enhance the frequency of chromosomal aberrations, which could result in a higher risk of blood cell mutations (Oladipo 2018; Khodkar et al. 2019). Considering their high toxicity, persistence nature, and bio-accumulation potentials, the United Nations Environment Programme Governing Council and the United States Environmental Protection Agency (USEPA) classified some pesticides as persistent organic pollutants (Mahour et al. 2014; Matthies et al. 2016). Therefore, complete mineralization (conversion into less harmful compounds) for these pollutants is mandatory. As alternatives to the commonly used conventional approaches for pesticide treatment, advanced oxidation processes are particularly attractive because they can mineralize highly toxic and hazardous organic pollutants. Transition metal-based metal–organic frameworks (MOFs) have shown efficient catalytic properties and good stability for advanced oxidation processes. This subsection presents a comprehensive overview of the recent progress in utilizing MOFs for pesticide degradation from wastewater.

Zhong et al. (2020) designed Cu_2O/MIL(Fe/Cu) composite by growing Cu_2O on MIL-100(Fe) as a photo-Fenton catalyst for the degradation of thiacloprid (pesticide banned for its carcinogenicity and reproductive toxicity). Cu_2O onto the MOF surface was introduced to improve the visible-light absorption, leading to an increased catalytic rate for pesticide degradation as compared to constituent photocatalysts. After MOF modification, the charge transfers between copper oxide and MIL(Fe/Cu) improved via Cu bridges. A reduction in bandgap from 2.5 to 1.3 eV was observed, which increased the Fe^{2+}/Fe^{3+} redox reaction. Cu_2O/MIL(Fe/Cu) achieved 100% of thiacloprid

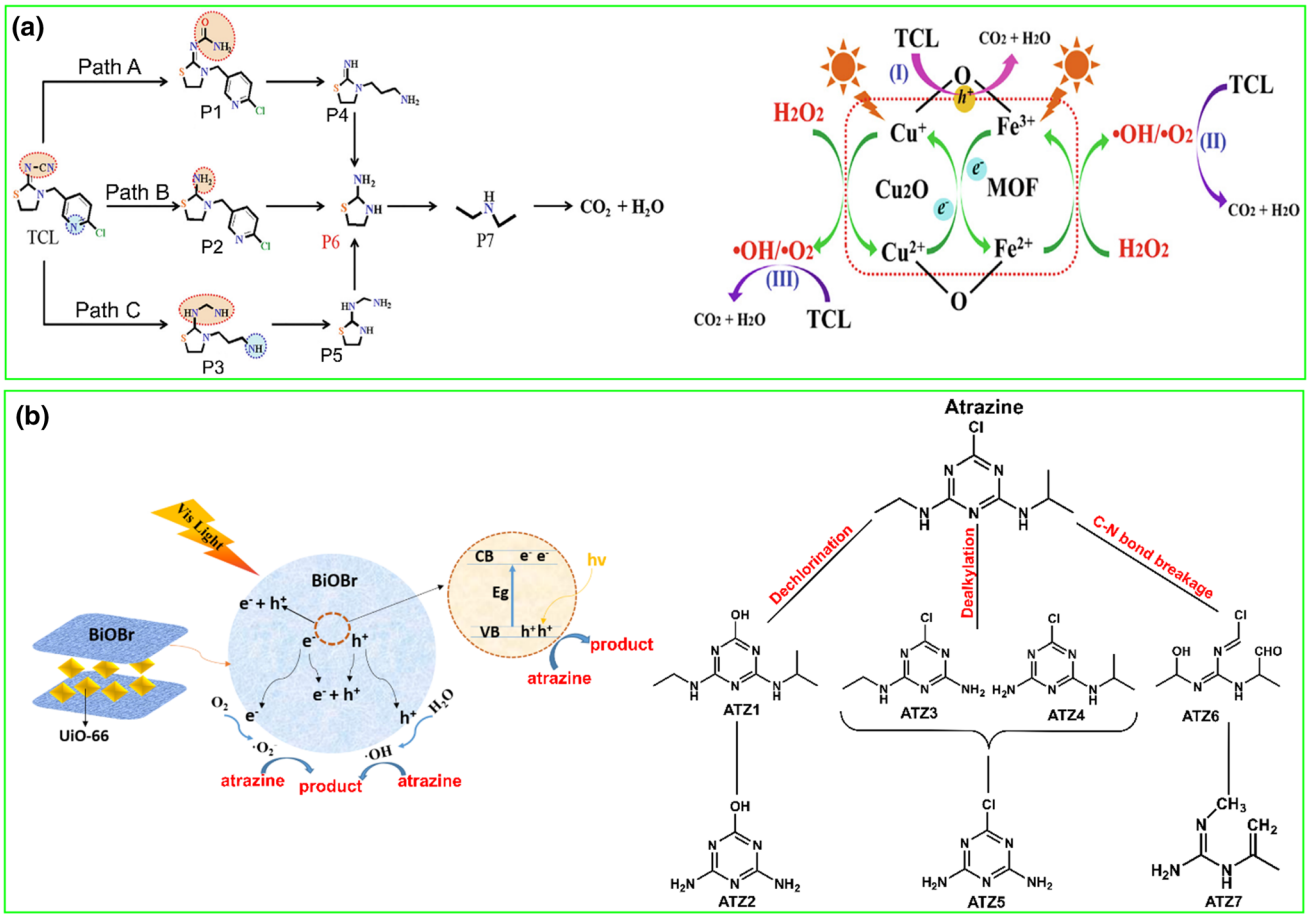

Fig. 8 **a** Photo-Fenton catalytic thiacloprid degradation pathway from the resulting intermediates. The possible reaction mechanism for photo-Fenton degradation of thiacloprid employing Cu_2O/MIL(Fe/Cu) (Reprinted with permission from (Zhong et al. 2020), **b** Interaction mechanism for photo-Fenton degradation of atrazine employing BiOBr/UiO-66. Degradation steps from the resulting intermediates in atrazine degradation (Reprinted with permission from (Xue et al. 2018))

degradation in 18 min, with 82.3% of mineralization after 80 min. Density functional theory (DFT) study corroborated that the amount of Cu on the modified MOF could enhance electron transition and photosensitivity. Under UV/visible-light irradiation, the photogenerated e^- drove Fe^{3+}/Fe^{2+} and Cu^{2+}/Cu^+ redox reactions. The holes and $^{\cdot}OH/O_2^{\cdot-}$ radicals (from H_2O_2) were responsible for the photocatalytic degradation of pesticides. During the process, reactive species ($^{\cdot}OH$, $O_2^{\cdot-}$) attacked the cyanoimino group (–CN), followed by the cleaving of the heterocyclic ring (Fig. 8a) (Zhong et al. 2020).

The pore size in MOF is an essential factor in controlling the catalytic process as pores of appropriate sizes allow the incoming and outgoing molecules in the cavities, which could help maintain the active site density. The microporous MOFs can adsorb small molecules; meanwhile, mesoporous MOF composites with open cavities provide sites for high catalytic activity. M.MIL-100(Fe)@ZnO nanospheres were used for the photocatalytic degradation of atrazine. M.MIL-100 (Fe)@ZnO nanospheres showed a 92% degradation and 49% mineralization of atrazine within 120 min. Improved molecular diffusion through mesopores in the modified MOF favored the process, which was not observed in the microporous MIL-100(Fe). Also, ZnO nanospheres incorporated in the MOF pores improved the charged separation efficiency by lowering the charge recombination rate of MIL-100(Fe) (Ahmad et al. 2019). Xue et al. (2018) evaluated the photocatalytic response of BiOBr/UiO-66 MOF for atrazine degradation. The modified MOF degraded atrazine with an insignificant loss in the activity after four cycles. The presence of competing impurities and anions in mineral water, tap water, and river water lowered the atrazine degradation performance. The degradation process is inhibited when anions are presented in the wastewater, as anions like nitrate and bicarbonate are powerful radical scavengers. The $^{\cdot}OH$, $O_2^{\cdot-}$, and h^+ are the reactive species involved in the atrazine degradation process over BiOBr/UiO-66. The generated radicals attacked atrazine molecules leading to dechlorination, dealkylation, and C–N bond dissociation (Fig. 8b) (Xue et al. 2018). A novel UiO-66/$CdIn_2S_4$ heterojunction nanocomposite was developed to mineralize triclosan from wastewater. Modified MOF with $CdIn_2S_4$ had a lower charge recombination rate than parent MOF, which enhanced the mineralization efficiency of the modified material. The nanocomposite showed six times higher efficiency than $CdIn_2S_4$ with 90% mineralization after 180 min. The main reactive species present in the degradation process were e^-, $O_2^{\cdot-}$, h^+, and $^{\cdot}OH$, which were important for pesticide mineralization. The nanocomposite maintained high photocatalytic activity even after four cycles (Bariki et al. 2020). Thus, MOF-based composites are potential photocatalysts for the remediation of pesticides from wastewater.

Degradation of phenolic compounds

Phenols are organic compounds commonly present in wastewaters from oil refineries, petrochemical, pharmaceuticals, paper, textile, and food industries (Farzaneh et al. 2010; Martínková et al. 2016; Villegas et al. 2016). The United States Environmental Protection Agency has designated phenolic compounds as priority pollutants. Though lethal effects in humans are not documented, humans exposed to phenol (> 1 mg L^{-1}) in drinking water could cause skin rashes, irregular breathing, muscle weakness, weight loss, or gastrointestinal symptoms such as diarrhea and nausea (Mohammadi et al. 2015; Villegas et al. 2016). Heterogeneous photocatalysts could harness solar energy for the in situ generation of reactive species ($^{\cdot}OH$, $O_2^{\cdot-}$), which are capable of mineralizing phenolic contaminants even at low concentrations (Chun et al. 2000; Ahmed et al. 2010).

Garcia's research group was one of the pioneers in proposing the use of metal–organic frameworks (MOFs) as photocatalysts for the degradation of pollutants (Alvaro et al. 2007; Llabrés i Xamena et al. 2007). The organic linkers are thought to behave as light-absorbing chromophores able to harvest photons from a wide region of the solar spectrum, while the metal ions in the scaffold are responsible for the photocatalytic activity. MOF-5 exhibited similar photocatalytic activity as commercial TiO_2 P25 and ZnO when comparing the moles of phenol degraded per metal ion in the material. This comparison originated from the fact that terephthalic units in MOF-5 are thought to be inactive (Alvaro et al. 2007). Additionally, a reverse shape selectivity (*i.e.,* large molecules are degraded faster than small molecules) during the photocatalytic degradation of phenol and 2,6-di-*tert*-butylphenol using MOF-5 was reported (Llabrés i Xamena et al. 2007). This characteristic behavior was reciprocated by Wang et al. (2017) during photocatalytic degradation of phenol using MOFs obtained with transition metals (M=Co, Zn, Ni, Cd) as nodes and 5-aminoisophthalic acid as the organic linker. The large pore size of the framework (Zn > Cd > Co > Ni) disfavored the photocatalytic degradation of phenol, indicating that small pore size is needed to grasp and further degrade the phenol molecules. Also, solubility was proposed to play an important role during the photocatalytic degradation of phenol, while [ZnL(H_2O)] and [CdL(H_2O)H_2O were insoluble, [CoL(H_2O)] was partially soluble, and [Ni-$(HL)_2(H_2O)_2$] was completely soluble in water, which may have led to the homogeneous Fenton reaction (Wang et al. 2017).

The photocatalytic activity of MOF can be enhanced by controlling the specific surface area. Masoomi et al. (2016) improve the photocatalytic degradation of phenol under UV/visible light by enhancing the specific surface area of TMU-5 by incorporating a varying proportion of Cd^{2+} ions (Masoomi et al. 2016). A close relationship between specific surface area and photocatalytic degradation of 2-chlorophenol has been reported over three MOFs composed of dicarboxyl-functionalized Fe(III)-salen complexes and Zn and Cd nodes. The highest photocatalytic degradation rate was recorded over Zn(Fe–L)Cl. It is assumed that the higher the specific surface area, the more exposed are the metal centers of the framework for interaction and photocatalytic activity (Li et al. 2015a). The photocatalytic degradation of other phenolic compounds has also been performed using MOF. [Zn(BDC)(DMF)] photocatalyst has been reported to degrade 97% of *p*-nitrophenol under 15 min of solar illumination. Apart from MOF being highly reusable for photocatalytic degradation of *p*-nitrophenol, the possible reduction of *p*-nitrophenol into *p*-aminophenol over [Zn(BDC)(DMF)] was an important and promising process for the transformation of a pollutant into a valuable chemical for the preparation of drugs (Samuel et al. 2018). There is a common agreement regarding the mechanism followed during the degradation of phenolic compounds. The highly reactive $^{\cdot}OH$ radicals are considered as the main species involved in the photocatalytic reaction. These are generated in situ by direct oxidation of hydroxyl ions or water molecules (Li et al. 2015a; Wu et al. 2015; Masoomi et al. 2016; Gong et al. 2019a) or by H_2O_2 reduction (Liang et al. 2015; Zhang et al. 2015; Khandan et al. 2018; Samuel et al. 2018; Ahmad et al. 2019; Li et al. 2019c). In some research works, $O_2^{\cdot-}$ radicals are another reactive species involved in the photodegradation mechanism formed by photogenerated electron transfer to adsorbed oxygen molecules (Alvaro et al. 2007; Masoomi et al. 2016; Gong et al. 2019a; Hu et al. 2019).

The formation of composites is a widely employed strategy to improve the performance of the MOF. The mechanism responsible for performance improvement depends on the type of material coupled with the photocatalyst. Liang et al. (2015) incorporated palladium particles in MIL-100(Fe) to form Pd@MIL-100(Fe). Deposition of Pd improved the visible-light-harvesting ability of MOF and increased the separation of charge carriers, avoiding recombination of electron–hole pairs in the photocatalyst. In this way, a 65% degradation and 20% mineralization of bisphenol A were possible in 240 min under visible light (Liang et al. 2015). Likewise, platinum particles were employed to improve the transfer of photogenerated electrons to H_2O_2 in Pt-UiO-66-NH_2 MOF and boost phenol degradation (Chen et al. 2020c). The coupling of MOF with magnetic ferrite nanoparticles is another viable strategy to improve the photocatalytic activity, coupled with the easy recovery of the MOF from reaction media. Magnetic Fe_3O_4/MIL-53(Fe) nanocomposite was fabricated by the solvothermal method (Zhang et al. 2015). Improved visible-light-induced degradation of *p*-nitrophenol was observed as compared to conventional metal oxides. Iron oxides are also known for improving the performance by a photo-Fenton coupled process. Gong et al. (2019a) reported the development of Fe_3O_4@-GO@MIL-100(Fe) composites with a large surface area of 1048.1 $m^2\ g^{-1}$ and a pore volume of 0.4 $cm^3\ g^{-1}$ as compared to Fe_3O_4@GO (surface area $\sim$ 79.4 $m^2\ g^{-1}$ and pore volume $\sim$ 0.1 $cm^3\ g^{-1}$). While the Fe_3O_4@GO degraded 40% of 2,4-dichlorophenol, Fe_3O_4@GO@MIL-100(Fe) nanocomposite degraded 100% of the pollutant in visible light/H_2O_2 system (Gong et al. 2019a).

MOFs coupled with conventional photocatalysts form Z-scheme photocatalysts with better charge separation. Cobalt and nickel-metal nodes and organic linkers were combined with $CuWO_4$ to form [CoNi(μ_3-tp)$_2$(μ_2-pyz)$_2$]/$CuWO_4$ composite. Apart from the lower recombination of charge carriers, the MOF/$CuWO_4$ composite had a large surface area, which led to a fourfold increase in the photocatalytic degradation performance for *p*-nitrophenol (Ramezanalizadeh and Manteghi 2018). Hu et al. (2019) reported the coupling of NH_2-MIL-125(Ti) with BiOCl for the photocatalytic degradation of bisphenol A under visible light. Band edge positions were sketched from X-ray photoelectron spectroscopy and UV–visible diffuse reflectance spectroscopy measurements. The study confirmed the formation of the heterojunction, which lowered the charge recombination rate and improved the degradation of bisphenol A. It is important to mention that NH_2-MIL-125(Ti) alone did not exhibit good photocatalytic activity (Hu et al. 2019). Ahmad et al. (2019) formed a ZnO decorated MIL-100(Fe) composite for the degradation of phenol and bisphenol A. The composite exhibited improved performance in comparison to the constituent photocatalysts. This behavior was attributed to the larger surface area that improved the contact with the pollutant and the photo-Fenton coupled process promoted by iron in the MOF (Ahmad et al. 2019). A similar effect was observed in g-C_3N_4/PDI@NH_2-MIL-53(Fe) composite synthesized by the solvothermal method. The matching of the conduction band of the photocatalysts facilitated a faster charge transfer and separation of photo-induced electron–hole pairs. Moreover, the formation of $^{\cdot}OH$ through H_2O_2 reduction was promoted by iron species in the framework. Bisphenol A and *p*-nitrophenol were degraded fully after 10 and 30 min, respectively (Li et al. 2019c). Though most of the studies lack the degradation pathway of pollutants, which makes it difficult to understand the underlying degradation mechanism and impact of

the study, Meng et al. (2017) reported visible-assisted degradation of bisphenol A over PCN-222. The GC–MS analysis confirmed a new peak at m/z ∼ 108 along with the characteristic peak of bisphenol A at m/z ∼ 213. This peak was assigned to *p*-benzoquinone, which was an intermediate product. Since *p*-benzoquinone is a resonating structure of *p*-hydroquinone, it could be assumed that singlet oxygen produced in the process cleaved and oxidized the single bonds to yield phenol like species in the initial stage. The high concentration of p-benzoquinone in the solution after 2 h suggested that the radicals were partly successful in ring-opening, which led to incomplete mineralization (Meng et al. 2017). Such drawbacks could be eliminated by adding oxidants, which could enhance the degradation rate and at the same time could increase the mineralization efficiency.

Metal–organic frameworks for air decontamination

Large emissions from industrial units, thermal power plants, incinerators, and automobiles are rich in toxic gases like SO_x, NO_x, volatile organic compounds, volatile sulfur-organic compounds, NH_3, and H_2S. The complex atmospheric chemistry of these gases aided by solar radiation and water vapors leads to photochemical smog, acid rain, and the greenhouse effect, which pose a severe threat to human health and the environment. Long-term exposure to air pollutants causes asthma, lung cancer, psychological complications, autism, and low birth weight. Sporadic events, like the historic 1952 Great Smog of London and 1966 New York City smog, or the more recent, 2015 Southeast Asian haze have shown the extent of deterioration done by the anthropogenic activities the air quality. The need of the hour is to develop effective and affordable technologies to trap and eliminate these gaseous pollutants. Many physicochemical processes including absorption, membrane separation, and cryogenic distillation have been developed for the removal of toxic components of gas streams. The absorption of toxic gas in a solvent is highly dependent on the strength of the interaction of gas molecules with the solvent. For sour gas sweetening, alkanolamines are a widely used class of chemical solvents, which selectively absorb acidic gases (CO_2 and H_2S) by dissociation. Though absorption is an efficient process, continuous loss of solvent, high energy consumption for the regeneration of spent solvent, and relatively low recovery of absorbed gas limit the process (Vega et al. 2020; Shah et al. 2017). Membrane treatment of toxic gas is attractive when the pressure of feed gas is high and is more suitable for the treatment of natural gas near the source. Moreover, the process does not require large space for operation, unlike the solvent absorption process. The process is limited by slow mass transfer at ambient conditions and periodic membrane replacement. For lowering the operational cost, membrane-solvent hybrid processes have been proposed. These gas–liquid membrane contactors offer high surface area per unit contactor volume with promisingly large H_2S/CO_2 selectivity (Shah et al. 2017). Researchers are focused on the adsorptive and catalytic removal of gaseous pollutants from the contaminated air. So far, numerous solid adsorbents like zeolites, lime, active carbon, metal oxides, and silica, in the pristine or modified form, have been extensively reported for the removal of $SO_x/NO_x/CO_x$ pollutants (Rezaei et al. 2015). The adsorptive and catalytic removal of toxic gases is in limelight for decades and appreciated for their technical simplicity and operation at ambient conditions. One of the limiting factors is the low surface area for sorbent-sorbate interactions. Large surface area coupled with transition metals (for adsorption/catalytic degradation) in metal–organic frameworks (MOFs) has attracted the environmental researchers to explore these materials for the detoxification of contaminated air. Moreover, tunable MOFs provide possible modifications in the structure and functionality for selective removal of toxic gases. In this section, we have provided discussions on the role of MOFs in the removal of major inorganic and organic gaseous pollutants. In the literature, it has been well established that MOFs have significantly high $NO_x/SO_x/CO_x$ adsorption capacities as compared to other porous solid adsorbents (Rezaei et al. 2015). For this reason, the review has reserved discussions and comparisons among different MOFs.

Inorganic sulfur compounds

Hydrogen sulfide (H_2S) and sulfur dioxide (SO_2) are the common atmospheric sulfur pollutants, which are majorly contributed by biogenic activities, farm activities, and thermal plants. These sulfur compounds in the oxidized form as SO_3 are responsible for the formation of acid rains that severely deteriorates the water quality. These gases are known to be toxic to humans, even at a low concentration. Though the exposure of more than 100 ppm of H_2S or SO_2 is found deadly for humans, the lower concentration (∼ below 1 ppm) of these gaseous pollutants could cause discomfort. The USEPA has fixed 15 ppb and 30 ppb, as the yearly average exposure limit for H_2S and SO_2, respectively. To reach such a low threshold requires special adsorbents with large surface area and high density of active sites. The open metal sites (electron-deficient) of a highly porous metal–organic framework (MOF) could strongly interact with H_2S (Lewis base or electron-pair donor) and SO_2 (σ-donor/π-acceptor), responsible for the extremely high adsorption capacity of MOFs. Many MOFs

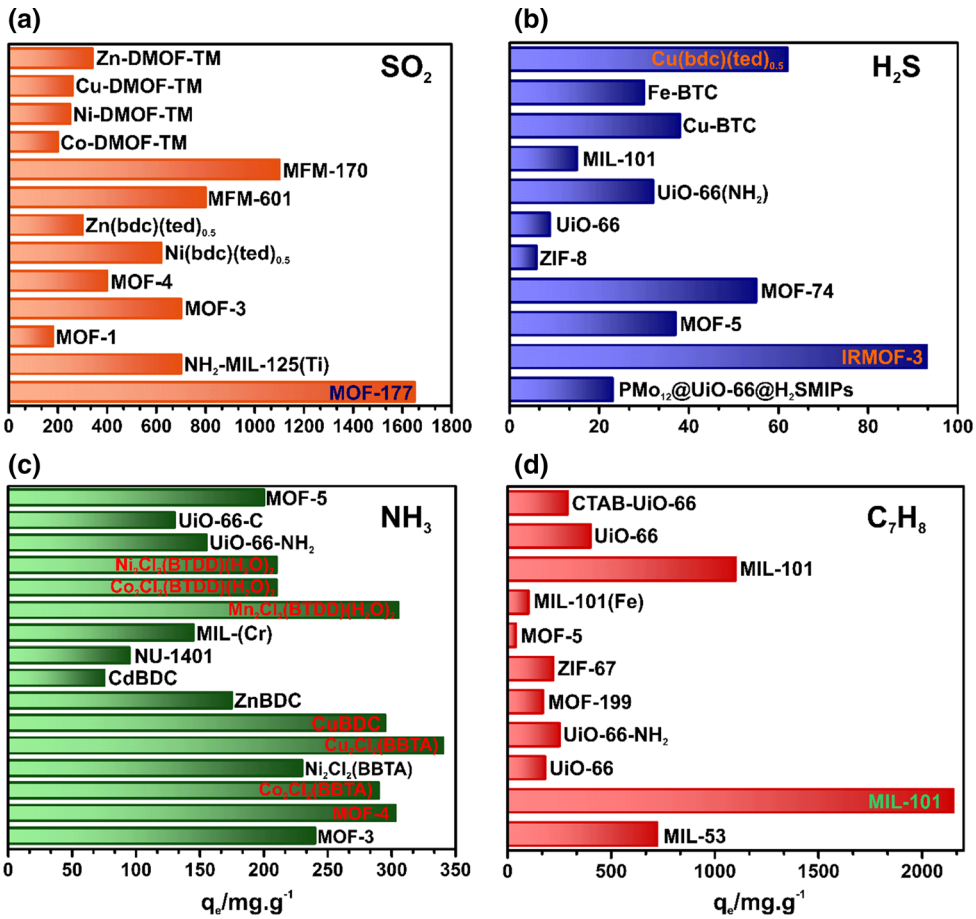

Fig. 9 **a** SO_2 adsorption efficiency of metal–organic frameworks (MOFs) (Tan et al. 2013; Glomb et al. 2017; Carter et al. 2018; Hungerford et al. 2018; Brandt et al. 2019; Smith et al. 2019), **b** H_2S adsorption capacity of MOFs (Liu et al. 2017a; Huang and Wang 2019), **c** NH_3 adsorption capacity of metal–organic frameworks (MOFs, Morris et al. 2011; Rieth et al. 2016; Glomb et al. 2017; Chen et al. 2018b; Rieth and Dinca 2018; Zhang et al. 2020b), **d** Toluene adsorption capacity of MOFs (Yang et al. 2011; Bahri et al. 2016; Vellingiri et al. 2016a; Zhang et al. 2019c, d)

with 3*d* transition metals as the nodes have been studied for the adsorptive removal of SO_2 from flue gases (Fig. 9a). Hungerford et al. (2018) developed pillared MOFs, M-DMOF-TM with Co^{2+}, Ni^{2+}, Cu^{2+}, and Zn^{2+} as the metal node for SO_2 removal. Though the MOFs showed good physisorption of dry SO_2, the SO_2 adsorption in 85% humidity led to the structural collapse due to the formation of sulfate/sulfite acid. The stability trend: Co < Ni < Cu > Zn in the humid condition was explained by the metal–ligand bond strength (in the same order as predicted by the Irving-Williams series) (Hungerford et al. 2018).

Glomb et al. (2017) reported significantly higher SO_2 adsorption capacity for Zn-based MOFs with urea-functionalized dicarboxylate linkers in the dry conditions, probably due to the high polarity of the gas molecules and the involvement of hydrogen bonding with the N–H and C=O bonds of the linker. Even for the dry SO_2, the diffraction pattern of MOF-1 showed broadening of reflections and a higher amorphous background, which hinted toward the partial decomposition of the MOF network (Glomb et al. 2017). The highest SO_2 adsorption capacity of 1645 mg g^{-1} was reported for MOF-177, which was linked to its exceptionally high surface area of 4100 m^2 g^{-1} and a total pore volume of 1.51 cm^3 g^{-1}. The MOF-177 showed poor adsorption behavior at low partial pressures, which limited its application for selective SO_2 adsorption from lowly concentrated flue gas (< 500 ppm). Moreover, the MOF-177 showed a 55% decrease in the surface area after dry SO_2 adsorption, making it unsuitable for humid SO_2 (Brandt et al. 2019).

The higher adsorption of SO_2 onto $Ni(BDC)(TED)_{0.5}$ than its Zn analog was reported by Tan et al. (2013), where the Ni-MOF adsorbed 291 and 638 mg g^{-1} of SO_2 at 0.11 and 1.13 bar, respectively (Tan et al. 2013). Since Zn-based MOFs have been predicted to be less stable for SO_2 adsorption, the obvious choices for practical applications are Ni- and Cu-based MOFs. The more pragmatic approach toward using the MOFs for selective uptake of SO_2 from flue gas was recorded for the fluorinated MOF. The breakthrough experiments with the KAUST-7 recorded high SO_2 uptake of 89.6 mg g^{-1} (500 ppm, SO_2/N_2: 0.05/99.95 mixture) and 0.64 mg g^{-1} (500 ppm, $SO_2/CO_2/N_2$: 0.05/10/89.95). The analog MOF, KAUST-8, showed even higher uptake of 102.4 mg g^{-1} (500 ppm, SO_2/N_2: 0.05/99.95 mixture). The fluorinated MOFs were stable for the adsorption of dry and 40% humid SO_2, which was reflected in their respective X-ray diffraction pattern for used MOFs (Tchalala et al. 2019).

Smith et al. (2019) developed a thermally and chemically stable MOF, MFM-170, for the selective and reversible uptake of SO_2 from flue gases. MFM-170 retained its structural integrity for ten weeks of exposure to moist SO_2. The SO_2 adsorption capacity of MFM-170 (1240 mg g^{-1}) decreased to 1037 mg g^{-1} for MFM-170·H_2O, where the water molecules at the Cu(II) site of MFM-170 reduced the adsorption capacity. The in situ single-crystal X-ray diffraction pattern of MFM-170•5.46SO_2 confirmed six distinct binding sites with the open Cu(II) sites as the thermodynamically favored binding site for SO_2 molecules. Exceptional SO_2/CO_2 selectivity was noticed in the breakthrough studies for fully activated and water-saturated MFM-170 (Smith et al. 2019).

Wang et al. (2020) reported theoretical considerations on the SO_2/CO_2 selectivity of Cu(II) sites of CuBTC MOF. The shorter bond distance and high binding energy for [Cu^{2+}···O=S=O] interactions than that for [Cu^{2+}···O=C=O], as calculated from the grand canonical Monte Carlo and density functional theory analysis suggested strong electrostatic interaction of SO_2 with the Cu^{2+} sites (Wang et al. 2020). The SO_2 adsorption onto Cu_2(2,3-pyrazinedicarboxylate)$_2$(pyrazine), named as CPL-1 MOF, with SO_2/CO_2 (9), SO_2/N_2 (368), and SO_2/CH_4 (74) selectivity was possible via molecular sieving effect. The density functional theory -based static binding energy of SO_2 molecules (36.3 kJ mol^{-1}) on CPL-1 MOF was found significantly higher than of CO_2 molecules (13.8 kJ mol^{-1}), which accounted for the SO_2/CO_2 selectivity. The density functional theory calculations predicted O–(hydroxyl and carbonyl) and H–(pzdc ligands)-based binding sites in CPL-1, where the SO_2 molecules were trapped by $S^{\delta+}$···$O^{\delta-}$ electrostatic interactions at a distance of 2.70 Å and $O^{\delta-}$···$H^{\delta+}$ hydrogen bonds at a distance of 2.19–2.85 Å. In this work, the authors were able to prepare MOF in kilogram scale with similar crystallinity and performance at a fabrication cost of $230 kg^{-1} (Zhang et al. 2020a). The exceptional selectivity of MFM-170, SO_2/CO_2 (35), SO_2/N_2 (944), SO_2/CO (203), and SO_2/CH_4 (260), coupled with zero loss in the SO_2 adsorption performance for 50 adsorption/desorption cycles, made MFM-170 as one of the suitable MOF for the capture of SO_2 from flue gases (Smith et al. 2019).

For the selective adsorption of H_2S from syngas, Liu et al. (2017a) reported numerous MOFs with different organic linkers and Cr, Fe, Cu, Zn, and Zr as transition metal nodes (Fig. 9b). Among all the MOFs studies, Cu- and Zn-containing MOFs showed better adsorption performances due to the strong covalent interaction of the H_2S molecules with free Zn and Cu sites. The chemisorption process was driven by the formation of Cu–S and Zn–S bonds at the expense of weak Cu–O and Zn–O bonds, respectively. For other MOFs, including MIL-101(Cr), UiO-66, and ZIF-8, reversible adsorption behavior with poor selectivity was recorded due to the involvement of physical forces. Considering the trade-off between H_2S/CO_2 selectivity and uptake, UiO-66 and MIL-101(Cr) were chosen as promising MOFs for H_2S capture (Liu et al. 2017a). Alivand et al. (2019) reported selective H_2S adsorption using conventional MIL-101(Cr) and improved MIL-101(Cr) with excess ligand-clusters. Apart from the improvement in the surface and porous properties, the modified MOF had ∼ 60% more H_2S adsorption capacity than the conventional one. The increased adsorption behavior was attributed to the creation of unsaturated Cr^{3+} sites for stronger interactions of polar gases at low pressures (Alivand et al. 2019).

One of the many observations reported by Liu et al. (2017a) was the significantly higher adsorption of H_2S onto the amine analog of UiO-66 as compared to the parent MOF. Apart from reversible adsorption of H_2S molecules in the tetrahedron aromatic cage of the UiO-66, the reactive interaction of $-NH_2$ groups with H_2S (forming NH_3HS) led to irreversible adsorption of H_2S over UiO-66-NH_2 (Liu et al. 2017a). Joshi et al. (2018) made detailed observations on the enhanced H_2S uptake from natural gas simulant mixtures by amine analogs of UiO-66(Zr), MIL-125(Ti), and MIL-101(Cr). In the fixed-bed experiments with 1% H_2S/99% CH_4 and 1% H_2S/10% CO_2/89% CH_4 test mixtures, the trend: MIL-125 < UiO-66 < MIL-101 observed for the adsorption capacity was following the pore diameter. The MOFs showed decreased H_2S uptake in the presence of CO_2 in the test mixtures except for MIL-101. The presence of hydroxyl groups in MIL-125 and UiO-66 served as the CO_2 physisorption sites, which were absent in MIL-101. The study suggested adsorptive uptake of H_2S over amine analogs with a higher H_2S/CO_2 selectivity from natural gas (Joshi et al. 2018). Monte Carlo molecular simulation was performed by Sokhanvaran et al. (2019) to understand the adsorption of H_2S, CO_2, and CH_4 onto parent and hydroxyl-functionalized MIL-47(V). The simulated adsorption selectivity of the MOF was in the order $H_2S/CH_4 > H_2S/CO_2 > CO_2/CH_4$. Polar H_2S molecules interacted more strongly with the polar functionality of the MOF than the CO_2 molecules, which is nonpolar with a weak electrical quadrupole moment (Sokhanvaran et al. 2019). Thus, theoretical and experimental considerations showed that MOFs own intrinsic selectivity for H_2S molecules in multi-component systems with a higher proportion of CO_2 and CH_4 molecules, which is a good indication for their utilization in the desulfurization of natural gas. In most of these studies, the regeneration of MOFs was poor, which led to the non-reusability of MOFs for a large number of cycles.

The thermal catalytic conversion of H_2S to sulfur using MOF as a catalyst is a more feasible approach toward the

desulfurization process. Liu et al. (2017a) hinted toward converting H_2S to S_8 at 200 °C onto MIL-100(Fe) gel. The temperature was sufficient to break the energy barrier, which led to the transfer of an electron from S to Fe, resulting in the reduction of Fe(III) and the production of S_8 in the pores of MOF (Liu et al. 2017a). Zheng et al. (2020) presented a detailed study on the catalytic conversion of H_2S over three Fe-based MOFs, MIL-100, MIL-101, and MIL-53. The Fe-MOF showed superior H_2S conversion performance than commercial Fe_2O_3, where the trend: MIL-100 (100%) > MIL-101 (79%) > MIL-53 (77%) at 100 °C followed matched with the trend observed for surface area and the concentration of Lewis acid sites. The density functional theory calculations predicted larger H_2S adsorption energy (E_{ads} ~ 0.96 eV) with shorter Fe–S bond length (2.788 Å) for MIL-100 as compared to those observed for MIL-101 (E_{ads} ~ 0.31 eV, Fe–S ~ 2.806 Å), which further confirmed the stronger binding of H_2S onto MIL-100 (Zheng et al. 2020). In the context of adsorption-degradation duality, TiO_2@MIL-101(Cr) was developed for the UV-assisted photo-oxidation of H_2S. The TiO_2-coated MOF showed improved H_2S conversion efficiency with a higher degree of reusability without any regeneration (Sheng et al. 2017). Thus, catalytic or photocatalytic conversion of H_2S using MOFs are preferred methods for the desulfurization process.

Inorganic nitrogen compounds

Nitrogen oxides (NO and NO_2) are the primary pollutants responsible for the formation of photochemical smog, acid rain, and the destruction of the ozone layer. These gaseous pollutants are being added to the air from automobile combustion engines and thermal power plants. Adsorptive removal of NO_x is an unconventional approach, which is in the early stages of development. In the literature, reports on

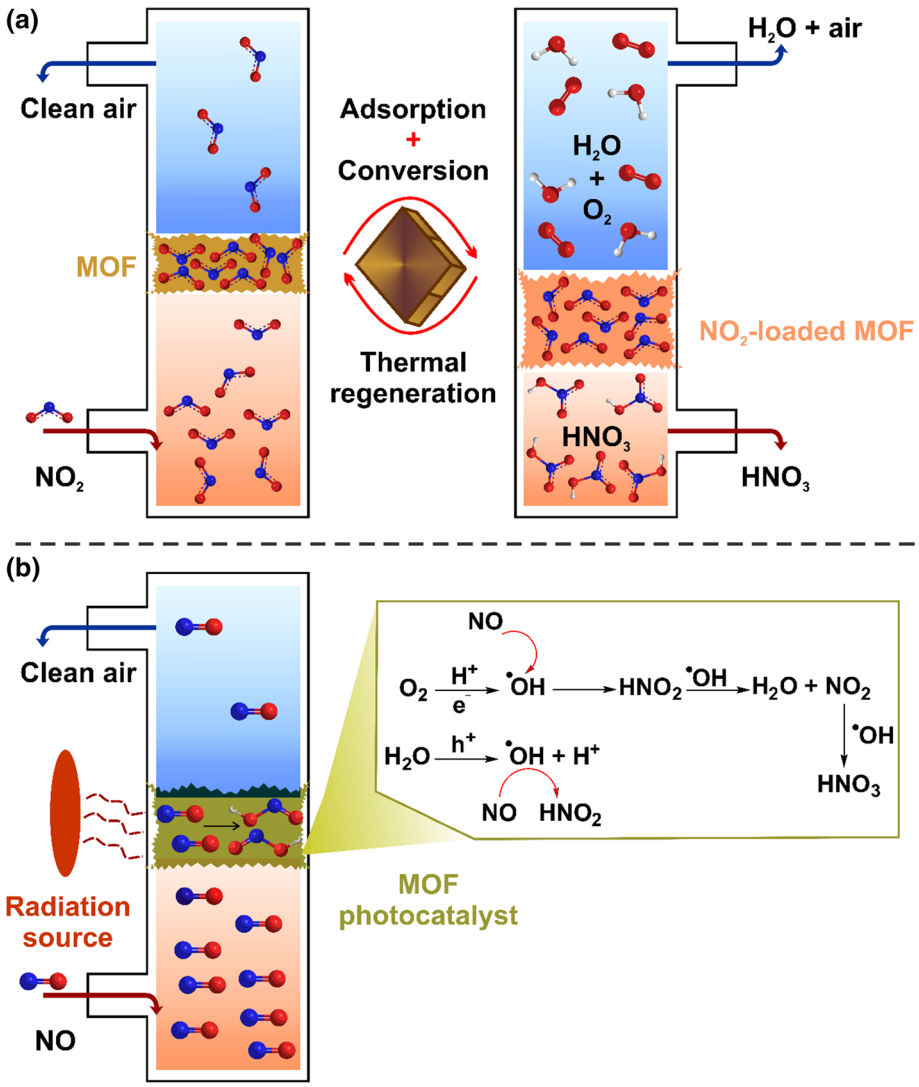

Fig. 10 **a** Adsorption and conversion of NO_2 into HNO_3 over a transition metal-based metal–organic framework (MOF), **b** photocatalytic conversion of NO_x to HNO_3/HNO_2 over a MOF as a powerful method for air clean-up and cheap production of HNO_3

adsorptive removal of NO_x using metal–organic frameworks (MOFs) are limited. But discussing these published works seems reasonable to compare the NO_x removal efficacy of MOFs via adsorptive and catalytic processes. Peterson et al. (2016) reported significant improvement in the NO_2 adsorption capacity of UiO-66-NH_2 (930 mg g^{-1}) over UiO-66 (400 mg g^{-1}) in the dry conditions. In 80% relative humidity, the adsorption capacity reached 1400 and 610 mg g^{-1} for UiO-66-NH_2 and UiO-66. Another feature of this study was the lower formation of NO during the adsorption process (4.5%) as compared to conventional active carbon (23%) (Peterson et al. 2016).

Li et al. (2019b) reported preferential and reversible adsorption of NO_2 over a Zn-based MOF, MFM-520, with a high degree of reusability. The in situ single-crystal X-ray diffraction study of NO_2@MFM-520 confirmed the dimerization of NO_2 to form N_2O_4, where each pore can accommodate one N_2O_4 molecule. The retention of N_2O_4 molecules in the pore was supported by sixteen hydrogen bonding ($O^{\delta-}\cdots H^{\delta+}$ $\sim$ 2.74 and 3.74 Å) interactions of aromatic –CH groups of linker and eight dipole interactions ($N^{\delta+}\cdots O^{\delta-}$ $\sim$ 3.68 Å) of carboxylate O atoms with the N_2O_4 molecule. The NO_2-loaded MOF soaked in water for 10 min yielded a 0.09 M HNO_3 solution. Moreover, the MOF was fully regenerated and showed no performance loss for 125 cycles. Thus, this MOF-based process could be used as a powerful method for air clean-up and cheap production of HNO_3 (as opposed to conventional energy-intensive oxidation of NH_3) (Fig. 10a) (Li et al. 2019b).

The selective catalytic reduction (SCR) of NO with NH_3 is an efficient post-treatment catalytic process to convert NO to N_2 for NO_x emission control. Though transition metal oxides are commonly used as catalysts for commercial applications, transition metal-based MOFs are expected to show even better results owing to a large surface area and porosity. Sun et al. (2018) studied the deNO_x efficacy of Ni-BDC in the selective catalytic reduction of the NH_3 process in the 100–500 °C range. More than 90% NO conversion was possible at a temperature of 275 °C, which decreased sharply after 440 °C due to the destabilization of the Ni-BDC framework (Sun et al. 2018). Better deNO_x performance was recorded for MnO_x@MIL-125(Ti), where the catalyst showed quantitative NO conversion in the range of 175–425 °C. The Mn oxide-MOF catalyst was a significant improvement over commercially used MnO_x/TiO_2 catalysts. The in situ diffuse reflectance infrared Fourier transform spectroscopy confirmed two kinds of NH_3 species on the surface of the MnO_x@MIL-125(Ti) catalyst, i.e., coordinated NH_3 on Lewis sites and NH_4^+ on Brønsted acid sites. The adsorption of NO and O_2 led to the formation of NO^-, NO_2^-, and NO_3^- on the surface of MnO_x@MIL-125(Ti). The two species, NO_2^- and NO_3^-, are active in the selective catalytic reduction reaction. Furthermore, the rapid disappearance of NO^- species in the presence of NH_3 predicted the formation of [$NO^-(NH_3)$], as possible intermediates, which rapidly decomposed into N_2 and H_2O (Sun et al. 2019a).

The catalytic removal of NO was studied as a synergy between CuBTC and the non-thermal plasma (NTP) process. The non-thermal plasma modified CuBTC (CuBTC-P) showed $\sim$ 98% NO removal as compared to 21 and 29%, respectively, for CuBTC and non-thermal plasma de-nitration process. The CuBTC-NTP synergetic method generated unsaturated Cu(II) sites, which were reduced to Cu(I) after electron capture during the non-thermal plasma discharge process. The primary process was reducing NO to N_2 by the high-energy electrons of non-thermal plasma and the Cu(I) active sites of CuBTC. The CuBTC-non-thermal plasma de-nitration synergetic method showed the merits of being effective at ambient temperature without reducing agents (as opposed to the conventional selective catalytic reduction method) (Gong et al. 2019b). Three isocompositional and structurally different Fe-based MOFs, MIL-53, MIL-88B, and MIL-101, have been explored as potential photocatalysts for converting NO to HNO_3. Among the three MOFs, MIL-101 showed better NO conversion efficiency of 76, 61, and 61% under solar, UV, and visible radiation, respectively (Fig. 10b). Also, the MOF was found highly stable, where conversion efficiency was more than 70% for eight consecutive cycles (Nguyen et al. 2018). To some extent, the involvement of transition-based MOFs in the selective catalytic reduction processes for reductive removal of NO_x seems a reasonable choice in the mitigation of NO_x from the polluted air.

Ammonia (NH_3) emitted in large quantities from livestock breeding, fertilizer application, and industrial production is another form of inorganic nitrogen that is considered toxic to living beings. Ammonia reacts with SO_2, NO_x, etc., to form $PM_{2.5}$ (fine particulate matter with an aerodynamic diameter of < 2.5 µm), which has been linked to respiratory disorders in densely polluted countries. NH_3 molecules are basic and have a high affinity for Lewis or Brønsted acidic active sites such as unsaturated Lewis acidic open metal sites of transition metal-based MOFs. In the literature, most of the studies dealing with the adsorptive removal of NH_3 molecules are focused on using MOFs with 3d transition metals as nodes (Fig. 9c).

Reith et al. (2016) reported three isostructural azolate MOFs with Mn, Co, and Ni as metal nodes for the adsorptive removal of NH_3. The three MOFs showed significantly higher NH_3 uptake than UiO-66-NH_2 at 1 bar and 298 K. The comparatively higher NH_3 uptake by $Mn_2Cl_2(BTDD)(H_2O)_2$ suggested MOF structural rearrangement, which resulted in the opening of a second coordination site on the Mn ions. These MOFs maintained

adsorption capacity for multiple cycles, even with the loss in surface area, suggesting good accessibility to NH_3-binding open metal sites (Rieth et al. 2016).

The study by Rieth and Dinca (2018) developed another series of isoreticular azolate MOFs containing Co, Ni, and Cu as the nodes and 1H,5H-benzo(1,2- d),(4,5-d′)bistriazole) (BBTA) as the linker. The BBTA series was a significant improvement over the larger-pore bis(1H-1,2,3-triazolo[4,5-b],[4′,5′-i])dibenzo[1,4]dioxin) (BTDD) series in the NH_3 uptake capacity. The smaller pore in BBTA series allowed increased hydrogen-bonding interactions of the metal-bound NH_3 molecules with the additional NH_3 molecules adsorbed in the pore, which is less likely to occur in the larger-pore BTDD series. The breakthrough performance of Co_2Cl_2BBTA in 80% relative humidity was nearly 45% lower than in dry conditions, which was still superior to conventional adsorbents like zeolites and AC (Rieth and Dinca 2018). A series of MOFs with terephthalic acid (BDC) as the linker, Cu(BDC), Zn(BDC), and Cd(BDC) was synthesized for the removal of low concentrates of NH_3 from polluted air. The adsorption of NH_3 onto MOF led to the structural changes, where 3D (Cu(BDC) and Cd(BDC)) and 2D (Zn(BDC)) MOFs transformed into 1D MOFs. The high polarity and coordination ability of NH_3 molecules with the metal nodes resulted in the formation of metal-NH_3 bonds at the expense of framework metal-linker bonds. The regeneration and reversibility of the framework were possible after 80 min of heating at 220 °C under vacuum. Though the overall regeneration process was energy-intensive, Cu(BDC) showed reusability for ten adsorption-regeneration cycles (Chen et al. 2020d).

Volatile aromatic compounds

Volatile aromatic compounds, including benzene and benzene homologs (toluene, xylene, ethylbenzene, etc.), are ubiquitous in the polluted urban atmosphere primarily released by chemical processing industries. These pollutants are difficult to degrade and linked to respiratory disorders and cancers in human beings. Even at low concentrations, these gaseous pollutants could cause human discomforts in the indoor environment. Thus, the olfactory threshold for benzene, toluene, and *p*-xylene has been set to 2.70, 0.33, and 0.06 ppm, respectively (Vellingiri et al. 2016b). Adsorption technology, with the aid of active carbon, amorphous silica, or zeolites, has been frequently adapted for the mitigation of benzene and its analogs (Kim et al. 2020). Though these adsorbents are cost-effective, limited surface area and binding sites have disfavored their adsorption efficacies. A major segment of metal–organic frameworks (MOFs) has one or more phenyl rings in their structural linkers, the phenyl ring of volatile aromatic compounds could interact with the MOF surface via π–π interactions similar to those observed in active carbon. Another strong interactive force favorable to the adsorption process is the cation-π interaction between the metal node of a MOF and the phenyl ring of volatile aromatic compounds. Though there are several volatile aromatic compounds of environmental interests, this subsection is limited to a discussion on benzene and toluene removal with some perspectives on other volatile aromatic compounds.

In the literature, reports are available on the adsorptive removal of several volatile aromatic compounds onto transition metal-based MOFs, MIL-101(Cr) (Yang et al. 2011), MOF-199(Cu) (Vellingiri et al. 2016b), and Cu-MOF (Yang et al. 2015). Yang et al. (2015) demonstrated exceptional volatile aromatic compounds adsorption capacity over a porous Cr-based MOF, MIL-101 (Yang et al. 2011). The maximum adsorption capacity was recorded for benzene (1291 mg g^{-1}), whereas the minimum was for m-xylene (727 mg g^{-1}). The odd adsorptive behavior was not supported by the polarity of the volatile molecules (Yang et al. 2015), which suggested that the cation-π interactions were not the driving forces in the adsorption of the compounds. The possible reason could be the matching of the molecular volume of volatile aromatic compounds with that of the cylindrical pore size and volume of MOF. Volatile aromatic compounds molecules are considered as rectangular solids shape, where benzene, toluene, ethylbenzene, and *p*-xylene have a plane diameter smaller than those of o-xylene and m-xylene. The volatile aromatic compounds molecule with smaller plane diameter could easily enter the pores of comparable size as compared to larger plane diameter molecules, which was the main reason behind significant adsorption of benzene due to the least diameter (Yang et al. 2011).

For Cu-MOF with azolate linkers, the larger-sized xylene or ethylbenzene was preferred more than the smaller-sized benzene and toluene, suggesting the absence of host–guest selectivity. One of the possible explanations for this behavior was the hydrophobic interactions between the alkyl-branched aromatics with the *n*-C_4H_9-filled pores of MOF (Yang et al. 2015). The adsorptive removal of benzene has been performed over CuBTC and MIL-101, where the adsorption capacity was 450 and 900 mg g^{-1}, respectively. Based on the enthalpy and performance considerations, it was established that CuBTC adsorbed benzene via strong interactions as compared to the MIL-101, but the later had higher adsorption capacity due to a larger cavity volume (Belarbi et al. 2019). MIL-(Cr)-Z1 with an adsorption capacity of 766 mg g^{-1} in 80% relative humidity was a good adsorbent for the removal of benzene in humid conditions. The adsorption performance decreased as a function of increasing temperature,

suggesting weak physical interaction of benzene onto the MOF (Zhu et al. 2017).

Vellingiri et al. (2016a) reported toluene adsorption onto six MOFs with higher adsorption capacity recorded for UiO-66(NH_2) and ZIF-67 (Fig. 9d). The hydrogen bonding between the methyl of toluene and –N–H bonds of UiO-66(NH_2) and ZIF-67 dominated over the π-π interactions. The involvement of physical forces in the adsorption process led to a lowering in the toluene adsorption capability of MOFs with the increasing temperature. MOFs other than UiO-66(NH_2) performed poorly in 25% relative humidity due to the competitive nature of water molecules with toluene for the binding sites. Based on the adsorption capacity and reusability, UiO-66(NH_2) was screened out as the best performing MOF in the study (Vellingiri et al. 2016a). Bahri et al. (2016) reported one of the highest adsorption capacities for toluene over MIL-101(Cr), where the larger surface area and mesoporous cavities favored the adsorption of toluene molecules. The 30% relative humidity seriously affected the performance of MIL-101 with a ∼ 80% loss in the toluene uptake. MIL-53 had a good resistance against the humidity with adsorption capacity dipping to 692 mg g^{-1} at 30% relative humidity from 730 mg g^{-1} in dry conditions. In the case of MIL-101, Cr^{3+} metal sites preferably interacted with polar H_2O molecules, forming water clusters on the MOF surface and preventing the volatile aromatic compound molecules from reaching the binding sites. On the contrary, the interactions between H_2O and carboxylate and hydroxy groups via hydrogen bonding led to the MOF structure's deformation. The flexible framework allowed the expansion of pores and compensated for the loss due to the pore filling of MOF with water molecules (Bahri et al. 2016). Besides adsorption, photocatalytic degradation is another powerful method for the remediation of volatile aromatic compounds. Zhang et al. (2016) reported visible-light-induced degradation of toluene over NH_2-MIL-101(Fe). The MOF photocatalyst adsorbs in the entire UV/visible range with a bandgap of 1.32 eV. The photocatalyst was able to degrade ∼ 80% of toluene in 600 min, which was considerably faster than P25 Degussa, which was due to the organic-linker-to-metal-cluster charge transfer in MOF, increasing the photo-charge separation efficiency (Zhang et al. 2016).

Li et al. (2020) proposed adsorption–oxidation removal of toluene using MIL-88B. In the first step, MOF was used as an adsorbent and adsorb 100% of 460 ppm toluene gas. In the second stage, the MOF acted as a photocatalyst and converted 85% of the adsorbed toluene into CO_2 under a 100 mW cm^{-2} solar irradiation within 60 min. The MOF showed similar adsorption–oxidation performances for benzene and *p*-xylene. Besides good conversion efficiency, the MOF showed remarkable reusability with only a 6% loss in the performance after 100 adsorption–oxidation cycles (Li et al. 2020). In an unconventional approach, TiO_2 nanoparticles-incorporated NH_2-UiO-66 was studied for the photocatalytic degradation of styrene under visible light. After 600 min of illumination, the MOF degraded ∼ 99% of styrene with a mineralization efficiency of 35% (Yao et al. 2018). The mineralization efficiency in the foremost factor in judging the applicability of the photocatalytic process. Though visible illumination is partially effective in mineralization, the evolution of the metal oxide-integrated MOF hybrids could resolve the issue.

Volatile sulfur-organic compounds

Representative volatile sulfur-organic compounds, including methyl mercaptan, dimethyl sulfide, and dimethyl disulfide, are colorless and odorous gases. These can cause skin and eye irritation in humans at a very low concentration and could be lethal if exposed to a high concentration. The emission of volatile sulfur-organic compounds is primarily linked to industrial sources like oil refineries, pharmaceuticals, tanneries, and paper mills. According to Pearson's hard-soft acid–base theory, volatile sulfur-organic compounds (soft bases) preferentially interact with soft Lewis acid sites (Cu^{2+}, Zn^{2+}, Co^{2+}, and Ni^{2+}) via acid–base interactions. In the literature, multiple reports have been dedicated to the use of Cu-based metal–organic frameworks (MOFs), especially MOF-199 for the adsorptive removal of volatile sulfur-organic compounds (Li et al. 2015b; Ma et al. 2016; Deng et al. 2018). Deng et al. (2018) utilized chemically and thermally activated MOF-199 for the adsorption of volatile sulfur-organic compounds in single and multi-component studies. The best performance was shown by chemically and thermally treated MOF-199-T2, where the adsorption capacity for methyl mercaptan, dimethyl sulfide, and dimethyl disulfide was 14.6, 10.6, and 21.2 mg g^{-1}, respectively. The low energy requirement for the breaking of C–S (259 kJ mol^{-1}) and S–S (266 kJ mol^{-1}) bonds as compared to the C–H bonds (347 kJ mol^{-1}) and the high affinity of Cu sites to form CuS favored the adsorption of dimethyl disulfide over other volatile sulfur-organic compounds in a multi-component study. Moreover, the presence of two methyl groups and larger size promoted the van der Waals interactions between dimethyl disulfide molecules and the aromatic groups of MOF. These interactive forces and the preferential adsorption of dimethyl disulfide were further validated by the density functional theory calculations (Deng et al. 2018). Li et al. (2015b) reported ethyl mercaptan and dimethyl sulfide adsorption over MOF-199. The deconvoluted X-ray photoelectron spectra of Cu 2p and S 2p confirmed the presence of Cu–S–C_2H_5 species and the formation of CuS, which was visible

as the MOF turned black (Li et al. 2015b). Similar results were observed for methyl mercaptan adsorption onto MOF-199. The MOF showed significantly better methyl mercaptan adsorption performance than the commercial AC, where the maximum adsorption capacity of 75 mg g^{-1} was recorded for 5 ppm methyl mercaptan concentration (Ma et al. 2016).

Wang et al. (2019a) developed a reduced CuBTC (Cu(I)/Cu(II)-BTC) to remove dimethyl disulfide with the adsorption capacity of 147 mg(S) g^{-1}. The density functional theory calculation predicted higher interaction energy of dimethyl disulfide with the Cu(I)/Cu(II)-BTC structure (70.65 kJ mol^{-1}) than the parent Cu(II)-BTC (20.28 kJ mol^{-1}), confirming stronger interaction of dimethyl disulfide with Cu(I) sites (Wang et al. 2019a). Other than Cu-based MOF, Zn-based MOF, IRMOF-3 (Wang et al. 2014), and HKUST-1 (Ma et al. 2018) have been explored for the adsorption of volatile sulfur-organic compounds. Wang et al. (2014) studied ethyl mercaptan and dimethyl sulfide adsorption onto IRMOF-3 in a fixed-bed reactor. The adsorption capacities decreased as a function of increasing temperature, suggesting the involvement of physical forces in the volatile sulfur-organic compounds adsorption process. The physisorption of volatile sulfur-organic compounds was further confirmed by X-ray photoelectron spectroscopy, where the peaks associated with ZnS (161.7 eV) and elemental S (164.4 eV) were absent, and the "S" peaks corresponding to volatile sulfur-organic compounds were observed (Wang et al. 2014).

Chemical warfare agents

Though a sizable population in the world may never experience chemical warfare agents in their lifetime, these toxicants have been given the utmost priorities in war-torn nations. The Geneva protocol of 1925 prohibited the use of these compounds, but could not prevent the development and stockpiling of these weapons of mass destruction. As preventive measures against the use of chemical warfare agents in wars, accidental leakage of chemical warfare agents in production units, and for the destruction of existing stockpiles, several effective detoxification strategies have been proposed. The adsorptive or catalytic removal of these hazardous compounds is explored as these methods are significantly fast and effective. In the literature, metal–organic frameworks (MOFs) have been studied both as adsorbents and catalysts for chemical warfare agentś removal on many occasions, which deserves a brief discussion in this review. Soman, sarin and o-ethyl S-[2-(diisopropylamino)ethyl]-methylphosphonothioate are organophosphate compounds, which are considered as nerve agents. The systematic molecular simulation study by Agrawal et al. (2018) on the adsorptive interactions of simulants (dimethyl methylphosphonate DMMP and dimethyl *p*-nitrophenyl phosphate) and real (soman and sarin) chemical warfare agents with ~ 3000 different MOFs. The study confirmed that simulants are as good as chemical warfare agents for adsorption study (Agrawal et al. 2018).

In the literature, most of the papers published on the removal of chemical warfare agents simulants are centered on the use of Zr-based MOFs, especially parent and analogs of UiO-66 and UiO-67 (Ploskonka and DeCoste 2019; Ruffley et al. 2019; Wang et al. 2019c). Ploskonka and DeCoste (2019) studied multiple G-nerve agents and stimulants hydrolysis onto four Zr-MOFs, UiO-66, UiO-67, NU-1000, and PCN-222 in the N-ethylmorpholine buffer solution (pH 10). All the four MOFs showed faster hydrolysis of sarin with a half-life ($t_{1/2}$) in the range of 2–7 min. The dimethyl *p*-nitrophenyl phosphate hydrolysis was comparatively slow ($t_{1/2}$ ~ 17–19 min) and reached 100% within 120 min. The adsorption of G agents or simulants onto UiO-66 and UiO-67 occurred at uncoordinated Zr sites via organophosphate group of the adsorbate (Ploskonka and DeCoste 2019).

In another recent study, Harvey et al. (2019) employed density functional theory-calculated infrared spectroscopy to resolve the binding sites of sarin molecules onto UiO-66. Though the study predicted three additional binding sites, ZrOH, fully coordinated Zr site, and μ_3-OH for sarin molecules, the under-coordinated Zr was the preferred sites for sarin adsorption (Harvey et al. 2019). The hydrolysis was facilitated through hydrogen bonding between the bridged hydroxyl group and the leaving group of the adsorbate molecule. A water molecule hydrogen-bonded to a neighboring Zr–OH initiated a nucleophilic attack on the P, forming P–OH and the leaving P–X. The P–X bond's scission was done by the Brønsted acidic nature of the neighboring Zr–OH_2 site. A similar mechanism was proposed for NU-1000 and PCN-222, but with the addition of another pathway. The terminal –OH on the same Zr atoms on which the organophosphate interacted was utilized in the hydrolysis process (Ploskonka and DeCoste 2019). The theoretically calculated energy of terminal displacement of Zr–OH_2 groups by the sarin molecules by Momeni and Cramer highlighted the importance of the displacement process in the overall reaction kinetics. The study predicted faster kinetics for UiO-66 than NU-1000, which was experimentally observed in the study (Momeni and Cramer 2018).

The role of moisture on the hydrolysis of dimethyl *p*-nitrophenyl phosphate was probed by Wang et al. (2019c), where UiO-66, UiO-66-NH_2, and NU-1000 wetted with different amounts of water were tested for dimethyl *p*-

nitrophenyl phosphate hydrolysis. Overall, the water loading favored the hydrolysis process, where higher activity and faster kinetics were recorded for MOFs soaked with 400 wt% water (Wang et al. 2019c). Ruffley et al. (2019) reported the adsorption of dimethyl methylphosphonate onto differently functionalized UiO-67-X, with X as −H, $-CH_3$, −SH, $-NH_2$, $-N_3$,$-NO_2$, −Br, and −Cl. Based on the density functional theory calculations, UiO-67-NH_2, UiO-67-CH_3, and UiO-67 showed strong, intermediate, and weak binding with dimethyl methylphosphonate, respectively (Ruffley et al. 2019).

Bis(2-chloroethyl) sulfide, commonly known as mustard gas, was used during World War I. It is a notorious chemical warfare agent with cytotoxic, vesicant, and blistering effects on exposed skin. The extent of damage reported in World War I, continuous use of this chemical warfare agents in the post-world war era, and a large stockpile of bis(2-chloroethyl) sulfide in all major countries have forced researchers to develop remediation strategies to counter the damaging effects of bis(2-chloroethyl) sulfide in the future. The safety guidelines prohibit the use of bis(2-chloroethyl) sulfide in the laboratory scale, and for this reason, studies using 2-chloroethyl ethyl sulfide as a bis(2-chloroethyl) sulfide simulant have been reported in the literature. Buru et al. (2020) developed $H_5PV_2Mo_{10}O_{40}$-incorporated NU-1000 activated by heat (PV_2Mo_{10}@NU-1000–80 °C) and supercritical CO_2 (PV_2Mo_{10}@NU-1000-scCO_2). In the study, though 100% 2-chloroethyl ethyl sulfide conversion was possible with PV_2Mo_{10}@NU-1000–80 °C and PV_2Mo_{10}@NU-1000-scCO_2, the reaction rate was slow, and instead of forming non-toxic singly oxidized 2-chloroethyl ethyl sulfoxide, doubly oxidized 1-chloro-2-(ethylsulfonyl)ethane was majorly formed as the oxidation product in all experimental cases (Buru et al. 2020). The same group reported another polyoxometalate ($H_3PW_{12}O_{40}$)-incorporated NU-1000 (PW_{12}@NU-1000) for the oxidative conversion of 2-chloroethyl ethyl sulfide. The MOF ($t_{1/2}$ ∼ 13 min) and $H_3PW_{12}O_{40}$ ($t_{1/2}$ ∼ 5 min) showed selective toward 1-chloro-2-(ethylsulfonyl)ethane and 2-chloroethyl ethyl sulfoxide products, respectively. The heated MOF-polyoxometalate hybrid (PW_{12}@NU-1000-120 °C) decreased the $t_{1/2}$ value to 3 min with intermediate 2-chloroethyl ethyl sulfoxide selectivity of ∼ 59%. Supercritical CO_2-activated MOF-polyoxometalate hybrid (PW_{12}@NU-1000-scCO_2) had $t_{1/2}$ of 1 min and 90% preference to 2-chloroethyl ethyl sulfoxide. This variation in the selectivity could be due to the involvement of different mechanisms occurring on the MOF node or the polyoxometalate. An easy diffusion of the substrate to polyoxometalate in mesopores and rapid oxidation of sulfide led to the selective formation of singly oxidized products (Buru et al. 2018).

Buru et al. (2018) studied photocatalytic oxidation of 2-chloroethyl ethyl sulfide using porphyrin- (PCN-222), pyrene- (NU-1000), and perylene- (UMCM-313) based MOFs under light-emitting diode. PCN222, NU-1000, and UMCM-313 had $t_{1/2}$ value of 11, 6, and 4 min, respectively, in the bulk state, which was following the measured singlet oxygen quantum yield, $\Phi(^1O_2)^*$ of the corresponding linkers (porphyrin ∼ 0.38, pyrene ∼ 0.40, and perylene ∼ 0.45). The higher Φ value for a photosensitizer decreased the half-life of the 2-chloroethyl ethyl sulfide oxidation reaction. All three MOFs were found selective and generated the singly oxidized product, which is considered crucial in the implementation of MOFs in mustard gas oxidation. The thin films of MOF showed delayed photo-oxidation of 2-chloroethyl ethyl sulfide, but the turnover frequencies were ten times higher than those observed in the bulk MOF. The increased activity was linked to the lower MOF loading and greater MOF exposure to the incident radiation (Buru et al. 2018). The photo-oxidation of 2-chloroethyl ethyl sulfide is fast in pure O_2 and gets significantly delayed in the air (Liu et al. 2015). The faster oxidative 2-chloroethyl ethyl sulfide conversion over MOFs in the presence of air makes the process convenient from a practical standpoint. Zhang et al. (2018) reported photo-oxidation of 2-chloroethyl ethyl sulfide onto photoactive UiO-68-TBTD. The MOF was faster in selective oxidation of 2-chloroethyl ethyl sulfide to 2-chloroethyl ethyl sulfoxide ($t_{1/2}$ ∼ 3 min) in the air than H_2-TBTD ($t_{1/2}$ ∼ 6.5 min) (Zhang et al. 2018). This study was a significant improvement over the previously published one on the grounds of practicality and reusability.

Since protective gears like masks and suits are deployed to save humans from the toxic effects of chemical warfare agents, MOFs like UiO-66-NH_2 integrated into fibers (Dwyer et al. 2018; Kim et al. 2018; Chen et al. 2019b; Shen et al. 2019) or self-supported filters (Liang et al. 2018a) have been explored for the purpose. Liang et al. (2018a) developed Zr-MOF filters by growing UiO-66, UiO-67, and UiO-66-NH_2 onto the ZrO_2 nanofiber mat as the source of Zr ions. The orchestrated Zr-MOF filters were evaluated for the catalytic hydrolysis of chemical warfare agent surrogate dimethyl *p*-nitrophenyl phosphate in an N-ethylmorpholine buffer solution (pH 10). In 60 min, UiO-66-NH_2 and UiO-67 showed 100% dimethyl *p*-nitrophenyl phosphate conversion to *p*-nitrophenoxide, whereas it was 90% for UiO-66. The $t_{1/2}$ values were in the order of UiO-66-NH_2 (1.9 min) > UiO-67 (6.6 min) > UiO-66 (21.3 min). The faster degradation kinetics of UiO-66-NH_2 was due to the involvement of amine-group (Brønsted base) in the nucleophilic attack on the soft carbon center of dimethyl *p*-nitrophenyl phosphate molecules (Wang et al. 2019c). Moreover, the larger pore size of UiO-67 favored the diffusion process and allowed easy access of active

sites to dimethyl *p*-nitrophenyl phosphate molecules (Liang et al. 2018a).

Shen et al. (2019) integrated UiO-66-NH_2 in cellulose sponge for the catalytic hydrolysis of dimethyl *p*-nitrophenyl phosphate in an N-ethylmorpholine buffer solution. The MOF-cellulose sponge and MOF powder showed similar dimethyl *p*-nitrophenyl phosphate conversion performance after 100 min, where the $t_{1/2}$ value was 8 and 9 min, respectively. Apart from being good catalysts, the sponge showed high mechanical strength until 32 kPa (Shen et al. 2019). UiO-66-NH_2 was successfully grown on the surface of cotton fabric, which was used for the adsorption and hydrolysis of soman. In a more direct approach, the ability of MOF-cotton fabric to withstand chemical warfare agents was tested using an aerosol vapor–liquid assessment group (device to analyze military protective fabrics). The study reported a 20-fold and 10-fold dip in the soman and bis(2-chloroethyl)sulfide permeability of MOF-cotton fabric compared to the cotton fabric. Moreover, the conversion of toxic soman to non-toxic methylphosphonic acid was feasible (Kim et al. 2018). Thus, it is possible to integrate such MOF-fiber hybrids in chemical warfare agent resistant protective suits. The more realistic situation in battlefields requires the destruction of chemical warfare agents without the need for water and toxic organic bases. The possible replacement of N-ethylmorpholine is a solid-phase base like polyethyleneimine. The Zr-MOF/polyethyleneimine composites were developed by a simple vortex mixing of MOF powder and polyethyleneimine particles.

The MOF-808/polyethyleneimine showed a quantitative conversion of dimethyl *p*-nitrophenyl phosphate under 50% relative humidity in 960 min ($t_{1/2}$ ~ 96 min). The possible real-world application of MOF/polyethyleneimine composites was further explored by coating MOF-808/polyethyleneimine composite on a flexible fiber. The kinetics of dimethyl *p*-nitrophenyl phosphate conversion was even faster on the MOF-808/polyethyleneimine/fiber, where in the same experimental condition; the complete conversion was possible within 240 min ($t_{1/2}$ ~ 24 min). The MOF-808/polyethyleneimine/fiber completely hydrolyzed soman and o-ethyl S-[2-(diisopropylamino)ethyl]-methylphosphonothioate within 60 min. The MOF/polyethyleneimine/fiber showed remarkable tolerance in different conditions experienced in a warzone like wet and dry perspiration, CO_2-rich air, gasoline-rich atmosphere, and after exposure to air for 100 days. The overall impression of this study was that the MOF/polyethyleneimine/fiber could be successfully integrated into protective suits (Fig. 11) (Chen et al. 2019b).

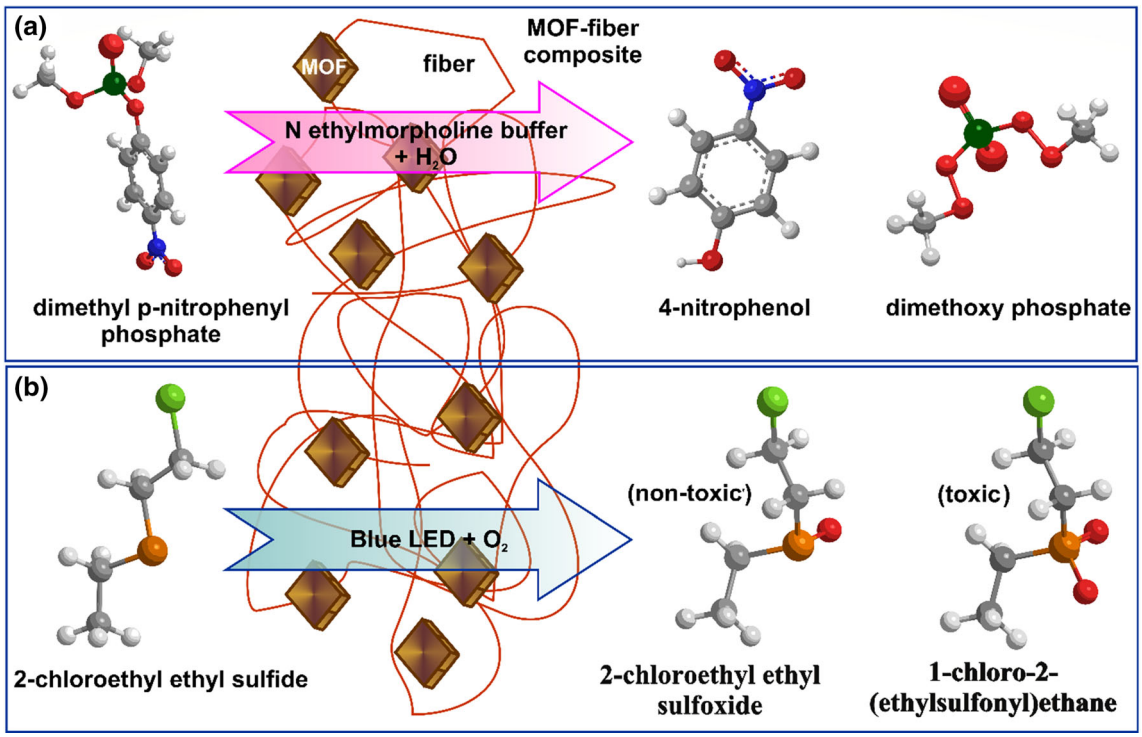

Fig. 11 Hydrolysis of dimethyl *p*-nitrophenyl phosphate in N-ethylmorpholine buffer over metal–organic framework (MOF)-fiber composite and destruction of 2-chloroethyl ethyl sulfide over MOF-fiber composite in O_2/blue light-emitting diode system. Atom color legend: C, gray; N, blue; O, red; S, orange; P; green, Cl, light green; H, white

Challenges and perspectives

The challenges being faced by old and new technologies are the driving force for the development of new functional materials that can eliminate toxicants present in water and air. Metal–organic frameworks (MOFs) are a sub-class of inorganic–organic hybrids with notable and advantageous physicochemical properties suitable for capturing pollutants and degrading them into non-toxic by-products by different chemical reactions. Though the commercialization of MOFs for remediation of contaminated water and air is in the infancy period and need proper exploration, the literature has been enriched with numerous related publications, which have been reviewed here.

Transition metal-based MOFs in the form of monometallic MOFs, bimetallic MOFs, and composites have the potential to eliminate toxic organic pollutants from wastewater of varying origins. These are novel catalysts for degrading and mineralizing organic pollutants under low power UV/visible radiations, and ultrasonication, which make these materials energy-efficient. However, the possible use of MOFs in wastewater remediation requires high structural stability in the operating conditions. Though it has been claimed that MOFs are stable in a wide pH range, such reports are scarce and cannot be generalized and applied to all MOFs. Likewise, their stability against oxidants and radiation sources needs to be addressed along with the reusability. The best possible way to evaluate MOF's structural integrity is to subject them in acidic/basic solutions, oxidants, and radiation sources and then compare the X-ray diffraction patterns before and after exposure (Mateo et al. 2019). The use of toxic heavy metals (Cd, Cr, and Co), organic linkers (4,4-bipyridine and trimesic acid), solvents (ŃN-dimethylformamide, chloroform, and acetone) and probable toxicity of synthesized nanoscale MOF crystals could be a roadblock in their commercialization for wastewater treatment (Kumar et al. 2019). Another issue that is commonly ignored in these research works is the cost of fabricating MOFs. Since there is no good estimation of MOF's manufacturing cost, it is not easy to estimate and compare the cost-to-performance ratio with other conventional materials. Though limiting the number of organic linkers for MOF synthesis is not feasible, the least toxic transition metals like Fe and Zn can be prioritized. Moreover, toxic solvents can be fully removed by adopting solvent-free synthesis. Since the synthesis of MOF via solvent-free routes like liquid-assisted grinding and aqueous synthesis are comparatively cheaper (\$13–36 kg^{-1}) than organic solvent (solvothermal) synthesis (\$35–71 kg^{-1}), following alternative solvent-free routes could reduce the cost of production (DeSantis et al. 2017). Many of these studies also lack screening of degradation by-products and their toxicity and column studies with real wastewater from industrial and domestic sources. Another pitfall is that some of the pollutants like pesticides are toxic even at μg L^{-1} concentrations, and the studies should focus on achieving the minimum acceptable limit of such pollutants after the treatment process. The practical exploitation of MOFs needs a complete understanding of the reaction pathways and their applicability in real wastewater and needs to be explored in great length from commenting on its applicability in wastewater treatment facilities. Nevertheless, the field is in the flowering stage, and future works could help in deciding MOFs applicability in wastewater treatment.

MOFs were first studied for the capture and storage of nonpolar gases. So, application of MOFs in adsorptive or catalytic removal of inorganic and organic gaseous pollutants is evident. The transition metal-based MOFs, especially Cr- and Cu-based MOFs, have shown high adsorption capacity for toxic gases with high selectivity against CO_2 and CH_4. In the literature, more studies are focused on the adsorptive removal and less on the catalytic removal of gases. The high adsorption of gaseous pollutants at ambient conditions is favorable only if the process is reversible and repetitive for hundreds of cycles for economical use of the porous adsorbents. Though a handful of works are focused on discussing the reusability issues, many researchers chose not to report, which makes it difficult to compare the advantages of adsorption over catalysis. The catalytic removal of gaseous pollutants via thermal or photolytic reactions over MOFs is a more suitable approach. Some of the works have confirmed the significant conversion of toxic pollutants like NO_x into nitric and nitrous acid under the effect of solar or UV-irradiation. Also, the selective catalytic reduction of NO with NH_3 or thermal degradation of volatile organic sulfur compounds to yield S_8 makes MOFs, versatile catalysts for air detoxification. Though the MOFs have many advantages to highlight for gaseous pollutant removal, the materials are thermally unstable and degrade even at a low temperature of 300–400 °C. The thermal stability of MOFs can be improved by increasing the coordination forces with a proper choice of organic linkers and metal nodes. Moreover, metal nodes of MOFs, especially those containing transition metals, are hydrophilic and coordinated with water molecules, which lowers the active site density and compromises with the structural integrity by hydrolysis reactions. Developing hydrophobic MOFs by choosing hydrophobic linkers and grafting oleophilic functionalities on the open metal sites can prevent the inflow of water molecules, which will enhance the performance. Moreover, the MOF stability should be evaluated by keeping MOFs in different atmospheric conditions to see the deterioration of MOFs under atmospheric oxygen (Du et al. 2019). So far,

the studies on the air detoxification are limited to answering whether a MOF can remove a particular gaseous pollutant, and if yes, then to what extent? The future research works should address mineralization efficiency, the toxicity of by-products, reusability, and MOF stability. Other than that, the practical use of MOFs could be indoor air decontamination, which requires gas-phase studies at ultra-low concentrations (ppm) for many pollutants as the United States Environmental Protection Agency limit for such pollutants is in the ppb range.

Good progress has been made in evaluating MOFs for protection against chemical warfare agents as adsorbents or catalysts. Chemical warfare agents are a special class of toxic pollutants and need unique and expensive methods for removal. MOFs blended with natural or synthetic fibers, and their use in protective gear and suits will be a humanitarian effort in saving countless lives in war-torn nations. The studies dealing with MOFs for chemical warfare agentś removal have addressed many drawbacks of efficacy in different environmental conditions, regenerations, the toxicity of by-products, reusability, and possible testing in real conditions (using Aerosol Vapor–Liquid Assessment Group assessment). The overall impression is that there are higher chances of commercialization of MOFs in the military than in civilian applications. Every possible assumption of the commercialization of MOFs is based on the cost of fabrication, low eco-toxicity, and high efficacy without relying on secondary chemicals or processes. Therefore, looking for economic precursors is essential for an affordable method for MOF fabrication. The least-step approach toward finding an alternative for a multi-step process for the development of a MOF could be a cost-cutting alternative. A more systematic evaluation of MOF toxicity to humans and other living beings may be another convincing approach for betting over MOFs in the wastewater treatment process. Though the present development of MOFs for environmental applications is limited due to shallow understanding, MOF's role in the future is highly probable. We believe that in the coming years, transition metal-based MOFs could be an alternative to pre-existing adsorbents and catalysts and integrated into commercial air and gas decontamination processes.

The future of MOFs is dependent on the ease with which the synthesis technology could be transferred from academic/laboratory-scale to a large industrial scale. Methods for industrial production of MOFs should be scrutinized on various parameters, including cost, availability of raw materials, technical simplicity, yields, purity and quality of synthesized MOFs, and environmental impact of the process. The quality of the adopted methodology is commonly evaluated by the space-time yield of the synthesis reaction. Space-time yield is defined as the mass of a MOF produced in kilogram per cubic meter of the reaction mixture in one day of synthesis. Methods with high space-time yield values are considered best for large-scale production of MOFs. The space-time yield values of popular MOFs synthesized using different protocols have been discussed in the literature (Rubio-Martinez et al. 2017). There is no point in developing materials with a poor environment footprint for environmental applications. For this reason, along with parameters like space-time yield, hidden and largely ignored parameter, i.e., environmental footprint should be considered before commercializing the process. Many popular MOFs like HKUST-1, MOF-5, UiO-66 series, ZIF-67, and ZIF-8 manufactured by Badische Anilin und Soda Fabrik, MOF Apps, and MOF Technologies are commercially available on Sigma-Aldrich (Rubio-Martinez et al. 2017). To date, high cost is the most important factor that is preventing the MOFs from replacing conventional adsorbents for environmental applications. But, with the advancement of the field, new players are entering the market for the commercialization of lesser-known MOFs and will certainly introduce MOFs up to their use for real-world environmental applications.

Conclusion

This review deals with the environmental applications of metal–organic frameworks (MOFs) for air and water detoxification. The large surface area, tunable porosity, and ease of functionalization make the chemistry and applications of MOF-based materials attractive to materials scientists. Thus, the development of new photocatalysts and gas adsorbents are being boosted by the tailored synthesis of novel coordination polymers where the metallic node and the organic linker are chosen to improve the final application of the MOF. The most updated synthetic routes for transition metal-based MOFs are discussed. The electron-transfer properties of the metallic node and the organic linker define the photocatalytic activity of a MOF. The most commonly used transition metals are Fe, Cu, Cd, and Fe, whereas aromatic polycarboxylates and porphyrins are the preferred ligands. Combinations of the mentioned metals/ligands are proven to be the most effective for photodegradation of organic pollutants, which is driven by an adequate light-harvesting capacity, low recombination rate, and large surface area. At the same time, the use of two metals instead of one as metallic nodes increases the pore size and thus favors the gas adsorption process. Also, bimetallic MOFs are relatively stable and could act as reusable photocatalysts/adsorbents. The MOF-based materials exhibit high adsorption capacity for a large variety of inorganic and organic gaseous pollutants. MOF's commercialization is challenging due to its high production cost, but the growing number of business enterprises could

pave the path for large-scale synthesis of MOFs-based materials. The positive approach toward finding technologies to integrate MOFs in the consumer lives will be the driving force toward the commercialization of MOFs for environmental applications.

Acknowledgement Authors are very grateful for the funds [Project#20200451-001] provided by the "Korea Institute of Civil Engineering and Building Technology" (KICT), Republic of Korea. The authors thank LNCAE (Laboratorio Nacional de Conversión y Almacenamiento de Energía) and Laboratorio Nacional de Ciencia, Tecnología y Gestión Integrada del Agua (LNAGUA) for technical support. Authors would like to thank Grayson Gould, Reliance Canada for language editing.

References

Abazari R, Mahjoub AR (2018) Amine-functionalized Al-MOF$^{\#}$@-$_{y}^{x}Sm_2O_3$–ZnO: A visible light-driven nanocomposite with excellent photocatalytic activity for the photo-degradation of amoxicillin. Inorg Chem 57:2529–2545. https://doi.org/10.1021/acs.inorgchem.7b02880

Abdpour S, Kowsari E, Moghaddam MRA (2018) Synthesis of MIL-100(Fe)@MIL-53(Fe) as a novel hybrid photocatalyst and evaluation photocatalytic and photoelectrochemical performance under visible light irradiation. J Solid State Chem 262:172–180. https://doi.org/10.1016/j.jssc.2018.03.018

Agrawal M, Sava Gallis DF, Greathouse JA, Sholl DS (2018) How useful are common simulants of chemical warfare agents at predicting adsorption behavior? J Phys Chem C 122:26061–26069. https://doi.org/10.1021/acs.jpcc.8b08856

Ahmad M, Chen S, Ye F et al (2019) Efficient photo-Fenton activity in mesoporous MIL-100(Fe) decorated with ZnO nanosphere for pollutants degradation. Appl Catal B Environ 245:428–438. https://doi.org/10.1016/j.apcatb.2018.12.057

Ahmed S, Rasul MG, Martens WN et al (2010) Heterogeneous photocatalytic degradation of phenols in wastewater: A review on current status and developments. Desalination 261:3–18. https://doi.org/10.1016/j.desal.2010.04.062

Alivand MS, Shafiei-Alavijeh M, Tehrani NHMH et al (2019) Facile and high-yield synthesis of improved MIL-101(Cr) metal-organic framework with exceptional CO_2 and H_2S uptake; the impact of excess ligand-cluster. Microporous Mesoporous Mater 279:153–164. https://doi.org/10.1016/j.micromeso.2018.12.033

Alvaro M, Carbonell E, Ferrer B et al (2007) Semiconductor behavior of a metal-organic framework (MOF). Chem-A Eur J 13:5106–5112. https://doi.org/10.1002/chem.200601003

Azhar MR, Vijay P, Tadé MO et al (2018) Submicron sized water-stable metal organic framework (bio-MOF-11) for catalytic degradation of pharmaceuticals and personal care products. Chemosphere 196:105–114. https://doi.org/10.1016/j.chemosphere.2017.12.164

Bahri M, Haghighat F, Kazemian H, Rohani S (2016) A comparative study on metal organic frameworks for indoor environment application: Adsorption evaluation. Chem Eng J 313:711–713. https://doi.org/10.1016/j.cej.2016.10.004

Bariki R, Majhi D, Das K et al (2020) Facile synthesis and photocatalytic efficacy of UiO-66/$CdIn_2S_4$ nanocomposites with flowerlike 3D-microspheres towards aqueous phase decontamination of triclosan and H_2 evolution. Appl Catal B Environ 270:118882. https://doi.org/10.1016/j.apcatb.2020.118882

Bayliss PA, Ibarra IA, Pérez E et al (2014) Synthesis of metal-organic frameworks by continuous flow. Green Chem 16:3796–3802. https://doi.org/10.1039/c4gc00313f

Bedia J, Muelas-Ramos V, Peñas-Garzón M et al (2019) A review on the synthesis and characterization of metal organic frameworks for photocatalytic water purification. Catalysts 9:52. https://doi.org/10.3390/catal9010052

Belarbi H, Gonzales P, Basta A, Trens P (2019) Comparison of the benzene sorption properties of metal organic frameworks: Influence of the textural properties. Environ Sci Process Impacts 21:407–412. https://doi.org/10.1039/c8em00481a

Benito J, Sorribas S, Lucas I et al (2016) Langmuir-Blodgett films of the metal-organic framework MIL-101(Cr): Preparation, characterization, and CO_2 adsorption study using a QCM-based setup. ACS Appl Mater Interfaces 8:16486–16492. https://doi.org/10.1021/acsami.6b04272

Brandt P, Nuhnen A, Lange M et al (2019) Metal-organic frameworks with potential application for SO_2 separation and flue gas desulfurization. ACS Appl Mater Interfaces 11:17350–17358. https://doi.org/10.1021/acsami.9b00029

Buru CT, Platero-Prats AE, Chica DG et al (2018) Thermally induced migration of a polyoxometalate within a metal-organic framework and its catalytic effects. J Mater Chem A 6:7389–7394. https://doi.org/10.1039/c8ta02562b

Buru CT, Wasson MC, Farha OK (2020) $H_5PV_2Mo_{10}O_{40}$ polyoxometalate encapsulated in NU-1000 metal-organic framework for aerobic oxidation of a mustard gas simulant. ACS Appl Nano Mater 3:658–664. https://doi.org/10.1021/acsanm.9b02176

Cao J, Yang ZH, Xiong WP et al (2018) One-step synthesis of Co-doped UiO-66 nanoparticle with enhanced removal efficiency of tetracycline: Simultaneous adsorption and photocatalysis. Chem Eng J 353:126–137. https://doi.org/10.1016/j.cej.2018.07.060

Carter JH, Han X, Moreau FY et al (2018) Exceptional adsorption and binding of sulfur dioxide in a robust zirconium-based metal-organic framework. J Am Chem Soc 140:15564–15567. https://doi.org/10.1021/jacs.8b08433

Chandra R, Singh V, Tomar S, Nath M (2019) Multi-core-shell composite SnO_2NPs@ZIF-8: potential antiviral agent and effective photocatalyst for waste-water treatment. Environ Sci Pollut Res 26:23346–23358. https://doi.org/10.1007/s11356-019-05646-5

Chen DM, Zhang XJ (2019) A polyoxometalate template metal-organic framework with unusual $\{Cu_8(\mu_4\text{-}OH)_6\}^{10+}$ secondary building unit for photocatalytic dye degradation. Inorg Chem Commun 108:107523. https://doi.org/10.1016/j.inoche.2019.107523

Chen DM, Liu XH, Zhang NN et al (2018a) Immobilization of polyoxometalate in a cage-based metal-organic framework towards enhanced stability and highly effective dye degradation. Polyhedron 152:108–113. https://doi.org/10.1016/j.poly.2018.05.059

Chen Y, Zhang F, Wang Y et al (2018b) Recyclable ammonia uptake of a MIL series of metal-organic frameworks with high structural stability. Microporous Mesoporous Mater 258:170–177. https://doi.org/10.1016/j.micromeso.2017.09.013

Chen J, Chao F, Ma X et al (2019a) Synthesis of flower-like CuS/UiO-66 composites with enhanced visible-light photocatalytic performance. Inorg Chem Commun 104:223–228. https://doi.org/10.1016/j.inoche.2019.04.022

Chen Z, Ma K, Mahle JJ et al (2019b) Integration of metal-organic frameworks on protective layers for destruction of nerve agents under relevant conditions. J Am Chem Soc 141:20016–20021. https://doi.org/10.1021/jacs.9b11172

Chen J, Zhang X, Bi F et al (2020a) A facile synthesis for uniform tablet-like TiO_2/C derived from Materials of Institut Lavoisier-125(Ti) (MIL-125(Ti)) and their enhanced visible light-driven

photodegradation of tetracycline. J Colloid Interface Sci 571:275–284. https://doi.org/10.1016/j.jcis.2020.03.055
Chen L, Wang HF, Li C, Xu Q (2020b) Bimetallic metal-organic frameworks and their derivatives. Chem Sci 11:5369–5403. https://doi.org/10.1039/d0sc01432j
Chen SS, Hu C, Liu CH et al (2020c) De Novo synthesis of platinum-nanoparticle-encapsulated UiO-66-NH_2 for photocatalytic thin film fabrication with enhanced performance of phenol degradation. J Hazard Mater 397:122431. https://doi.org/10.1016/j.jhazmat.2020.122431
Chen Y, Du Y, Liu P et al (2020d) Removal of ammonia emissions via reversible structural transformation in M(BDC) (M=Cu, Zn, Cd) metal-organic frameworks. Environ Sci Technol 54:3636–3642. https://doi.org/10.1021/acs.est.9b06866
Cheng M, Lai C, Liu Y et al (2018) Metal-organic frameworks for highly efficient heterogeneous Fenton-like catalysis. Coord Chem Rev 368:80–92. https://doi.org/10.1016/j.ccr.2018.04.012
Cheng J, Hu T, Li W et al (2020) Stable zinc metal-organic framework materials constructed by fluorenone carboxylate ligand: multifunction detection and photocatalysis property. J Solid State Chem 282:121125. https://doi.org/10.1016/j.jssc.2019.121125
Chun H, Yizhong W, Hongxiao T (2000) Destruction of phenol aqueous solution by photocatalysis or direct photolysis. Chemosphere 41:1205–1209. https://doi.org/10.1016/S0045-6535(99)00539-1
Chung KT (2016) Azo dyes and human health: a review. J Environ Sci Heal-Part C Environ Carcinog Ecotoxicol Rev 34:233–261. https://doi.org/10.1080/10590501.2016.1236602
Clarivate Accelerating innovation (2019) Web of Science. https://login.webofknowledge.com/error/Error?Error=IPError&PathInfo=%2F&RouterURL=https%3A%2F%2Fwww.webofknowledge.com%2F&Domain=.webofknowledge.com&Src=IP&Alias=WOK5. Accessed 31 May 2020
De Andrade JR, Oliveira MF, Da Silva MGC, Vieira MGA (2018) Adsorption of pharmaceuticals from water and wastewater using nonconventional low-cost materials: a review. Ind Eng Chem Res 57:3103–3127. https://doi.org/10.1021/acs.iecr.7b05137
Demirbas A (2009) Agricultural based activated carbons for the removal of dyes from aqueous solutions: a review. J Hazard Mater 167:1–9. https://doi.org/10.1016/j.jhazmat.2008.12.114
Deng Y, Vellingiri K, Kim KH et al (2018) Activation strategies of metal-organic frameworks for the sorption of reduced sulfur compounds. Chem Eng J 350:747–756. https://doi.org/10.1016/j.cej.2018.06.006
DeSantis D, Mason JA, James BD et al (2017) Techno-economic analysis of metal-organic frameworks for hydrogen and natural gas storage. Energy Fuels 31:2024–2032. https://doi.org/10.1021/acs.energyfuels.6b02510
Dhakshinamoorthy A, Asiri AM, García H (2016) Metal-organic framework (MOF) compounds: photocatalysts for redox reactions and solar fuel production. Angew Chemie-Int Ed 55:5414–5445. https://doi.org/10.1002/anie.201505581
Diercks CS, Liu Y, Cordova KE, Yaghi OM (2018) The role of reticular chemistry in the design of CO_2 reduction catalysts. Nat Mater 17:301–307. https://doi.org/10.1038/s41563-018-0033-5
Du PD, Thanh HTM, To TC et al (2019) Metal-organic framework MIL-101: synthesis and photocatalytic degradation of remazol black B dye. J Nanomater 2019:6061275. https://doi.org/10.1155/2019/6061275
Dwyer DB, Lee DT, Boyer S et al (2018) Toxic organophosphate hydrolysis using nanofiber-templated UiO-66-NH_2 metal-organic framework polycrystalline cylinders. ACS Appl Mater Interfaces 10:25794–25803. https://doi.org/10.1021/acsami.8b08167
Fang XD, Yang LB, Dou AN et al (2018) Synthesis, crystal structure and photocatalytic properties of a Mn(II) metal-organic framework based on a thiophene-functionalized dicarboxylate ligand. Inorg Chem Commun 96:124–127. https://doi.org/10.1016/j.inoche.2018.08.017
Farzaneh F, Mehraban Z, Norouzi F (2010) Synthesis and utilization of a mesoporous nickel oxide as a novel catalyst for degradation of phenol. Environ Chem Lett 8:69–72. https://doi.org/10.1007/s10311-008-0193-7
Feng S, Wang R, Feng S et al (2019) Synthesis of Zr-based MOF nanocomposites for efficient visible-light photocatalytic degradation of contaminants. Res Chem Intermed 45:1263–1279. https://doi.org/10.1007/s11164-018-3682-8
Flügel EA, Ranft A, Haase F, Lotsch BV (2012) Synthetic routes toward MOF nanomorphologies. J Mater Chem 22:10119–10133. https://doi.org/10.1039/c2jm15675j
Gangu KK, Maddila S, Mukkamala SB, Jonnalagadda SB (2016) A review on contemporary metal-organic framework materials. Inorganica Chim Acta 446:61–74. https://doi.org/10.1016/j.ica.2016.02.062
Gao Y, Yu G, Liu K et al (2017) Integrated adsorption and visible-light photodegradation of aqueous clofibric acid and carbamazepine by a Fe-based metal-organic framework. Chem Eng J 330:157–165. https://doi.org/10.1016/j.cej.2017.06.139
Gascon J, Corma A, Kapteijn F, Llabres i Xamena FX (2014) Metal organic framework catalysis: quo vadis? ACS Catal 4:361–378. https://doi.org/10.1002/chin.201414255
Geisse AR, Ngule CM, Genna DT (2019) Removal of lead ions from water using thiophene-functionalized metal-organic frameworks. Chem Commun 56:237–240. https://doi.org/10.1039/c9cc09022c
Gil A, Assis FCC, Albeniz S, Korili SA (2011) Removal of dyes from wastewaters by adsorption on pillared clays. Chem Eng J 168:1032–1040. https://doi.org/10.1016/j.cej.2011.01.078
Glomb S, Woschko D, Makhloufi G, Janiak C (2017) Metal-organic frameworks with internal urea-functionalized dicarboxylate linkers for SO_2 and NH_3 adsorption. ACS Appl Mater Interfaces 9:37419–37434. https://doi.org/10.1021/acsami.7b10884
Gómez-Avilés A, Peñas-Garzón M, Bedia J et al (2019) Mixed Ti-Zr metal-organic-frameworks for the photodegradation of acetaminophen under solar irradiation. Appl Catal B Environ 253:253–262. https://doi.org/10.1016/j.apcatb.2019.04.040
Gong Q, Liu Y, Dang Z (2019a) Core-shell structured Fe_3O_4@-GO@MIL-100(Fe) magnetic nanoparticles as heterogeneous photo-Fenton catalyst for 2,4-dichlorophenol degradation under visible light. J Hazard Mater 371:677–686. https://doi.org/10.1016/j.jhazmat.2019.03.019
Gong X, Zhao R, Qin J et al (2019b) Ultra-efficient removal of NO in a MOFs-NTP synergistic process at ambient temperature. Chem Eng J 358:291–298. https://doi.org/10.1016/j.cej.2018.09.222
Gong X, Shu Y, Jiang Z et al (2020) Metal-organic frameworks for the exploitation of distance between active sites in efficient photocatalysis. Angew Chemie-Int Ed 59:5326–5331. https://doi.org/10.1002/anie.201915537
Guo X, Geng S, Zhuo M et al (2019) The utility of the template effect in metal-organic frameworks. Coord Chem Rev 391:44–68. https://doi.org/10.1016/j.ccr.2019.04.003
Gupta VK, Ali I, Saini VK et al (2005) Removal of dyes from wastewater using bottom ash. Ind Eng Chem Res 44:3655–3664. https://doi.org/10.1021/ie0500220
Gupta A, Viltres H, Gupta NK (2020a) Sono-adsorption of organic dyes onto $CoFe_2O_4$/Graphene oxide nanocomposite. Surf. Interfaces 20:100563. https://doi.org/10.1016/j.surfin.2020.100563
Gupta NK, Ghaffari Y, Bae J, Kim KS (2020b) Synthesis of coral-like α-Fe_2O_3 nanoparticles for dye degradation at neutral pH. J Mol Liq 301:112473. https://doi.org/10.1016/j.molliq.2020.112473

Gupta NK, Ghaffari Y, Kim S et al (2020c) Photocatalytic degradation of organic pollutants over MFe_2O_4 (M = Co, Ni, Cu, Zn) nanoparticles at neutral pH. Sci Rep 10:4942. https://doi.org/10.1038/s41598-020-61930-2

Han Y, Zhang L, Bai C et al (2018) Fabrication of AgI/MIL-53(Fe) composites with enhanced photocatalytic activity for rhodamine B degradation under visible light irradiation. Appl Organomet Chem 32:1–8. https://doi.org/10.1002/aoc.4325

Han X, Yang S, Schr M (2019) Porous metal-organic frameworks as emerging sorbents for clean air. Nat Rev Chem 3:108–118. https://doi.org/10.1038/s41570-019-0073-7

Hao OJ, Kim H, Chiang PC (2000) Decolorization of wastewater. Crit Rev Environ Sci Technol 30:449–505. https://doi.org/10.1080/10643380091184237

Harvey JA, McEntee ML, Garibay SJ et al (2019) Spectroscopically resolved binding sites for the adsorption of sarin gas in a metal-organic framework: insights beyond Lewis acidity. J Phys Chem Lett 10:5142–5147. https://doi.org/10.1021/acs.jpclett.9b01867

Hassan MM, Carr CM (2018) A critical review on recent advancements of the removal of reactive dyes from dyehouse effluent by ion-exchange adsorbents. Chemosphere 209:201–219. https://doi.org/10.1016/j.chemosphere.2018.06.043

He L, Dong Y, Zheng Y et al (2019) A novel magnetic MIL-101(Fe)/TiO_2 composite for photo degradation of tetracycline under solar light. J Hazard Mater 361:85–94. https://doi.org/10.1016/j.jhazmat.2018.08.079

He X, Chen DR, Wang WN (2020) Bimetallic metal-organic frameworks (MOFs) synthesized using the spray method for tunable CO_2 adsorption. Chem Eng J 382:122825. https://doi.org/10.1016/j.cej.2019.122825

Howarth AJ, Peters AW, Vermeulen NA et al (2017) Best practices for the synthesis, activation, and characterization of metal-organic frameworks. Chem Mater 29:26–39. https://doi.org/10.1021/acs.chemmater.6b02626

Hu Q, Di J, Wang B et al (2019) In-situ preparation of NH_2 -MIL-125(Ti)/BiOCl composite with accelerating charge carriers for boosting visible light photocatalytic activity. Appl Surf Sci 466:525–534. https://doi.org/10.1016/j.apsusc.2018.10.020

Huang Y, Wang R (2019) Highly selective separation of H_2S and CO_2 using a H_2S-imprinted polymers loaded on a polyoxometalate@Zr-based metal-organic framework with a core-shell structure at ambient temperature. J Mater Chem A 7:12105–12114. https://doi.org/10.1039/c9ta01749f

Huang W, Jing C, Zhang X et al (2018) Integration of plasmonic effect into spindle-shaped MIL-88A(Fe): steering charge flow for enhanced visible-light photocatalytic degradation of ibuprofen. Chem Eng J 349:603–612. https://doi.org/10.1016/j.cej.2018.05.121

Hungerford J, Bhattacharyya S, Tumuluri U et al (2018) DMOF-1 as a representative MOF for SO_2 adsorption in both humid and dry conditions. J Phys Chem C 122:23493–23500. https://doi.org/10.1021/acs.jpcc.8b06819

Jadhav SA, Garud HB, Patil AH et al (2019) Recent advancements in silica nanoparticles based technologies for removal of dyes from water. Colloids Interface Sci Commun 30:100181. https://doi.org/10.1016/j.colcom.2019.100181

Jiang D, Xu P, Wang H et al (2018) Strategies to improve metal organic frameworks photocatalyst's performance for degradation of organic pollutants. Coord Chem Rev 376:449–466. https://doi.org/10.1016/j.ccr.2018.08.005

Jiang Y, Liu C, Huang A (2019) EDTA-functionalized covalent organic framework for the removal of heavy-metal ions. ACS Appl Mater Interfaces 11:32186–32191. https://doi.org/10.1021/acsami.9b11850

Jones OA, Lester JN, Voulvoulis N (2005) Pharmaceuticals: a threat to drinking water? Trends Biotechnol 23:163–167. https://doi.org/10.1016/j.tibtech.2005.02.001

Joshi JN, Zhu G, Lee JJ et al (2018) Probing metal-organic framework design for adsorptive natural gas purification. Langmuir 34:8443–8450. https://doi.org/10.1021/acs.langmuir.8b00889

Kang YS, Lu Y, Chen K et al (2019) Metal-organic frameworks with catalytic centers: from synthesis to catalytic application. Coord Chem Rev 378:262–280. https://doi.org/10.1016/j.ccr.2018.02.009

Khan NA, Jhung SH (2015) Synthesis of metal-organic frameworks (MOFs) with microwave or ultrasound: rapid reaction, phase-selectivity, and size reduction. Coord Chem Rev 285:11–23. https://doi.org/10.1016/j.ccr.2014.10.008

Khandan FM, Afzali D, Sargazi G, Gordan M (2018) Novel uranyl-curcumin-MOF photocatalysts with highly performance photocatalytic activity toward the degradation of phenol red from aqueous solution: effective synthesis route, design and a controllable systematic study. J Mater Sci: Mater Electron 29:18600–18613. https://doi.org/10.1007/s10854-018-9978-z

Khasevani SG, Gholami MR (2018) Engineering a highly dispersed core@shell structure for efficient photocatalysis: a case study of ternary novel BiOI@MIL-88A(Fe)@g-C_3N_4 nanocomposite. Mater Res Bull 106:93–102. https://doi.org/10.1016/j.materresbull.2018.05.024

Khasevani SG, Gholami MR (2019a) Evaluation of the reaction mechanism for photocatalytic degradation of organic pollutants with MIL-88A/BiOI structure under visible light irradiation. Res Chem Intermed 45:1341–1356. https://doi.org/10.1007/s11164-018-3681-9

Khasevani SG, Gholami MR (2019b) Synthesis of BiOI/$ZnFe_2O_4$-metal-organic framework and g-C_3N_4-based nanocomposites for applications in photocatalysis. Ind Eng Chem Res 58:9806–9818. https://doi.org/10.1021/acs.iecr.8b05871

Khasevani SG, Mohaghegh N, Gholami MR (2017) Kinetic study of navy blue photocatalytic degradation over Ag_3PO_4/$BiPO_4$@-MIL-88B(Fe)@g-C_3N_4 core@shell nanocomposite under visible light irradiation. New J Chem 41:10390–10396. https://doi.org/10.1039/c7nj01968h

Khodkar A, Khezri SM, Pendashteh AR et al (2019) A designed experimental approach for photocatalytic degradation of paraquat using α-Fe_2O_3@MIL-101(Cr)@TiO_2 based on metal-organic framework. Int J Environ Sci Technol 16:5741–5756. https://doi.org/10.1007/s13762-018-1941-2

Kim KC (2018) Design strategies for metal-organic frameworks selectively capturing harmful gases. J Organomet Chem 854:94–105. https://doi.org/10.1016/j.jorganchem.2017.11.017

Kim MK, Kim SH, Park M et al (2018) Degradation of chemical warfare agents over cotton fabric functionalized with UiO-66-NH_2. RSC Adv 8:41633–41638. https://doi.org/10.1039/c8ra06805d

Kim S, Gupta NK, Bae J, Kim KS (2020) Structural variations and generation of binding sites in Fe-loaded ZSM-5 and silica under the effect of UV-irradiation and their role in enhanced BTEX abatement from gas streams. J Hazard Mater 384:121274. https://doi.org/10.1016/j.jhazmat.2019.121274

Klimakow M, Klobes P, Thünemann AF et al (2010) Mechanochemical synthesis of metal-organic frameworks: a fast and facile approach toward quantitative yields and high specific surface areas. Chem Mater 22:5216–5221. https://doi.org/10.1021/cm1012119

Kökçam-Demir Ü, Goldman A, Esrafili L et al (2020) Coordinatively unsaturated metal sites (open metal sites) in metal-organic frameworks: design and applications. Chem Soc Rev 49:2751–2798. https://doi.org/10.1039/c9cs00609e

Kumar P, Anand B, Tsang YF et al (2019) Regeneration, degradation, and toxicity effect of MOFs: opportunities and challenges. Environ Res 176:108488. https://doi.org/10.1016/j.envres.2019.05.019

Lee YR, Kim J, Ahn WS (2013) Synthesis of metal-organic frameworks: a mini review. Korean J Chem Eng 30:1667–1680. https://doi.org/10.1007/s11814-013-0140-6

Lee YR, Jang MS, Cho HY et al (2015) ZIF-8: a comparison of synthesis methods. Chem Eng J 271:276–280. https://doi.org/10.1016/j.cej.2015.02.094

Li J, Yang J, Liu YY, Ma JF (2015a) Two heterometallic-organic frameworks composed of iron(III)-salen-based ligands and d^{10} metals: gas sorption and visible-light photocatalytic degradation of 2-chlorophenol. Chem-A Eur J 21:4413–4421. https://doi.org/10.1002/chem.201406349

Li Y, Wang LJ, Fan HL et al (2015b) Removal of sulfur compounds by a copper-based metal organic framework under ambient conditions. Energy Fuels 29:298–304. https://doi.org/10.1021/ef501918f

Li WJ, Tu M, Cao R, Fischer RA (2016) Metal-organic framework thin films: electrochemical fabrication techniques and corresponding applications & perspectives. J Mater Chem A 4:12356–12369. https://doi.org/10.1039/c6ta02118b

Li H, Li Q, He Y et al (2017) Two novel porous MOFs with square-shaped cavities for the removal of toxic dyes: adsorption or degradation? New J Chem 41:15204–15209. https://doi.org/10.1039/c7nj02904g

Li B, Ma J-G, Cheng P (2018a) Silica-protection-assisted encapsulation of Cu_2O nanocubes into a metal-organic framework (ZIF-8) to provide a composite catalyst. Angew Chemie 130:6950–6953. https://doi.org/10.1002/ange.201801588

Li G, Zhao S, Zhang Y, Tang Z (2018b) Metal-organic frameworks encapsulating active nanoparticles as emerging composites for catalysis: recent progress and perspectives. Adv Mater 30:1–43. https://doi.org/10.1002/adma.201800702

Li R, Chen Z, Cai M et al (2018c) Improvement of sulfamethazine photodegradation by Fe(III) assisted MIL-53(Fe)/percarbonate system. Appl Surf Sci 457:726–734. https://doi.org/10.1016/j.apsusc.2018.06.294

Li Y, Jiang J, Fang Y et al (2018d) TiO_2 nanoparticles anchored onto the metal-organic framework NH_2-MIL-88B(Fe) as an adsorptive photocatalyst with enhanced fenton-like degradation of organic pollutants under visible light irradiation. ACS Sustain Chem Eng 6:16186–16197. https://doi.org/10.1021/acssuschemeng.8b02968

Li H, Zhang J, Yao Y et al (2019a) Nanoporous bimetallic metal-organic framework (FeCo-BDC) as a novel catalyst for efficient removal of organic contaminants. Environ Pollut 255:113337. https://doi.org/10.1016/j.envpol.2019.113337

Li J, Han X, Zhang X et al (2019b) Capture of nitrogen dioxide and conversion to nitric acid in a porous metal-organic framework. Nat Chem 11:1085–1090. https://doi.org/10.1038/s41557-019-0356-0

Li Y, Fang Y, Cao Z et al (2019c) Construction of g-C_3N_4/PDI@MOF heterojunctions for the highly efficient visible light-driven degradation of pharmaceutical and phenolic micropollutants. Appl Catal B Environ 250:150–162. https://doi.org/10.1016/j.apcatb.2019.03.024

Li P, Kim S, Jin J et al (2020) Efficient photodegradation of volatile organic compounds by iron-based metal-organic frameworks with high adsorption capacity. Appl Catal B Environ 263:118284. https://doi.org/10.1016/j.apcatb.2019.118284

Liang R, Luo S, Jing F et al (2015) A simple strategy for fabrication of Pd@MIL-100(Fe) nanocomposite as a visible-light-driven photocatalyst for the treatment of pharmaceuticals and personal care products (PPCPs). Appl Catal B Environ 176–177:240–248. https://doi.org/10.1016/j.apcatb.2015.04.009

Liang H, Yao A, Jiao X et al (2018a) Fast and sustained degradation of chemical warfare agent simulants using flexible self-supported metal-organic framework filters. ACS Appl Mater Interfaces 10:20396–20403. https://doi.org/10.1021/acsami.8b02886

Liang Q, Jin J, Liu C et al (2018b) Fabrication of the ternary heterojunction $Cd_{0.5}Zn_{0.5}S$@UIO-66@g-C_3N_4 for enhanced visible-light photocatalytic hydrogen evolution and degradation of organic pollutants. Inorg Chem Front 5:335–343. https://doi.org/10.1039/c7qi00638a

Liu SQ, Cheng S, Luo L et al (2011) Degradation of dye rhodamine B under visible irradiation with Prussian blue as a photo-Fenton reagent. Environ Chem Lett 9:31–35. https://doi.org/10.1007/s10311-009-0242-x

Liu Y, Howarth AJ, Hupp JT, Farha OK (2015) Selective photooxidation of a mustard-gas simulant catalyzed by a porphyrinic metal-organic framework. Angew Chemie-Int Ed 54:9001–9005. https://doi.org/10.1002/anie.201503741

Liu J, Wei Y, Li P et al (2017a) Selective H_2S/CO_2 separation by metal-organic frameworks based on chemical-physical adsorption. J Phys Chem C 121:13249–13255. https://doi.org/10.1021/acs.jpcc.7b04465

Liu J, Zhu DD, Guo CX et al (2017b) Design strategies toward advanced MOF-derived electrocatalysts for energy-conversion reactions. Adv Energy Mater 7:1–26. https://doi.org/10.1002/aenm.201700518

Liu B, Vellingiri K, Jo SH et al (2018a) Recent advances in controlled modification of the size and morphology of metal-organic frameworks. Nano Res 11:4441–4467. https://doi.org/10.1007/s12274-018-2039-3

Liu CX, Zhang WH, Wang N et al (2018b) Highly efficient photocatalytic degradation of dyes by a copper–triazolate metal-organic framework. Chem-A Eur J 24:16804–16813. https://doi.org/10.1002/chem.201803306

Liu N, Jing C, Li Z et al (2019) Effect of synthesis conditions on the photocatalytic degradation of rhodamine B of MIL-53(Fe). Mater Lett 237:92–95. https://doi.org/10.1016/j.matlet.2018.11.079

Llabrés i Xamena FX, Corma A, Garcia H (2007) Applications for metal-organic frameworks (MOFs) as quantum dot semiconductors. J Phys Chem C 111:80–85. https://doi.org/10.1021/jp063600e

Lou Z, Xiao X, Huang M et al (2019) Acrylic acid-functionalized metal-organic frameworks for Sc(III) selective adsorption. ACS Appl Mater Interfaces 11:11772–11781. https://doi.org/10.1021/acsami.9b00476

Ma X, Liu H, Li W et al (2016) Reactive adsorption of low concentration methyl mercaptan on a Cu-based MOF with controllable size and shape. RSC Adv 6:96997–97003. https://doi.org/10.1039/c6ra18593b

Ma X, Peng S, Li W et al (2018) Efficient removal of low concentration methyl mercaptan by HKUST-1 membrane constructed on porous alumina granules. Cryst Eng Comm 20:407–411. https://doi.org/10.1039/c7ce01922j

Mahmoodi NM, Abdi J, Oveisi M et al (2018) Metal-organic framework (MIL-100 (Fe)): synthesis, detailed photocatalytic dye degradation ability in colored textile wastewater and recycling. Mater Res Bull 100:357–366. https://doi.org/10.1016/j.materresbull.2017.12.033

Mahour R, Khan MF, Forbes S, Perez-Estrada LA (2014) Pesticides and herbicides. Water Environ Res 86:1545–1578. https://doi.org/10.2175/106143014x14031280668777

Malik A, Nath M (2019) Multicore-shell nanocomposite formed by encapsulation of WO_3 in zeolitic imidazolate framework (ZIF-

8): as an efficient photocatalyst. J Environ Chem Eng 7:103401. https://doi.org/10.1016/j.jece.2019.103401

Martínez-Huitle CA, Brillas E (2009) Decontamination of wastewaters containing synthetic organic dyes by electrochemical methods: a general review. Appl Catal B Environ 87:105–145. https://doi.org/10.1016/j.apcatb.2008.09.017

Martínková L, Kotik M, Marková E, Homolka L (2016) Biodegradation of phenolic compounds by Basidiomycota and its phenol oxidases: a review. Chemosphere 149:373–382. https://doi.org/10.1016/j.chemosphere.2016.01.022

Masoomi MY, Bagheri M, Morsali A, Junk PC (2016) High photodegradation efficiency of phenol by mixed-metal-organic frameworks. Inorg Chem Front 3:944–951. https://doi.org/10.1039/c6qi00067c

Mateo D, Santiago-Portillo A, Albero J et al (2019) Long-term photostability in terephthalate metal-organic frameworks. Angew Chemie-Int Ed 58:17843–17848. https://doi.org/10.1002/anie.201911600

Matthies M, Solomon K, Vighi M et al (2016) The origin and evolution of assessment criteria for persistent, bioaccumulative and toxic (PBT) chemicals and persistent organic pollutants (POPs). Environ Sci Processes Impacts 18:1114–1128. https://doi.org/10.1039/C6EM00311G

McGrath DT, Ryan MD, Macinnis JJ et al (2019) Selective decontamination of the reactive air pollutant nitrous acid: via node-linker cooperativity in a metal-organic framework. Chem Sci 10:5576–5581. https://doi.org/10.1039/c9sc01357a

Mehta JP, Tian T, Zeng Z et al (2018) Sol-gel synthesis of robust metal-organic frameworks for nanoparticle encapsulation. Adv Funct Mater 28:1705588. https://doi.org/10.1002/adfm.201705588

Mei W, Song H, Tian Z et al (2019) Efficient photo-Fenton like activity in modified MIL-53(Fe) for removal of pesticides: regulation of photogenerated electron migration. Mater Res Bull 119:110570. https://doi.org/10.1016/j.materresbull.2019.110570

Meng A, Chaihu L, Chen H et al (2017) Ultrahigh adsorption and singlet-oxygen mediated degradation for efficient synergetic removal of bisphenol A by a stable zirconium-porphyrin metal-organic framework. Sci Rep 7:6297. https://doi.org/10.1038/s41598-017-06194-z

Mohammadi S, Kargari A, Sanaeepur H et al (2015) Phenol removal from industrial wastewaters: a short review. Desalin Water Treat 53:2215–2234. https://doi.org/10.1080/19443994.2014.883327

Momeni MR, Cramer CJ (2018) Dual role of water in heterogeneous catalytic hydrolysis of sarin by zirconium-based metal-organic frameworks. ACS Appl Mater Interfaces 10:18435–18439. https://doi.org/10.1021/acsami.8b03544

Morris W, Doonan CJ, Yaghi OM (2011) Postsynthetic modification of a metal-organic framework for stabilization of a hemiaminal and ammonia uptake. Inorg Chem 50:6853–6855. https://doi.org/10.1021/ic200744y

Naimi Joubani M, Zanjanchi MA, Sohrabnezhad S (2020) The carboxylate magnetic-zinc based metal-organic framework heterojunction: fe_3O_4-COOH@ZIF-8/Ag/Ag_3PO_4 for plasmon enhanced visible light Z-scheme photocatalysis. Adv Powder Technol 31:29–39. https://doi.org/10.1016/j.apt.2019.09.034

Nguyen HP, Matsuoka M, Kim TH, Lee SW (2018) Iron(III)-based metal-organic frameworks as potential visible light-driven catalysts for the removal of NO_x: a solution for urban air purification. J Photochem Photobiol A Chem 367:429–437. https://doi.org/10.1016/j.jphotochem.2018.09.008

Notar Francesco I, Fontaine-Vive F, Antoniotti S (2014) Synergy in the catalytic activity of bimetallic nanoparticles and new synthetic methods for the preparation of fine chemicals. ChemCatChem 6:2784–2791. https://doi.org/10.1002/cctc.201402252

Oladipo AA (2018) MIL-53 (Fe)-based photo-sensitive composite for degradation of organochlorinated herbicide and enhanced reduction of Cr(VI). Process Saf Environ Prot 116:413–423. https://doi.org/10.1016/j.psep.2018.03.011

Oladipo AA, Vaziri R, Abureesh MA (2018) Highly robust $AgIO_3$/MIL-53 (Fe) nanohybrid composites for degradation of organophosphorus pesticides in single and binary systems: application of artificial neural networks modelling. J Taiwan Inst Chem Eng 83:133–142. https://doi.org/10.1016/j.jtice.2017.12.013

Oladipo AA, Gazi M, Ifebajo AO, et al (2020) Photocatalytic degradation of toxic pesticides. In: Photocatalysts in Advanced Oxidation Processes for Wastewater Treatment. Wiley, pp 93–138. https://doi.org/10.1002/9781119631422.ch4

Patel M, Kumar R, Kishor K et al (2019) Pharmaceuticals of emerging concern in aquatic systems: chemistry, occurrence, effects, and removal methods. Chem Rev 119:3510–3673. https://doi.org/10.1021/acs.chemrev.8b00299

Peterson GW, Mahle JJ, Decoste JB et al (2016) Extraordinary NO_2 removal by the metal-organic framework UiO-66-NH_2. Angew Chemie-Int Ed 55:6235–6238. https://doi.org/10.1002/anie.201601782

Pirsaheb M, Moradi N (2020) Sonochemical degradation of pesticides in aqueous solution: investigation on the influence of operating parameters and degradation pathway-a systematic review. RSC Adv 10:7396–7423. https://doi.org/10.1039/c9ra11025a

Ploskonka AM, DeCoste JB (2019) Insight into organophosphate chemical warfare agent simulant hydrolysis in metal-organic frameworks. J Hazard Mater 375:191–197. https://doi.org/10.1016/j.jhazmat.2019.04.044

Pratim Bag P, Sahoo P (2020) Designing metal-organic frameworks based photocatalyst for specific photocatalytic reactions: a crystal engineering approach. In: Green photocatalysts for energy and environmental process, pp 142–176. https://doi.org/10.1007/978-3-030-17638-9_6

Prosser RS, Sibley PK (2015) Human health risk assessment of pharmaceuticals and personal care products in plant tissue due to biosolids and manure amendments, and wastewater irrigation. Environ Int 75:223–233. https://doi.org/10.1016/j.envint.2014.11.020

Racles C, Zaltariov MF, Silion M et al (2019) Photo-oxidative degradation of doxorubicin with siloxane MOFs by exposure to daylight. Environ Sci Pollut Res 26:19684–19696. https://doi.org/10.1007/s11356-019-05288-7

Ramezanalizadeh H, Manteghi F (2018) Synthesis of a novel MOF/$CuWO_4$ heterostructure for efficient photocatalytic degradation and removal of water pollutants. J Clean Prod 172:2655–2666. https://doi.org/10.1016/j.jclepro.2017.11.145

Ranft A, Betzler SB, Haase F, Lotsch BV (2013) Additive-mediated size control of MOF nanoparticles. CrystEngComm 15:9296–9300. https://doi.org/10.1039/c3ce41152d

Rawtani D, Khatri N, Tyagi S, Pandey G (2018) Nanotechnology-based recent approaches for sensing and remediation of pesticides. J Environ Manage 206:749–762. https://doi.org/10.1016/j.jenvman.2017.11.037

Rayaroth MP, Aravind UK, Aravindakumar CT (2016) Degradation of pharmaceuticals by ultrasound-based advanced oxidation process. Environ Chem Lett 14:259–290. https://doi.org/10.1007/s10311-016-0568-0

Reinsch H (2016) "Green" synthesis of metal-organic frameworks. Eur J Inorg Chem 2016:4290–4299. https://doi.org/10.1002/ejic.201600286

Rezaei F, Rownaghi AA, Monjezi S et al (2015) SO_x/NO_x removal from flue gas streams by solid adsorbents: a review of current challenges and future directions. Energy Fuels 29:5467–5486. https://doi.org/10.1021/acs.energyfuels.5b01286

Rieth AJ, Dinca M (2018) Controlled gas uptake in metal-organic frameworks with record ammonia sorption. J Am Chem Soc 140:3461–3466. https://doi.org/10.1021/jacs.8b00313

Rieth AJ, Tulchinsky Y, Dincã M (2016) High and reversible ammonia uptake in mesoporous azolate metal-organic frameworks with open Mn Co, and Ni sites. J Am Chem Soc 138:9401–9404. https://doi.org/10.1021/jacs.6b05723

Rojas S, Horcajada P (2020) Metal-organic frameworks for the removal of emerging organic contaminants in water. Chem Rev 120:8378–8415. https://doi.org/10.1021/acs.chemrev.9b00797

Rubio-Martinez M, Avci-Camur C, Thornton AW et al (2017) New synthetic routes towards MOF production at scale. Chem Soc Rev 46:3453–3480. https://doi.org/10.1039/c7cs00109f

Ruffley JP, Goodenough I, Luo TY et al (2019) Design, Synthesis, and characterization of metal-organic frameworks for enhanced sorption of chemical warfare agent simulants. J Phys Chem C 123:19748–19758. https://doi.org/10.1021/acs.jpcc.9b05574

Safaei M, Foroughi MM, Ebrahimpoor N et al (2019) A review on metal-organic frameworks: synthesis and applications. TrAC-Trends Anal Chem 118:401–425. https://doi.org/10.1016/j.trac.2019.06.007

Sajjadi S, Khataee A, Bagheri N et al (2019) Degradation of diazinon pesticide using catalyzed persulfate with Fe_3O_4@MOF-2 nanocomposite under ultrasound irradiation. J Ind Eng Chem 77:280–290. https://doi.org/10.1016/j.jiec.2019.04.049

Samuel MS, Bhattacharya J, Parthiban C et al (2018) Ultrasound-assisted synthesis of metal organic framework for the photocatalytic reduction of 4-nitrophenol under direct sunlight. Ultrason Sonochem 49:215–221. https://doi.org/10.1016/j.ultsonch.2018.08.004

Sánchez-Sánchez M, Getachew N, Díaz K et al (2015) Synthesis of metal-organic frameworks in water at room temperature: salts as linker sources. Green Chem 17:1500–1509. https://doi.org/10.1039/c4gc01861c

Sarkar S, Banerjee A, Halder U et al (2017) Degradation of synthetic azo dyes of textile industry: a sustainable approach using microbial enzymes. Water Conserv Sci Eng 2:121–131. https://doi.org/10.1007/s41101-017-0031-5

Shah MS, Tsapatsis M, Siepmann JI (2017) Hydrogen sulfide capture: from absorption in polar liquids to oxide, zeolite, and metal–organic framework adsorbents and membranes. Chem Rev 117:9755–9803. https://doi.org/10.1021/acs.chemrev.7b00095

Shen C, Mao Z, Xu H et al (2019) Catalytic MOF-loaded cellulose sponge for rapid degradation of chemical warfare agents simulant. Carbohydr Polym 213:184–191. https://doi.org/10.1016/j.carbpol.2019.02.044

Sheng H, Chen D, Li N et al (2017) Urchin-inspired TiO_2@MIL-101 double-shell hollow particles: adsorption and highly efficient photocatalytic degradation of hydrogen sulfide. Chem Mater 29:5612–5616. https://doi.org/10.1021/acs.chemmater.7b01243

Smith GL, Eyley JE, Han X et al (2019) Reversible coordinative binding and separation of sulfur dioxide in a robust metal-organic framework with open copper sites. Nat Mater 18:1358–1365. https://doi.org/10.1038/s41563-019-0495-0

Sokhanvaran V, Gomar M, Yeganegi S (2019) H2S separation from biogas by adsorption on functionalized MIL-47-X (X =–OH and–OCH3): a simulation study. Appl Surf Sci 479:1006–1013. https://doi.org/10.1016/j.apsusc.2019.02.152

Stock N, Biswas S (2012) Synthesis of metal-organic frameworks (MOFs): routes to various MOF topologies, morphologies, and composites. Chem Rev 112:933–969. https://doi.org/10.1021/cr200304e

Sun Q, Liu M, Li K et al (2017) Synthesis of Fe/M (M = Mn Co, Ni) bimetallic metal organic frameworks and their catalytic activity for phenol degradation under mild conditions. Inorg Chem Front 4:144–153. https://doi.org/10.1039/C6QI00441E

Sun X, Shi Y, Zhang W et al (2018) A new type Ni-MOF catalyst with high stability for selective catalytic reduction of NO_x with NH_3. Catal Commun 114:104–108. https://doi.org/10.1016/j.catcom.2018.06.012

Sun H, Liu Z, Wang Y et al (2019a) Novel metal-organic framework supported manganese oxides for the selective catalytic reduction of NO_x with NH_3: promotional role of the support. J Hazard Mater 380:120800. https://doi.org/10.1016/j.jhazmat.2019.120800

Sun H, Zhang H, Mao H et al (2019b) Facile synthesis of the magnetic metal-organic framework $Fe_3O_4/Cu_3(BTC)_2$ for efficient dye removal. Environ Chem Lett 17:1091–1096. https://doi.org/10.1007/s10311-018-00833-1

Tan K, Canepa P, Gong Q et al (2013) Mechanism of preferential adsorption of SO_2 into two microporous paddle wheel frameworks M(bdc)(ted)0.5. Chem Mater 25:4653–4662. https://doi.org/10.1021/cm401270b

Tang J, Wang J (2018) Metal organic framework with coordinatively unsaturated sites as efficient fenton-like catalyst for enhanced degradation of sulfamethazine. Environ Sci Technol 52:5367–5377. https://doi.org/10.1021/acs.est.8b00092

Tang J, Wang J (2020) Iron-copper bimetallic metal-organic frameworks for efficient Fenton-like degradation of sulfamethoxazole under mild conditions. Chemosphere 241:125002. https://doi.org/10.1016/j.chemosphere.2019.125002

Tarkwa JB, Oturan N, Acayanka E et al (2019) Photo-Fenton oxidation of Orange G azo dye: process optimization and mineralization mechanism. Environ Chem Lett 17:473–479. https://doi.org/10.1007/s10311-018-0773-0

Tchalala MR, Bhatt PM, Chappanda KN et al (2019) Fluorinated MOF platform for selective removal and sensing of SO_2 from flue gas and air. Nat Commun 10:1–10. https://doi.org/10.1038/s41467-019-09157-2

Tian H, Peng J, Du Q et al (2018) One-pot sustainable synthesis of magnetic MIL-100(Fe) with novel Fe_3O_4 morphology and its application in heterogeneous degradation. Dalt Trans 47:3417–3424. https://doi.org/10.1039/c7dt04819j

Tilgner D, Friedrich M, Verch A et al (2018) A metal-organic framework supported nonprecious metal photocatalyst for visible-light-driven wastewater treatment. Chem Photo Chem 2:349–352. https://doi.org/10.1002/cptc.201700222

Tiwari A, Sagara PS, Varma V, Randhawa JK (2019) Bimetallic metal organic frameworks as magnetically separable heterogeneous catalysts and photocatalytic dye degradation. ChemPlusChem 84:136–141. https://doi.org/10.1002/cplu.201800546

UNESCO (2019) Water and climate change. In: International encyclopedia of geography, pp 1–6

Vaitsis C, Sourkouni G, Argirusis C (2019) Metal organic frameworks (MOFs) and ultrasound: a review. Ultrason Sonochem 52:106–119. https://doi.org/10.1016/j.ultsonch.2018.11.004

Vega F, Baena-Moreno FM, Fernández LMG et al (2020) Current status of CO_2 chemical absorption research applied to CCS: towards full deployment at industrial scale. Appl Energy 260:114313. https://doi.org/10.1016/j.apenergy.2019.114313

Vellingiri K, Kumar P, Deep A, Kim K (2016a) Metal-organic frameworks for the adsorption of gaseous toluene under ambient temperature and pressure. Chem Eng J 307:1116–1126. https://doi.org/10.1016/j.cej.2016.09.012

Vellingiri K, Szulejko JE, Kumar P et al (2016b) Metal organic frameworks as sorption media for volatile and semi-volatile organic compounds at ambient conditions. Sci Rep 6:27813. https://doi.org/10.1038/srep27813

Villegas LGC, Mashhadi N, Chen M et al (2016) A short review of techniques for phenol removal from wastewater. Curr Pollut Reports 2:157–167. https://doi.org/10.1007/s40726-016-0035-3

Vu HT, Tran LT, Le GH et al (2019) Synthesis and application of novel Fe-MIL-53/GO nanocomposite for photocatalytic degradation of reactive dye from aqueous solution. Vietnam J Chem 57:681–685. https://doi.org/10.1002/vjch.201900055

Wang SS, Yang GY (2015) Recent advances in polyoxometalate-catalyzed reactions. Chem Rev 115:4893–4962. https://doi.org/10.1021/cr500390v

Wang XL, Fan HL, Tian Z et al (2014) Adsorptive removal of sulfur compounds using IRMOF-3 at ambient temperature. Appl Surf Sci 289:107–113. https://doi.org/10.1016/j.apsusc.2013.10.115

Wang H, Yuan X, Wu Y et al (2015) Synthesis and applications of novel graphitic carbon nitride/metal-organic frameworks mesoporous photocatalyst for dyes removal. Appl Catal B Environ 174–175:445–454. https://doi.org/10.1016/j.apcatb.2015.03.037

Wang H, Yuan X, Wu Y et al (2016) In situ synthesis of In2S3 at MIL-125(Ti) core-shell microparticle for the removal of tetracycline from wastewater by integrated adsorption and visible-light-driven photocatalysis. Appl Catal B Environ 186:19–29. https://doi.org/10.1016/j.apcatb.2015.12.041

Wang Y, Zhang LJ, Zhang R et al (2017) Porous metal-organic frameworks with 5-aminoisophthalic acid as platforms for functional applications about high photodegradation efficiency of phenol. Cryst Growth Des 17:6531–6540. https://doi.org/10.1021/acs.cgd.7b01190

Wang D, Jiang H, Tan J et al (2019a) Manipulating oxidation states of copper within Cu-BTC using $Na_2S_2O_3$ as a new strategy for enhanced adsorption of sulfide. Ind Eng Chem Res 58:19503–19510. https://doi.org/10.1021/acs.iecr.9b04349

Wang H, Cui PH, Shi JX et al (2019b) Controllable self-assembly of CdS@NH_2-MIL-125(Ti) heterostructure with enhanced photodegradation efficiency for organic pollutants through synergistic effect. Mater Sci Semicond Process 97:91–100. https://doi.org/10.1016/j.mssp.2019.03.016

Wang H, Mahle JJ, Tovar TM et al (2019c) Solid-phase detoxification of chemical warfare agents using zirconium-based metal organic frameworks and the moisture effects: analyze via digestion. ACS Appl Mater Interfaces 11:21109–21116. https://doi.org/10.1021/acsami.9b04927

Wang H, Bai JQ, Yin Y, Wang SF (2020) Experimental and numerical study of SO_2 removal from a CO_2/SO_2 gas mixture in a Cu-BTC metal organic framework. J Mol Graph Model 96:107533. https://doi.org/10.1016/j.jmgm.2020.107533

Wei Y, Wang B, Cui X et al (2018) Highly advanced degradation of thiamethoxam by synergistic chemisorption-catalysis strategy using MIL(Fe)/Fe-SPC composites with ultrasonic irradiation. ACS Appl Mater Interfaces 10:35260–35272. https://doi.org/10.1021/acsami.8b12908

Wu XY, Qi HX, Ning JJ et al (2015) One silver(I)/tetraphosphine coordination polymer showing good catalytic performance in the photodegradation of nitroaromatics in aqueous solution. Appl Catal B Environ 168–169:98–104. https://doi.org/10.1016/j.apcatb.2014.12.024

Xue Y, Wang P, Wang C, Ao Y (2018) Efficient degradation of atrazine by BiOBr/UiO-66 composite photocatalyst under visible light irradiation: environmental factors, mechanisms and degradation pathways. Chemosphere 203:497–505. https://doi.org/10.1016/j.chemosphere.2018.04.017

Yang K, Sun Q, Xue F, Lin D (2011) Adsorption of volatile organic compounds by metal-organic frameworks MIL-101: influence of molecular size and shape. J Hazard Mater 195:124–131. https://doi.org/10.1016/j.jhazmat.2011.08.020

Yang F, Liu QK, Ma JP et al (2015) Reversible adsorption and separation of chlorocarbons and BTEX based on Cu(II)-metal organic framework. CrystEngComm 17:4102–4109. https://doi.org/10.1039/c5ce00547g

Yang FW, Li YX, Ren FZ et al (2019a) Toxicity, residue, degradation and detection methods of the insecticide triazophos. Environ Chem Lett 17:1769–1785. https://doi.org/10.1007/s10311-019-00910-z

Yang X, Liang T, Sun J et al (2019b) Template-directed synthesis of photocatalyst-encapsulating metal-organic frameworks with boosted photocatalytic activity. ACS Catal 9:7486–7493. https://doi.org/10.1021/acscatal.9b01783

Yao P, Liu H, Wang D et al (2018) Enhanced visible-light photocatalytic activity to volatile organic compounds degradation and deactivation resistance mechanism of titania confined inside a metal-organic framework. J Colloid Interface Sci 522:174–182. https://doi.org/10.1016/j.jcis.2018.03.075

Yap MH, Fow KL, Chen GZ (2017) Synthesis and applications of MOF-derived porous nanostructures. Green Energy Environ 2:218–245. https://doi.org/10.1016/j.gee.2017.05.003

Zeng L, Guo X, He C, Duan C (2016) Metal-organic frameworks: versatile materials for heterogeneous photocatalysis. ACS Catal 6:7935–7947. https://doi.org/10.1021/acscatal.6b02228

Zhang C, Ai L, Jiang J (2015) Solvothermal synthesis of MIL-53(Fe) hybrid magnetic composites for photoelectrochemical water oxidation and organic pollutant photodegradation under visible light. J Mater Chem A 3:3074–3081. https://doi.org/10.1039/c4ta04622f

Zhang Z, Li X, Liu B et al (2016) Hexagonal microspindle of NH_2-MIL-101(Fe) metal-organic frameworks with visible-light-induced photocatalytic activity for the degradation of toluene. RSC Adv 6:4289–4295. https://doi.org/10.1039/c5ra23154j

Zhang H, Nai J, Yu L, Lou XW (2017) Metal-organic-framework-based materials as platforms for renewable energy and environmental applications. Joule 1:77–107. https://doi.org/10.1016/j.joule.2017.08.008

Zhang WQ, Cheng K, Zhang H et al (2018) Highly efficient and selective photooxidation of sulfur mustard simulant by a triazolobenzothiadiazole-moiety-functionalized metal-organic framework in air. Inorg Chem 57:4230–4233. https://doi.org/10.1021/acs.inorgchem.8b00106

Zhang H, Chen S, Zhang H et al (2019a) Carbon nanotubes-incorporated MIL-88B-Fe as highly efficient Fenton-like catalyst for degradation of organic pollutants. Front Environ Sci Eng 13:18. https://doi.org/10.1007/s11783-019-1101-z

Zhang R, Du B, Li Q et al (2019b) α-Fe_2O_3 nanoclusters confined into UiO-66 for efficient visible-light photodegradation performance. Appl Surf Sci 466:956–963. https://doi.org/10.1016/j.apsusc.2018.10.048

Zhang X, Yang Y, Lv X et al (2019c) Adsorption/desorption kinetics and breakthrough of gaseous toluene for modified microporous-mesoporous UiO-66 metal organic framework. J Hazard Mater 366:140–150. https://doi.org/10.1016/j.jhazmat.2018.11.099

Zhang X, Yang Y, Song L et al (2019d) Enhanced adsorption performance of gaseous toluene on defective UiO-66 metal organic framework: equilibrium and kinetic studies. J Hazard Mater 365:597–605. https://doi.org/10.1016/j.jhazmat.2018.11.049

Zhang Y, Chen Z, Liu X et al (2020a) Efficient SO_2 removal using a microporous metal-organic framework with molecular sieving effect. Ind Eng Chem Res 59:874–882. https://doi.org/10.1021/acs.iecr.9b06040

Zhang Y, Zhang X, Chen Z et al (2020b) A flexible interpenetrated zirconium-based metal-organic framework with high affinity toward ammonia. Chemsuschem 13:1710–1714. https://doi.org/10.1002/cssc.202000306

Zhao H, Chen Y, Peng Q et al (2017) Catalytic activity of MOF(2Fe/Co)/carbon aerogel for improving H2O2 and ·OH generation in solar photo–electro–Fenton process. Appl Catal B Environ 203:127–137. https://doi.org/10.1016/j.apcatb.2016.09.074

Zhao X, Zhang S, Yan J et al (2018) Polyoxometalate-based metal-organic frameworks as visible-light-induced photocatalysts. Inorg Chem 57:5030–5037. https://doi.org/10.1021/acs.inorgchem.8b00098

Zheng TR, Qian LL, Li M et al (2018) A bifunctional cationic metal-organic framework based on unprecedented nonanuclear copper(II) cluster for high dichromate and chromate trapping and highly efficient photocatalytic degradation of organic dyes under visible light irradiation. Dalt Trans 47:9103–9113. https://doi.org/10.1039/c8dt01685b

Zheng XX, Fang ZP, Dai ZJ et al (2020) Iron-based metal-organic frameworks as platform for H_2S selective conversion: structure-dependent desulfurization activity. Inorg Chem 59:4483–4492. https://doi.org/10.1021/acs.inorgchem.9b03648

Zhong X, Lu Y, Luo F et al (2018) A nanocrystalline POM@MOFs catalyst for the degradation of phenol: effective cooperative catalysis by metal nodes and POM guests. Chem-A Eur J 24:3045–3051. https://doi.org/10.1002/chem.201705677

Zhong Z, Li M, Fu J et al (2020) Construction of Cu-bridged Cu_2O/MIL(Fe/Cu) catalyst with enhanced interfacial contact for the synergistic photo-Fenton degradation of thiacloprid. Chem Eng J 395:125184. https://doi.org/10.1016/j.cej.2020.125184

Zhu H, Liu D (2019) The synthetic strategies of metal-organic framework membranes, films and 2D MOFs and their applications in devices. J Mater Chem A 7:21004–21035. https://doi.org/10.1039/c9ta05383b

Zhu SY, Yan B (2018) Photofunctional hybrids of TiO_2 and titanium metal-organic frameworks for dye degradation and lanthanide ion-tuned multi-color luminescence. New J Chem 42:4394–4401. https://doi.org/10.1039/c7nj04786j

Zhu SR, Liu PF, Wu MK et al (2016) Enhanced photocatalytic performance of BiOBr/NH_2-MIL-125(Ti) composite for dye degradation under visible light. Dalt Trans 45:17521–17529. https://doi.org/10.1039/c6dt02912d

Zhu M, Hu P, Tong Z et al (2017) Enhanced hydrophobic MIL(Cr) metal-organic framework with high capacity and selectivity for benzene VOCs capture from high humid air. Chem Eng J 313:1122–1131. https://doi.org/10.1016/j.cej.2016.11.008